IDENTIFYING BIOLOGICALLY ACTIVE COMPOUNDS TO PROVIDE T CELL COSTIMULATION FOR CANCER IMMUNOTHERAPY

IDENTIFYING BIOLOGICALLY ACTIVE COMPOUNDS TO PROVIDE T CELL COSTIMULATION FOR CANCER IMMUNOTHERAPY

Kaylyn Bacchiocchi

Masters of Biochemistry and Biomedical Sciences Thesis

July 2021

Table of Contents:

ABSTRACT

Adoptive cell therapy (ACT) is a powerful cancer immunotherapy platform, where T lymphocytes are collected from cancer patients, expanded *ex vivo*, and infused back into the patient as a cellular drug. Genetic modification with chimeric receptors redirects T cell tumour-specificity. While ACT is a clinical success in many cancers, it is dependent on T cell proliferation following infusion, where robust expansion is a predictor of a positive outcome.

Costimulation is the activation of a class of receptors which provide maximal stimulatory signals to T cells, resulting in an enhancement of proliferation, survival, and memory. Costimulatory receptor signaling occurs in cooperation with the T cell receptor, and is provided by several receptor families that converge on costimulatory signaling pathways.

Chimeric receptors can be modified with costimulatory domains however, the non-canonical signaling can lead to overstimulation and serious toxicity in the clinic. We hypothesize that pharmacological costimulation can be used to boost T cell proliferation, where drug administration and dosage is controlled and the drug can cease to be administered should toxicities manifest. Small molecule costimulation may prove to be a useful approach to boost the efficacy of ACT as a cancer therapy.

The **objective** of my research project is to screen and characterize for small molecules that enhance T cell proliferation. Specifically, I will investigate the ability small molecule drugs to enhance T cell expansion following antigen-specific stimulation of T cells engineered with T cell antigen coupler (TAC) receptors.

Methods: I identified candidate small molecules with costimulatory effects on TAC T cells using two strategies. First, I generated a database of small molecules that were predicted to interact with costimulation pathways based on connectivity mapping, provided by the Broad Institute, using the transcriptomes of TAC T cells activated in the presence or absence of costimulation. As a second screening strategy, I developed a bioluminescent reporter system that was used for high throughput screening of small molecules libraries available at the Centre for Microbial and Chemical Biology. Following the identification of several hits, these compounds were tested *in vitro* for their modification to TAC T cell proliferation and function.

Results: We have identified several chemical classes of compounds which contributed to a robust increase in TAC T cell proliferation in the absence of costimulation, and have evaluated the top three drugs *in vitro* by proliferation and RNA sequencing assays. Ferutinin, and protein kinase C activating compounds mezerein and phorbol 12,13-dibutyrate, were found to robustly increase TAC T cell proliferation.

The **significance** of this project is to identify costimulatory small molecules to enhance the efficacy of T cell cancer therapy, and yield novel insight into the chemical space that modulates costimulation.

1. INTRODUCTION

1.1 Cancer Therapies

A cancer diagnosis is a fearful reality that most people either face themselves, or within their family or group of friends. In Canada, cancer is the leading cause of death where it is estimated that close to half of all Canadians will be diagnosed with cancer in their lifetime (Siegel, 2019). Of those who have been diagnosed, only 50% are expected to survive (Siegel, 2019).

Following diagnosis, a few primary treatment options are offered to the patient as a first line of care including surgery, radiation, and chemotherapy. Patients undergoing these treatments experience a deterioration in their quality of life, contributing to the lack of hope surrounding a cancer diagnosis. While these first line treatments have extended the lives of many individuals, they are highly invasive and cause permanent damage to normal tissues. Specifically, surgery and radiation treatments are limited by the accessibility of the tumour, and are a less successful treatment option for metastatic tumours. Chemotherapy involves the use of anti-proliferative compounds that target and kill rapidly dividing tumour cells (Huang, 2017), resulting in harmful off-target effects that can cause severe and wide-spread tissue damage. Potent anti-tumor activity as a result of these chemotherapeutic agents has hit a plateau in the last decade, where treatment efficacy is no longer able to surpass toxicity (Huang, 2017). There is currently an unmet need for safe and more effective cancer therapies.

1.2 T Cell Immune Surveillance

The development and survival of cancer is accredited to the failure of the immune system in recognizing and eliminating cancerous cells. Cancerous cells are created through the accumulation of several mutations that causes the loss of the cell's internal organization and ability to repair mutated DNA. As these cells accumulate independent mutations, they become dysfunctional and proliferate to form tumours. To the immune system, these cells resemble virus-infected cells, as their cellular organization has become reordered in comparison to a healthy cell (Parham, 2015). Necessary characteristics of cancer cells that derive from DNA mutations and result in a successful cancer cell lineage include the ability to stimulate their own growth, ignore growth-inhibiting signals, avoid apoptosis, develop connections to the blood supply, metastasize, and replicate constantly (Parham, 2015). The last hallmark characteristic needed for a successful cancer is the ability to successfully evade the immune system, where selective pressures from immune cells allows cancer cells to adapt in order to avoid death. In a perfect system, specific immune cells known as T lymphocytes patrol the body and eliminate cells that have developed an uncontrolled proliferative phenotype, or cancer. The caveat to this system is the genetic instability of cancerous cells, allowing tumours to adapt in response to selective pressures by the immune system. This phenomenon is also known as immune escape, where cancerous cells adapt to evade immune cell recognition and death. This is commonly seen in cancer patients as a result of immune infiltration in the tumour. Mechanisms of immune escape include downregulation of an immune-recognized surface receptors on cancer cells (otherwise known as cancer antigens), creating a hostile tumour microenvironment towards immune

cells, manipulating immune cells to become dysfunctional by upregulating markers of exhaustion or senescence, among other evasive mechanisms. These mechanisms result in tumour escape and the failure of the immune system to regulate cancer growth.

Immune surveillance is provided by circulating lymphocytes, with the main contributor to this system being T cells. Thymus-dependent lymphocytes, or T cells, are a type of immune cell that originate in the bone marrow from bone marrow stem cells and travel to the thymus to undergo maturation and gene rearrangement to develop antigen-specificity. T cells mediate immunity by recognizing a specific peptide sequence, or antigen, from a pathogen. Effector T cells are the subset of mature T cells that circulate between the blood and the lymph, in search of a specific pathogenic antigen. Effector T cell functions are performed through interactions with other cells in the body. A cytotoxic T cell activated by a pathogenic antigen is capable of killing the infected cell by releasing cytotoxic granules into the target cell, effectively inducing apoptosis, also known as programmed cell death. In the context of cancer, effector T cells are capable of killing antigen expressing cells by sequentially releasing cytotoxic granules into tumour cells in a serial-like fashion. A subset of these effector T cell clones become memory cells that persist in the body for decades, and are able to quickly respond and re-expand in the event of antigen recurrence. This allows memory T cells to recognize an antigen years later upon recurrence, and re-expand. However, in the case of a highly heterogeneous tumour, tumour cells that do not express an immune recognized antigen are the cells that escape immune recognition and can cause relapse, an example of immune escape.

1.2.1 The T cell receptor (TCR)

T cells possess an antigen binding domain referred to as a T cell receptor (TCR), where a single T cell expresses a number of identical TCRs on its cell surface. Each T cell clone expresses a unique antigen receptor that is produced as a result of gene rearrangement during T cell development. The TCR contains a variable region that displays high sequence variability that is generated during gene rearrangement and contributes to each unique T cell antigen specificity. Sequence variability spans across five human chromosomes to allow for a highly diverse population of T cells. Different T cell clones display TCRs with distinct antigen specificities, allowing for a diverse population and protection against peptide antigens derived from a variety of pathogens.

The TCR is a membrane-bound glycoprotein composed of two polypeptide chains that form an antigen binding site. TCRs naturally recognize one antigen depending on the TCR's unique combination of alpha and beta polypeptide domains (TCRα and TCRβ). The human TCR repertoire consists of $>10^8$ possible TCRs in the body at a given time (Lythe, 2016). The α:β chain associates with four membrane proteins, CD3γ, CD3δ, CD3ε and CD3ζ, to make up the CD3 complex. The association of these proteins on the T cell surface results in the formation of the T cell receptor complex, where the CD3ζ cytoplasmic domain activates intracellular signals in the event that an antigen has been recognized by the α:β chain. The α:β chain itself lacks signaling capabilities as a result of its short cytoplasmic tail. The formation of the T cell receptor complex is critical for the T cell to recognize its antigen, and mount an immune response.

1.3 Signal 1 – TCR: MHC interaction

T cells are termed naïve until they have become activated in the presence of their TCR-specific antigen. Upon activation of a naïve T cell, the cell undergoes transcriptional changes to become effector-like, and proliferates to form a population of T cell clones that are primed to respond against their antigen. T cell effector functions are executed following antigen-specific TCR interaction with a neighboring cell. The peptide antigen is presented to the T cell on the target cell's surface in the context of a large molecule termed a major histocompatibility complex (MHC). This MHC: peptide interaction with the TCR is termed 'Signal 1', and serves to activate both naïve and antigen experienced (effector) T cells. MHC molecules are polymorphic, where every individual possesses their own unique MHC molecule that is recognized by their own T cells. MHC molecules require the binding of a peptide to fold properly and form a stable complex, and continuously present foreign peptides on the cell surface, a phenomenon known as antigen presentation. Antigen presentation is required by T cells to mount an immune response. In the case of naïve T cells, antigen presentation and T cell activation occurs in the secondary lymphoid tissue. Once activated, the T cell undergoes a period of proliferation and expansion to form a large population of antigen-specific T cell clones, that are then capable of carrying out their specific effector T cell functions. T cell activation always requires signal 1, the interaction between an antigen-specific TCR and a peptide antigen presented by a MHC molecule on a neighboring antigen presenting cell.

1.3.1 TCR co-receptors

In healthy cells, the MHC molecule presents self-peptides that do not produce a T cell response, as the specificity of each TCR is directed against non-self-peptide antigens. The highly diverse TCR repertoire offers protection against a variety of antigens on a presented peptide. These foreign peptides are produced through the degradation of viral proteins in an infected human cell, or the degradation of whole pathogens by macrophages and dendritic cells, two specific types of immune cells. The T cell response is aimed at these two methods of infection, where two types of MHC molecules are responsible for the presentation of different types of pathogenic peptides. This accounts for two methods of MHC presentation: antigen presentation of intracellular pathogens, such as viruses by a MHC class I molecule, and extracellular pathogens, such as bacteria by a MHC class II molecule. Most cells express MHC class I molecules, however, only a few immune cell types express MHC class II molecules. These are macrophages, dendritic cells, and B cells.

These two MHC classes correspond with two types of effector T cells, cytotoxic T cells that recognize MHC class I intracellular peptides, and helper T cells that recognize MHC class II extracellular peptides. These cell types are distinguishable by specific cell-surface proteins, or their co-receptors, where cytotoxic T cells express a CD8 receptor and helper T cells express a CD4 receptor. These T cell co-receptors cooperate with the TCR to recognize peptide antigens by sterically binding their co-receptor to a structurally distinct binding site on their corresponding MHC molecule. The T cell TCR and co-receptor specifically recognize both the antigenic peptide and the MHC molecule. The primary function of CD8 T cells are to kill cells infected with an intracellular pathogen. CD4 T cells

help professional antigen presenting cells (APCs), otherwise known as macrophages and dendritic cells, that are presenting peptides from extracellular pathogens. Activated CD4 T cells help initiate an adaptive immune response by secreting cytokine and chemokines to activate these immune APCs, and help initiate a B cell response.

Effector CD8 T cells are cytotoxic in nature, and are responsible for killing infected target cells. These cytotoxic T cells are critical for the front line of defense against a pathogen, as they are capable of killing antigen-expressing cells in a serial-like fashion. In the context of cancer, cytotoxic CD8 T cells are the T cell subtype that exhibit cytotoxicity to directly kill antigen positive tumour cells. On the other hand, effector CD4 T cells comprise of five functional subtypes based on their cytokine secretion prolife, and function as helper cells to either activate or suppress different immune cells. These five helper subtypes include T_H1, T_H2, T_H17, T follicular helper cells (T_{FH}), and regulatory T cells (T_{reg}). Classically, T_H1 cells function to activate macrophages, T_H2 cells enhance the immune response to parasitic infections, T_H17 cells help immune cells respond to extracellular pathogens, T_{FH} cells aid in the B cell response, and T_{reg} cells possess the ability to suppress other effector T cell functions (Parham, 2015). The population of effector CD4 T cells in the body is highly diverse, where the five helper subtypes secrete distinct cytokine profiles that initiate different immune reactions. At the site of infection, alongside cytotoxic CD8 T cells, T_H1, T_H2, and T_H17 CD4 T cells are the helper subtypes that directly aid in the immune response. Both CD4 and CD8 co-receptors are critical to mount an effective adaptive immune response.

1.4 Signal 2 – T cell costimulation

Effector T cell activation requires signal 1 alone to mount an effective immune response. Circulating effector T cells in the blood and lymph have been primed against their target antigen, and do not require any additional help to proliferate and mount an immune response. However, naïve T cells require an extra signaling event, to become activated and undergo transcriptional changes to become an effector T cell. These additional signals are termed 'Signal 2', otherwise known as costimulation. Costimulatory signals provide naïve T cells with additional stimulation to reach their activation threshold. Without signal 2, these naïve T cells cannot divide or survive. Costimulatory receptors reside on all T cells, where a costimulatory molecule or ligand is required to activate and initiate costimulatory signaling cascades. Typically, these costimulatory ligands are provided by the target cell with the peptide: MHC complex that activates the T cell. The region of contact between these two cells is termed the T cell synapse, containing the central supramolecular activation complex (c-SMAC) and the peripheral SMAC (p-SMAC). The c-SMAC is a region on the T cell where the TCRs, co-receptors, co-stimulatory receptors, and CD2 adhesion molecules are concentrated. The p-SMAC makes up the outer ring around the c-SMAC, and houses integrins, such as LFA-1, and cell-adhesion molecules, such as ICAM-1. The T cell synapse allows for the organization of these signaling molecules during activation, and a concentrated area where intracellular signals are transmitted to the cell. Through the synapse formation, co-receptor and TCR signals synergize to activate the cell, where costimulatory signals enhance activation and phosphorylation of additional signaling pathways needed for proliferation and survival. In

naïve T cells, signal 1 and 2 results in gene transcription by downstream transcriptional activators NFAT (nuclear factor of activated T cells), NFκB (nuclear factor-κB), and AP-1 (activating protein-1) that induce T cell proliferation, differentiation, and effector T cell functions (Parham, 2015). T cell proliferation and differentiation also require the transcription and uptake of the cytokine interleukin-2 (IL-2), induced through the NFAT transcription factor. Secreted IL-2 delivers growth signals to T cells via autocrine or paracrine cytokine production. Costimulation signaling enhances the production of IL-2 (Parham, 2015).

Effector T cell activation can also be amplified through an additional family of receptor-ligand interactions, resulting costimulation. The ligation of these costimulatory receptors allows for a series of intracellular signaling cascades that modify the T cell response. Costimulation in addition to TCR binding on both naïve and effector T cells results in robust proliferation, survival, and memory responses (Song, 2012). However, costimulation can provide a boost to all T cells undergoing activation regardless of subtype, resulting in more potent anti-tumour activity. Costimulation by the CD28 receptor was first discovered in the late 1980s, as a CD28 monoclonal antibody provided signal 2 in combination with TCR stimulus to induce T cell activation (Jenkins, 1991). The identification of several receptors that share homology to CD28 were then discovered over the past two decades, leading to the definition of the CD28 receptor family (Esensten, 2017).

Costimulation can be provided by many classes of receptors that are constitutively expressed on T cells, including those belonging to the tumour necrosis factor receptor

superfamily (TNFRSF) and the immunoglobulin superfamilies (IgSF), and the interleukin 1 receptor and integrin families (Skånland, 2014). Co-signaling receptors are divided into superfamilies, families, and subfamilies, based on their protein structure and function (Chen, 2013).

1.4.1 Immunoglobulin superfamily (IgSF) costimulation

Within the IgSF, the most commonly characterized families are the CD28 and B7 families. Receptor members of the CD28 family primarily interact with members of the B7 family, where CD28 binds CD80 and CD86 molecules. The CD28 family is characterized by an extracellular immunoglobulin-like domain, and is not limited to costimulatory receptors. The CD28 family also includes the receptors CTLA4 and PD-1, known to play a role in inhibiting T cell effector functions. CD28 receptor expression can be found on approximately 80% of human CD4 T cells, and 50% of human CD8 T cells (Esensten, 2017).

Another IgSF group is the CD2/signaling lymphocytic activation molecule (SLAM) family, which includes CD2 and SLAM T cell costimulatory receptors (Chen, 2013). These family members are type I glycoproteins, where SLAM family members have at least one immunoreceptor tyrosine-based switch motif (ITSM) in their cytoplasmic tail. ITSMs on the cytoplasmic domain of SLAM receptors have high affinity for SLAM associated proteins (SAPs), consisting of a single SH2 domain (Cannons, 2011). Both SLAM and SAP are recruited to the T cell synapse during activation, where SAP competitively binds SLAM inducing SLAM phosphorylation to promote T cell activation, and prevent the binding of other SH2 domains that transmit inhibitory signals to the T cell (Cannons, 2011).

The engagement of the CD2 costimulatory T cell receptor by its ligand CD58 induces a costimulatory response T cells, leading to proliferation and cytokine production. The CD58/CD2 axis has been reported as the primary costimulatory pathway used in CD8 T cells lacking CD28 receptor expression (Leitner, 2015). Ligation of one or more costimulatory receptors results in an enhancement of T cell proliferation and survival. The engagement of these receptors alongside T cell activation stimulates additional intracellular signaling pathways, and can have a combinatorial effect.

T cell costimulation results in downstream activation of transcription factors to initiate T cell transition from G0/G1 to the S phase of the cell cycle, enhancement of cell survival, and cytokine production. Within the Ig superfamily, several receptors in the CD28 and CD2 families provide these stimulatory signals upon ligation. CD28 and CD2 are both constitutively expressed on T cells, with expression levels dependent on T cell subtype and activation status. The CD28 receptor is most commonly associated with its ligand B7 on APCs, otherwise known as CD80 or CD86. The CD2 receptor has been characterized as both an adhesion molecule and a costimulatory molecule, and is expressed to a higher degree on the surface of memory T cells (Demetriou, 2019). The T cell synapse is the interface between the T cell and an interacting APC. CD2 receptor ligation has been shown to alter the shape and size of the T cell synapse, leading to enhanced TCR aggregation and signaling (Demetriou, 2019). CD2 interaction with its ligand, CD58 (otherwise known as LFA-3) results in the formation of a distinct elongated synapse, defined by phalloidin (red) staining in figure 1A (Skånland, 2014). In comparison to CD28 costimulation, CD2 in addition to CD3 ligation results in a larger area of synapse (figure 1A). CD2 engagement

provides a boost to proximal TCR signaling cascades, including CD3ζ & SLP-76 phosphorylation.

Costimulation through CD28 induces potent NF-κB activation, and activation of protein kinase B (PKB, known as AKT) and mitogen-activated protein kinase/ Ras-Raf-MEK-ERK (MAPK/ERK) signaling pathways (Figure 1B). The NF-κB transcription factor regulates DNA transcription, cytokine production, and survival. The MAPK/ERK pathway is involved in the regulation of proliferation, differentiation, and survival. AP1/2 and NFAT transcription factors induced by CD28 ligation produce pro-inflammatory signals, and together regulate cell survival. CD2 engagement more potently induces phosphorylation of downstream transcription factor regulators ERK1/2. While CD28 and CD2 costimulation pathways converge to activate ERK1/2, they signal through distinct costimulation molecules and are initiated by sterically different receptor interactions within the T cell synapse.

A.

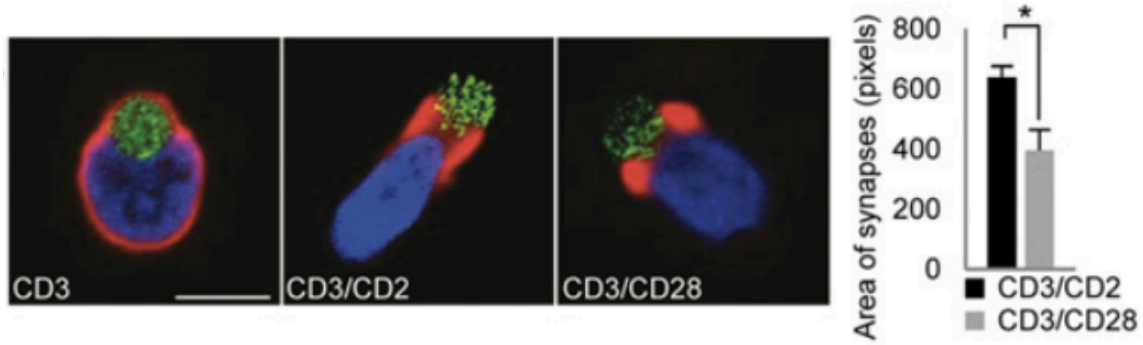

B.

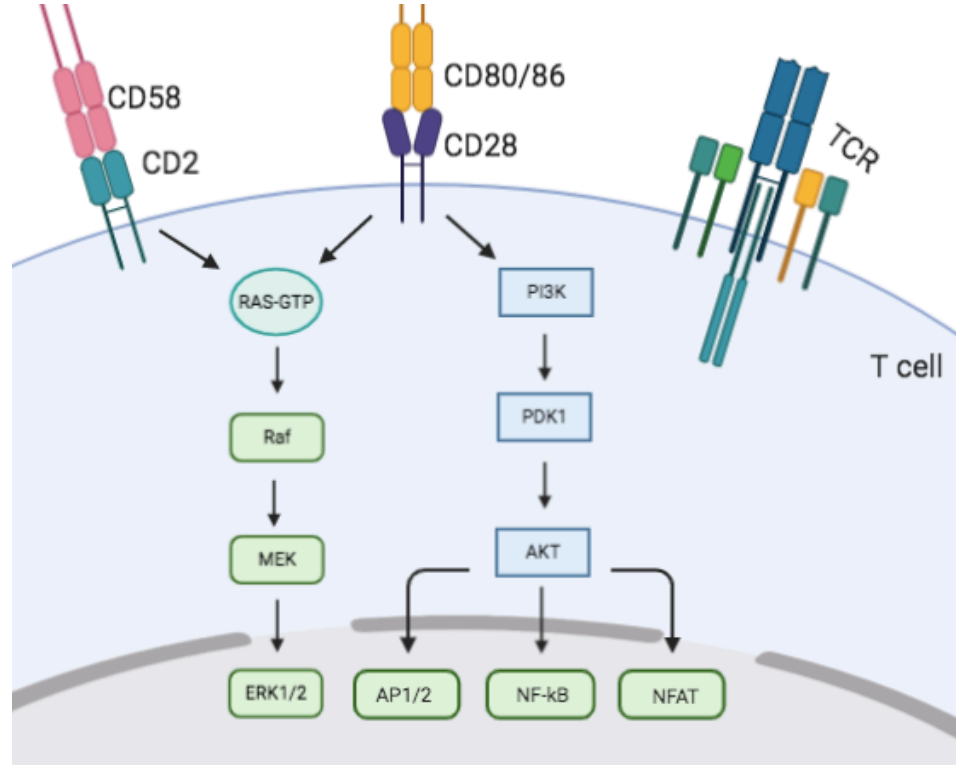

Figure 1: CD28 and CD2 costimulation results in different synapse formation and signaling pathways. A) Synapse formation with CD2 and CD28 co-stimulation. Localization of phalloidin (red), nucleus (blue) and bead (green) in T cells 20 min post-activation with anti-CD3, anti-CD3/CD2 or anti-CD3/CD28 antibody-coated beads (Skånland, 2014). **B)** CD28 and CD2 primary signaling pathways. CD28 has been characterized to primarily activate downstream AP1/2, NFκB and NFAT pathways (Chen, 2013). CD2 receptor signaling has been characterized to elicit strong ERK1/2 activation and nuclear translocation (Skånland, 2014). Figure made in Biorender.

1.5 Adoptive T cell therapy

Manipulation and use of the immune system for treating cancer is a rapidly growing avenue towards more effective therapies. A number of clinical trials in T cell immunotherapy are focused on adoptive cell therapy (ACT). In ACT, T cells are isolated from the patient, expanded *in vitro,* and reinfused back into the patient. The population of reinfused tumour infiltrating lymphocytes (TILs) relies on a high number of T cells to overwhelm and clear the tumour. Robust T cell expansion following adoptive transfer is used as a predictor of a positive outcome, as more tumour specific T cells are available to overcome the tumour burden (Borrie, 2018).

Novel treatments using adoptively transferred T cells have been shown to extend the survival of patients with B cell cancers, but have yet to display similar success in patients with solid tumours (Ramakrishna, 2020). T cell immunotherapy platforms are continually raising the expectations for treatment standards by achieving objective responses in previously untreatable cases.

1.5.1 Synthetic T cell receptors

One highly effective avenue of ACT available in the clinic is engineered T cell therapy. Here, the patient's own T cells are extracted and undergo proliferation *ex vivo* for therapy. The T cell product is engineered with synthetic T cell receptors, introduced into the T cell population via viral infection with a receptor-encoding plasmid. These synthetic receptors bypass the need for signal 1 (classical TCR activation), as they contain an antigen-specific receptor that functions independently of the native TCR peptide: MHC complex.

The most commonly used synthetic T cell receptor to date is the chimeric antigen receptor (CAR). Adoptive cell therapies using genetically engineered receptors, specifically CAR T cells, have had overwhelming success in B cell cancers (Ramakrishna, 2020). To deliver a highly specific cancer immunotherapy, CAR T cells are engineered with a synthetic single chain variable fragment (scFv) antibody fragment, targeted at a known cancer antigen. CAR T cell therapies bypass signal 1 (TCR activation) by using a synthetic extracellular antigen binding domain, coupled to an intracellular T cell activation domain, to signal independently of the TCR. However, an increase in inflammatory cytokines can occur as a result of CAR T cell therapy, characterized by systematic inflammation and toxic side-effects. These modifications drive the cell towards an activated cytotoxic state (Shimabukuro-Vornhagen, 2018). CAR T cell therapy has been successful in treating many liquid tumours, and will become a more prevalent cancer therapy as treatments become more accessible to patients (Schandevyl, 2018).

First generation CARs activate the T cell through their CD3ζ signaling domain when the extracellular scFv region is bound to a corresponding cancer antigen, to deliver signal 1 or activating signals to the T cell. Second and third generation CARs also deliver signal 2 to the T cell through one or more intracellular costimulatory domains (figure 2). Engineering intracellular costimulatory domains into chimeric T cell receptors has become an increasingly effective option to boost T cell expansion with ACT, and improve clinical success. Clinically available next generation CAR T cells include either one or multiple intracellular costimulatory domains such as CD28 and 41BB, that are activated upon antigen binding to the scFv (figure 2). These costimulatory signals directly activate

downstream pathways resulting in T cell proliferation and survival, and clinically desirable responses (Schandevyl, 2018).

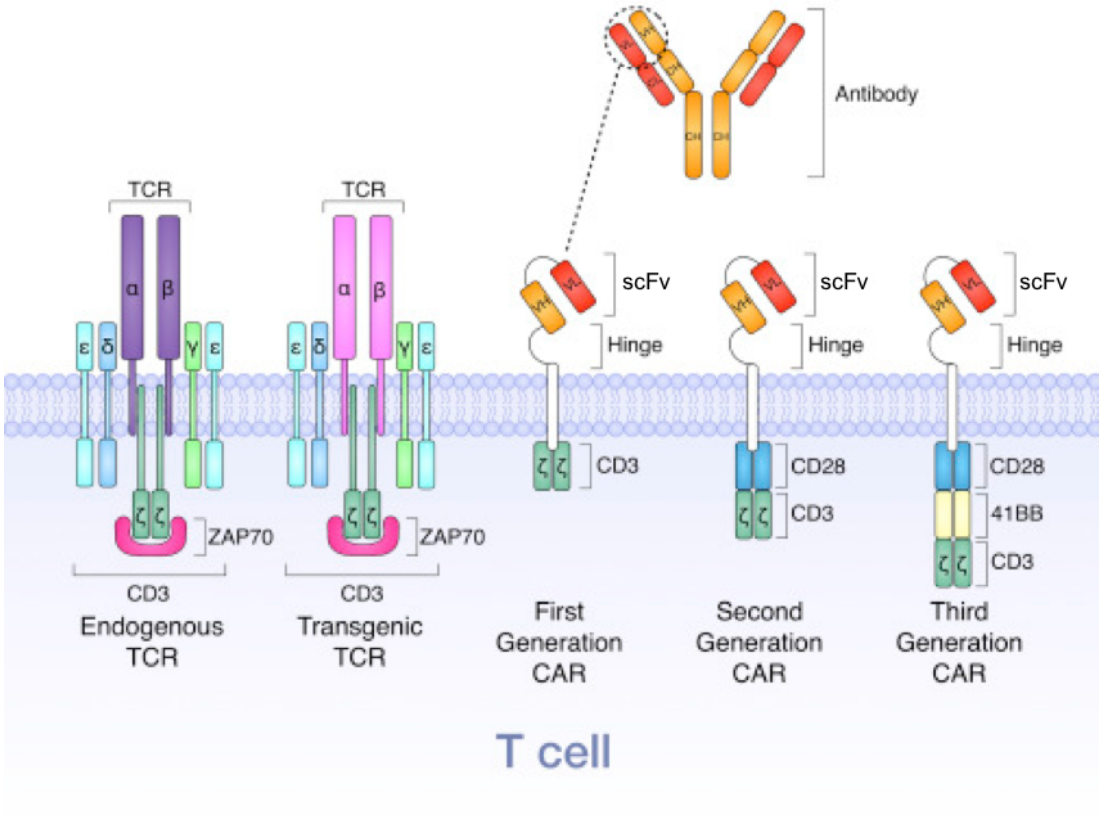

Figure 2: TCR vs. CAR signaling components. CAR T cells signal through the scFv antibody binding portion, and can include one or more costimulatory domains from the Ig superfamily (CD28) and TNF superfamily (41BB) of receptors (Borrie, 2018).

1.5.2 The TAC T cell receptor

Engineered T cells expressing a tumor-directing receptor have emerged as a highly promising cancer therapy, with one of them being the novel chimeric T cell antigen coupler (TAC) receptor currently undergoing clinical trials as a cell therapy. Unlike CAR T cells, the TAC T cell receptor co-opts the native TCR to redirect antigen specificity. TAC T cells have been shown to produce less off-target toxicities in a murine model of breast cancer,

than seen in comparable CAR T cell therapy (Helsen, 2018). The TAC receptor consists of an engineered CD4 co-receptor intracellular and transmembrane domain, connected to an extracellular CD3 epsilon-binding domain, and a distal antigen binding domain (figure 3) (Helsen, 2018). The receptor integrates the native TCR and its associated signaling and regulatory pathways, and demonstrates reduced pro-inflammatory cytokine production, little tonic signaling, and maintains a less exhausted phenotype while exerting robust anti-tumor efficacy (Helsen, 2018).

TAC T cells are fully functional despite the absence of costimulation built into the synthetic receptor. Unlike CAR T cells which function to become activated independently of the native TCR, TAC T cells activate the native T cell signaling pathways. TAC T cell activation is therefore modulated by pathways downstream of the TCR, which function to regulate activation, and consequently impact clonal expansion and anti-tumour activity.

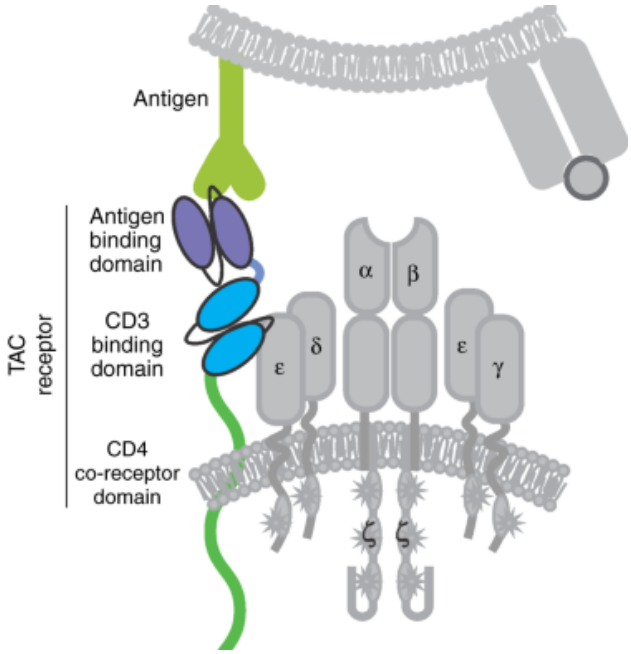

Figure 3: TAC T cell signaling components. TAC T cells co-opt the native TCR to redirect antigen specificity while retaining normal T cell signaling. The TAC T cell consists

of an engineered CD4 co-receptor intracellular and transmembrane domain, connected to an extracellular CD3 epsilon-binding domain, and a distal antigen binding domain (Helsen, 2018).

1.6 Pharmacologic manipulation of T cell function

Although T cell therapies have produced durable responses in the clinic, some patients do not respond or produce long lasting effects. A lack in response can be due to many factors. A predictor of a successful therapy is robust expansion and persistence of the T cell product following infusion (Borrie, 2018; Sterner, 2021; Tian, 2020; Zhang, 2020). The persistence of adoptively transferred T cells is important to mounting an effective response, as more T cells are available to clear the tumour burden. In a tumour microenvironment, T cells are constrained by the absence of costimulatory or cytokine signals that amplify T cell expansion and persistence. These supporting signals can be restored by small molecules that target pathways involved in T cell anti-tumour activity (Marro, 2019).

The benefit of using small molecules to deliver T cell signals is that they are relatively inexpensive to manufacture, have better bioavailability than biologics or monoclonal antibodies, and can be easily administered to patients receiving ACT (Marro, 2019). This is especially beneficial as small molecules are capable of accessing intracellular targets, unlike current antibody therapies, and can be distributed across a larger tumour area (Marro, 2019). This makes them an attractive therapeutic option for patients receiving T cell therapy. Small molecules also have a longer shelf life and can be dosed according to patient needs, allowing for the transient delivery of these T cell supporting signals.

One known signaling molecule related to costimulation is protein kinase C (PKC). Activation of the PKC complex provides signal 2 to T cells through activation of PKC-θ, most commonly turned on as a result of CD28 costimulation. TCR activation and costimulation by the native CD28 receptor triggers PKC-θ catalytic activation and translocation to the immunological synapse. These events initiate downstream signals to induce proliferation, including the activation of NF-κB, AP-1 and NFAT pathways (Wang, 2012). Small molecule PKC activators synergize with TCR engagement in T cells to increase intracellular calcium and induce activation, proliferation, and cytokine production (Kim, 2018). These small molecule compounds function to activate PKC- θ directly, and bypass the need for CD28 receptor stimulation.

Inhibitors of T cell signaling pathways that naturally inhibit T cell proliferation and anti-tumour function have also been explored, to boost T cell function and deliver stimulatory signals to T cells. Lacey et al. (2021) demonstrated a high throughput screen for inhibitors of hematopoietic progenitor kinase 1 (HPK1), where T cells treated with HPK1 inhibitors *in vivo* demonstrated enhanced activation and anti-tumour activity. An additional target, the V-domain Ig suppressor of T-cell activation (VISTA) receptor, is a known immune checkpoint that negatively regulates T cell anti-tumour function (Gabr, 2020). A small molecule blocking VISTA signaling *in vitro* was seen to enhance T cell proliferation and activation when co-cultured with cancer cell lines expressing VISTA (Gabr, 2020).

Cyclin-dependent kinase (CDK) and bromodomain (BRD) protein inhibitors have also been reported to increase anti-tumour T cell function in non-engineered T cells by

increasing cytotoxicity and type II interferon cytokine secretion (To, 2021). Specifically, the compound cyclopamine was found to induce antigen-dependent anti-tumour function in T cells and increase T cell proliferation. Cyclopamine is a Sonic Hedgehog (SHh) pathway inhibitor that has been shown to enhance T cell proliferation, IFNγ cytokine secretion and tumour cytotoxicity but only under hypoxic conditions, as seen in a solid tumour microenvironment (To, 2021). Many Hedgehog (Hh) inhibitors are currently undergoing clinical trials as anticancer drugs. Hh signaling is also known to play a large role in T cell function, where Hh signaling is induced in T cells following activation (Onishi, 2013).

Additional small molecules aimed at improving the success of adoptive T cell therapies include small molecule inhibitors of intermediary metabolic products that promote glycolic T cell metabolism (Waller, 2019). Inhibition of glycolic T cell metabolism during expansion was found to promote a metabolic prolife consistent with a memory T cell phenotype, allowing T cells to persist longer in a patient. These metabolic inhibitors were found to enhance the proliferative capacity of the engineered T cell product, and decrease the number of senescent-like T cells in culture (Waller, 2019).

Many activators of costimulatory pathways, such as PKC activators, and inhibitors of inhibitory pathways, such as CDK, BRD, HPK1, and VISTA, have been shown to promote T cell proliferation and anti-tumour function. Screening for compounds that can modulate these compounds may yield valuable agents for combining with ACT.

1.6.1 Methods of high-throughput screens

High throughput screening platforms for the discovery of compounds that enhance T cell anti-tumour function have become an increasingly popular avenue for improving T cell therapies (Marro, 2019). Several categories of high throughput T cell screening protocols have been reported recently to identify small molecule intervention that boost T cell function. Three methods used for quantifying these T cells responses are plate-based, imaging-based and cytometry-based assays. Each method offers its own benefits and limitations for number of parameters quantified vs speed of screening.

Plate based assays take advantage of a low number of parameters, with most screening protocols only observing one marker (Fouda, 2017). Plate-based screens are typically performed *in vitro*, in a 2-dimensional system. These systems primarily use luminescent or bioluminescent markers, to measure the intensity of a given parameter. Examples of these are red, green, or yellow fluorescent proteins, and firefly luciferase. Fluorescent proteins require no substrate and are measured through excitation. Firefly luciferase requires the addition of a D-luciferin substrate to initiate catalytic conversion and allow the cells to luminesce, where signal intensity is read by light emission (Fouda, 2017). Engineering methods such as lentiviral, mRNA or CRISPR-Cas9 (Dufva, 2020) allows a fluorescent or luminescent reporter to be inserted under the control of a specific gene promoter. Interferon gamma (IFN-γ) is used as a reporter to measure cytokine secretion as an indirect measure of T cell anti-tumour function (Ouyang, 2021). Reporter genes can also be inserted downstream of steadily expressed genes, to measure T cell proliferation or viability as a result of small molecule intervention. Ouyang et al. (2021) developed a high

throughput screen for 267 natural product small molecules to identify drugs that increase IFN-γ expression in human Jurkat T cell line. This study used a red fluorescent reporter system, where cells were engineered to express mCherry only when IFN-γ transcription was promoted. The output of this assay was a single measurement that directly represented the effect that these small molecules had on T cell IFN-γ expression. Grobben et al. (2020) developed a high throughput assay to discover inhibitors of arginase 1, a novel drug target for cancer immunotherapy. Arginase 1 is an enzymatic regulator of L-arginine, where arginase-1 activity has been found to reduce T cell anti-tumour efficacy. By monitoring the decrease in signal intensity of a L-arginine fluorescent probe, Arginase Gold, they measured arginase-1 enzymatic conversion rate as a result of small molecule inhibition over several time points (Grobben, 2020). This study is an excellent example of the flexibility of plate-based assays over short or long time courses, as a single reading of the plate is not endpoint. They applied their screening method to a library of 93,000 compounds, and found several hits. This demonstrates the high throughput capabilities of a plate-based screening system, as it returns a single intensity value for each well and is easily scalable. Plate based screening protocols are best suited for small molecule screens consisting of thousands of compounds. However, secondary screens are required to understand the effects of these drugs on T cell function, and elucidate the compound's mechanism of action.

The mid-tier high throughput T cell screening method is imaging based screens. These screens can be performed *in vitro* using a 2 or 3-dimensional system. In the case of reporter based imaging assays using one assay read-out, these assays do not need to be endpoint, and can be measured over a period of time. However, imaging screens typically

provide more than one assay read-out, using reporter systems similar to plate-based assays, or fluorescent cell stains. These methods are slower and lower throughput than plate-based screens, as an automated microscope is required to capture an image of each well on each plate. Automated fluorescent microscopes are commonly used for these screens and can capture a whole well at 2x magnification, to avoid stitching together multiple images (Eggert, 2006). The benefit to imaging based screens is the higher detail of information, and can inform on the shape and size of the 2 or 3-dimensional culture, and one or more fluorescent read-outs providing information on promoter activity, cell proliferation, viability, or cell death. To et al. (2021) conducted a 3-dimensional co-culture screen composed of tumour spheroids treated with T cells in the presence of small molecules. The activity of the top compound was discovered to be dependent on the oxygenation sate of the tumour microenvironment (To, 2021). A co-cultured 3-dimensional system was crucial to discovering a novel mechanism of action specific to hypoxic environments. Imaging based assays are best suited for the screening of a mid-sized library of small molecules, as they are more labour intensive depending on the number of parameters measured and wash steps required for each cell stain.

The last and most complex T cell screening protocol is cytometry-based assays. These assays include mass cytometry- and flow cytometry-based protocols. These are similar conceptually, where mass cytometry labels cell markers with antibodies bound to heavy metal ion tags, and flow cytometry uses antibodies bound to fluorophores. Both of these screening methods allow for a high detail of information and a large number of parameters. However, these cytometry-based staining protocols are highly complex, and

require multiple washes and fixing of cells. In T cell screening protocols, flow cytometry is more commonly used. Flow cytometry is a powerful tool, measuring shape and granularity of the cell, and the excitation of fluorophores by multiple lasers. As a T cell screen, flow cytometry permits the measure of multiple parameters in either an isolated or a co-cultured assay, where tumour cells can be labelled and gated out of the analysis (Edwards, 2015). With appropriate parameters chosen for analysis, a flow cytometry screen can deliver detailed information on T cell anti-tumour function, such as cytokine production, proliferation, and T cell and tumour viability. Santos et al. (2020) developed a flow cytometry based protocol monitoring cytotoxicity by measuring tumour viability via a CellTrace tracker dye (CFSE) and a dead cell stain (propidium iodide). This study presents a viable screening method for small libraries, or secondary screens with fewer compounds. Using CFSE and propidium iodide, they compared the change in ratio of T cells to tumour cells as a result of small molecule intervention and reported on tumour growth, death, and T cell persistence (Santos, 2020). Chen et al. (2018) developed a small molecule screening strategy for compounds that boost TCR signaling in mouse T cells. They investigated early (CD69) and late (CD25) markers of T cell activation by flow cytometry, following TCR activation in the presence of a small molecules derived from a kinase inhibitor library. To make this strategy high throughput, they conducted a viability pre-screen, where compounds that did not result in cell death at low concentrations were carried forward. This represents a viable option for flow cytometry screens, to pre-screen all compounds by measuring viability and rule out toxic compounds before engaging in a more complex screen. Marro et al. (2019) bypassed the complexity of antibody staining all

together in their flow cytometry based screen with mouse T cells. Similar to the Ouyang et al. (2021) plate-based screen, they engineered a florescent reporter, yellow fluorescent protein, downstream of the IFN-γ cytokine promoter to measure T cell anti-tumour activity. The use of a single fluorescent marker, measured by flow cytometry, simplified their screening process significantly and allowed for a higher throughput approach. However, an important limitation of both the Marro et al. (2019) and Chen et al. (2018) screen was the model used, as mouse T cell biology is known to differ from that of human T cells. Small molecules that resulted in desirable T cell activity in these screens may not reiterate the same mechanism of action seen in human T cells (Chen, 2018). In the case of large compound libraries, cytometry based screens may not be amenable for high throughput. Nonetheless, they can provide more information on T cell function than the other two screening approaches.

1.6.2 In silico screening through Connectivity Mapping

As alternative to physical screening, large-scale databases containing drug perturbation transcriptional profiles, such as the Connectivity Map (CMap) database, can be queried as a tool for drug discovery (Musa, 2018). Comparisons between the desired transcriptional profile associated with a condition of interest (eg. costimulated T cells) and established transcriptional profiles of cells treated with known drugs, enables the identification of drugs that may induce specific transcriptional changes associated with the condition of interest. The CMap approach can be used to predict the biochemical interactions of small molecules and discover drugs that target pathways related to disease, by using a collection of genomic and chemical information from thousands of drugs in the

CMap database (Musa, 2018). The phenotype of a disease or condition is described by a gene expression signature (a set of differentially expressed genes), and is used to query the collection of drug signatures from microarray experiments across several cell lines and drug concentrations. Build 02 is the most recent drug database (not including the most recent Library of Integrated Network-based Cellular Signatures (LINCS) database) offered by the Broad Institute containing 6100 instances of treatment-control pairs, with 1309 drugs, at 156 concentrations, 2 time points, and 5 cell lines (Musa, 2018; Subramanian, 2017). The desired gene signature is compared to the reference database of drug signatures to produce resulting positive (+1) or negative (-1) 'connectivity scores', determined by shared upregulated or downregulated genes. A positive connectivity score describes the degree of similarity between the gene expression and drug signatures, from 0 to +1. On the other hand, a negative connectivity score (from -1 to 0) describes the inverse similarity (Musa, 2018). The CMap approach is commonly used as a method to screen chemical compounds by matching gene signatures, described in the CMap database, to that of a desired profile. Following this computational approach to drug screening, compounds displaying a high connectivity score can be investigated further.

2. RATIONALE

TAC receptors were designed to deliver canonical signals through native TCR signaling. Previous data in our lab has demonstrated that TAC T cell proliferation can be enhanced by CD2-mediated costimulation and that survival may be enhanced by CD28-mediated costimulation. CD28 and CD2 costimulation have been shown to increase the number of dividing TAC T cells following antigen stimulation in figure 4 (red indicator), where the addition of CD86 and LFA-3 costimulatory ligands are seen to have a combinatorial effect.

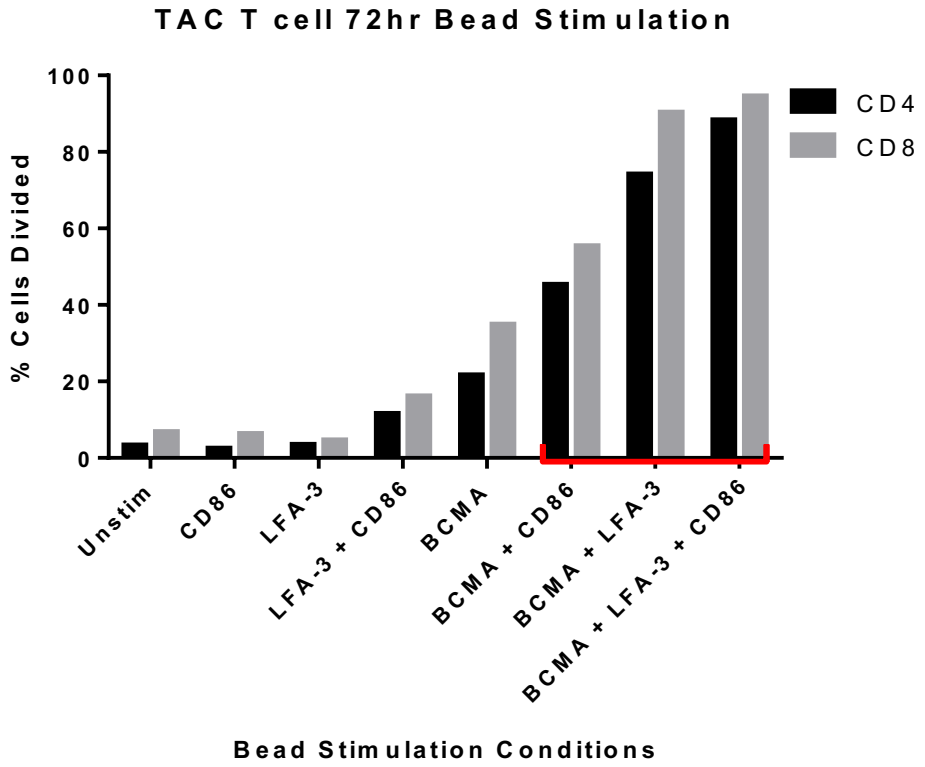

Figure 4: TAC T cell proliferation following 72hr stimulation with protein-coated beads. BCMA-specific TAC T cells stained with celltrace violet dye prior to stimulation. Cells were stimulated at a 1:1 ratio with beads coated with BCMA-Fc (31ng) and costimulatory (LFA-3, CD86) ligands. Quantification of MFI dye dilution and CD4/CD8

expression was measured after 72hours by flow cytometry. Red lines indicate antigen + costimulation conditions. (n=1) (unpublished data from Duane Moogk, Bramson lab).

Artificial costimulation in the form of small molecule drugs may boost the functionality of TAC T cells. Such agents could enable transient costimulation without the potential drawbacks of the CAR design, leading to non-canonical costimulatory signaling and excessive activation of the T cell. The purpose of my project is to find small molecule drugs that trigger signals downstream of costimulatory pathways, resulting in enhanced T cell proliferation and survival.

2.1 Hypothesis

We **hypothesize** that small molecules can be developed to activate costimulation in TAC T cells, to be used as a strategy to enhance T cell proliferation and survival for T cell therapies. The **significance** of this project is to yield novel insight into the chemical space that modulates costimulation, and set the stage for the development of costimulatory small molecules for T cell therapy.

2.2 Aims

2.2.1 Identifying small molecule targets of costimulation through RNAseq

We will be generating RNAseq data from T cells engineered with lentivirus encoding a BCMA-specific TAC receptor, stimulated with antigen-coated polystyrene beads in the presence or absence of LFA-3 and CD86. In addition to an unstimulated population, bead stimulation conditions will include antigen, and antigen + LFA-3/CD86 stimulated TAC T cells. RNA from cells stimulated with beads for 4 and 72hours will be sent for next generation Illumina sequencing at the Farncombe Metagenomics Facility at

McMaster University. Significant changes in RNA transcript levels will be compared across all samples in three biological replicates, and be used to derive a list of pathways involved in TAC T cell costimulation by LFA-3 and CD86 ligands. Small molecule drugs that are associated with comparable transcriptional changes as a result of costimulation will be identified through connectivity mapping, provided by the Broad institute (Subramanian, 2017). Our approach is designed to reveal potential drugs based on their known biological activity (Subramanian, 2017), and serve as a platform to pursue further testing of these small molecules for the enhancement of TAC T cell proliferation.

2.2.2 High throughput screening of biologically active compounds

Our second project aim is to screen a library of ~4000 biologically active compounds from McMaster's Center for Microbial Chemical Biology (CMCB) and characterize compounds that enhance T cell proliferation. Human T cells will be manufactured from healthy donor peripheral blood mononuclear cells (PBMCs) and transduced using an in-house retrovirus encoded with a T2A dual expressing system containing a chimeric TAC receptor and a reporter expressing firefly luciferase. Luciferase luminescence will be used an indirect measure of live cell number, where drug effects are evaluated against the fold differences in proliferation defined by positive and negative controls. These cells are known to proliferate sub-optimally in the presence of antigen alone, and are capable of expanding robustly in the presence of additional stimulatory signals. Screening protocols will be set-up within our screening facility at McMaster University, where we will screen the biologically active compound library with the use of high throughput screening (HTS) robotics.

2.2.3 Characterization of T cell costimulatory compounds

The hits from the connectivity map and high throughput screen will be tested for their effects on TAC T cells using standard functional assays to examine the drug's effect on TAC T cell proliferation, and survival.

3. RESULTS

3.1 TAC T cells activated in presence of costimulation

3.1.1 Costimulation of $CD4^+$ and $CD8^+$ sorted T cells

We performed stimulation experiments on unsorted T cells, $CD4^+$, and $CD8^+$ sorted T cells to investigate differences between T cell sub-types that may result in RNA transcription differences. Based on the functional differences we see between $CD4^+$ and $CD8^+$ T cells, CD4 and CD8 costimulation pathways may differ on a transcriptional level as detected by RNAseq. As a result, drugs elucidated from our connectivity map may be specific to $CD4^+$ or $CD8^+$ costimulation events, as these pathways may differ. In our analysis, we aimed to first identify drugs that are common to both T cell subtypes. To produce $CD4^+$ and $CD8^+$ sorted populations, PBMCs were positively selected for by CD4 or CD8 receptor and engineered with a lentivirus expressing a TAC receptor. For these studies, we opted to use a highly characterized in-house TAC receptor specific for BCMA, a target for multiple myeloma. $CD4^+$ and $CD8^+$ engineered T cell subtypes were cultured in isolation for 14-days. In parallel, we engineered whole PBMC with the same lentivirus to determine whether culturing $CD4^+$ and $CD8^+$ T cells separately influences their performance. For all cultures (sorted and unsorted), BCMA-specific TAC T cells were selected on day 7 based on expression of an NGFR transduction marker, to ensure we were using a highly-enriched population of TAC-engineered T cells. To assess the impact of costimulation on TAC T cells, we stimulated cells with BCMA antigen coated polystyrene beads with/without the costimulatory ligands CD86 and LFA-3. Sorted and unsorted cultures were stimulated with antigen-coated polystyrene beads on day 14, and monitored

over 72 hours to distinguish differences between sorted and unsorted TAC T cell populations. TAC T cells were stained with cell trace violet (CTV) dye prior to stimulation. CTV dilution provides a measure of the number of T cell divisions a cell undergoes post-stimulation, as each cell division dilutes the MFI of the CTV signal in half. The reported proliferation index of each stimulation condition was calculated based on the division index and % of cells divided (figure 5A). The total number of TAC T cells in each condition was calculated based on the ratio of counting beads to cells, measured by flow cytometry (figure 5B). Both the reported proliferation index and the total number of TAC T cells increased in the costimulation conditions. We see that costimulation enhanced the proliferation of both $CD4^+$ and $CD8^+$ T cells but the effect was greatest on TAC T cells generated from sorted populations (figure 5A, B). $CD4^+$ TAC T cells produced from sorted $CD4^+$ PBMCs displayed the greatest proliferation index.

As culturing $CD4^+$ and $CD8^+$ T cells in isolation results in enhanced proliferation compared to culturing the two cell types together, the RNAseq experiments were performed with TAC T cells generated from sorted $CD8^+$ and $CD4^+$ T cells.

A.

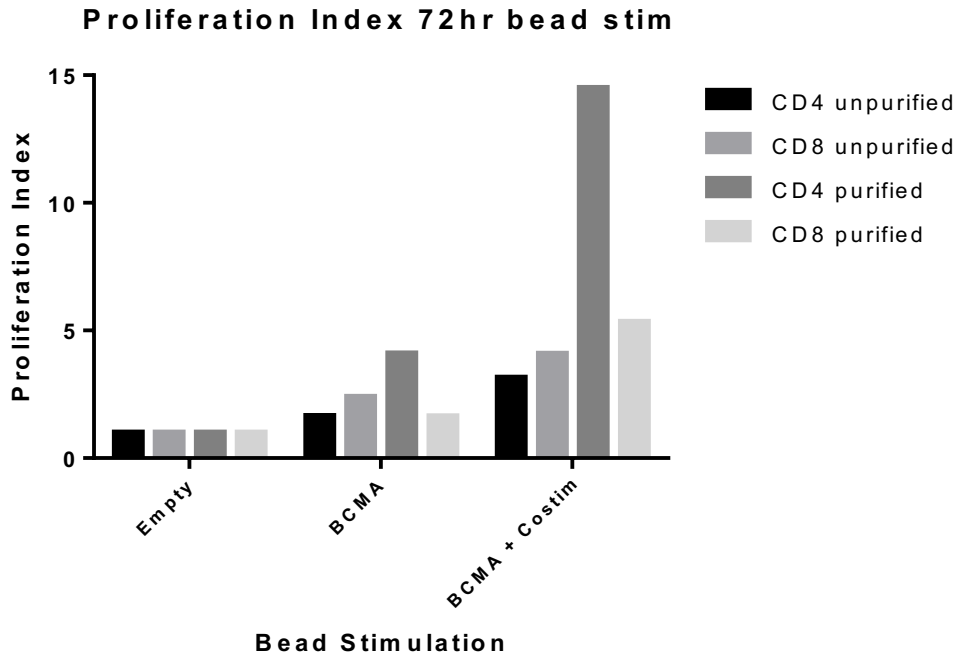

B.

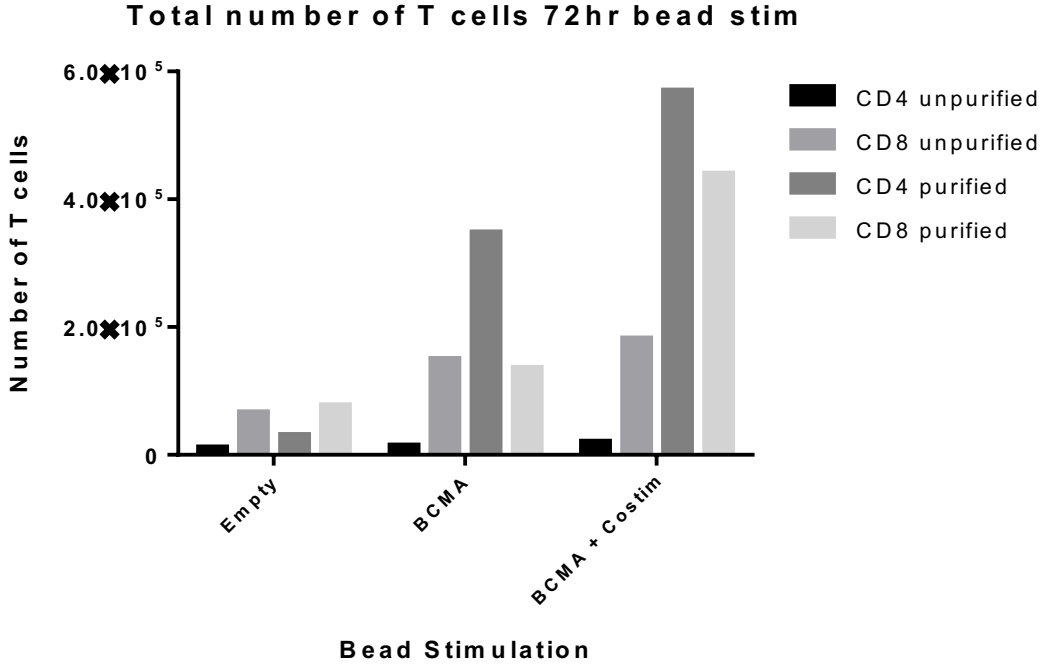

Figure 5: Proliferative capacity of TAC T cells stimulated for 72hours. T cells stimulated with 1:1 effector: target ratio of uncoated (empty), BCMA-coated, or BCMA+CD86+LFA3-coated beads in unsorted, $CD4^+$ sorted, and $CD8^+$ sorted

populations. MFI of CTV dye was captured by flow cytometry and analyzed on FCS Express software; demonstrated quantitatively as **A**) proliferation index (n=1), and **B**) the total number of TAC T cells in each well after 72hr stimulation, measured using the ratio of cells to counting beads (n=1).

3.1.2 RNA collection of costimulated TAC T cells

To generate transcriptional profiles of costimulated TAC T cells to be used for connectivity mapping, we generated TAC T cell products from 3 different donors to be stimulated with beads, as described in Section 3.1.1. Sorted $CD4^+$ and $CD8^+$ TAC T cells populations from each donor were stimulated on day 14 with antigen-coated beads with/ without CD86 and LFA-3 costimulation. At 4 and 72 hours post-stimulation, cells were collected, washed, and pelleted for RNA purification. We collected RNA at 4 hours as an early timepoint to capture changes in RNA levels upstream of major transcription factors that have been described to play a role in T cell proliferation. This early timepoint was chosen based on previous literature demonstrating that AP-1 transcription activity peaks at 8 hours, and NF-κB expression peaks at 24 hours-post activation (Jutz, 2016). At 72 hours-post T cell activation, AP-1 and NF-κB expression levels decline, with NFAT expression peaking at 72 hours (Jutz, 2016). With this in mind, we chose an early and a late post-activation timepoint to investigate the RNA transcriptional differences between stimulation conditions. In parallel with the RNA collections, we also performed a proliferation assay with T cells from each of the donors to confirm that the stimulatory conditions were performing as expected. Similar to the results shown in Figure 5, costimulation increased T cell proliferation with an effect that was more pronounced in $CD4^+$ TAC T cells (figure 6A) in comparison to $CD8^+$ TAC T cell (figure 6B).

A.

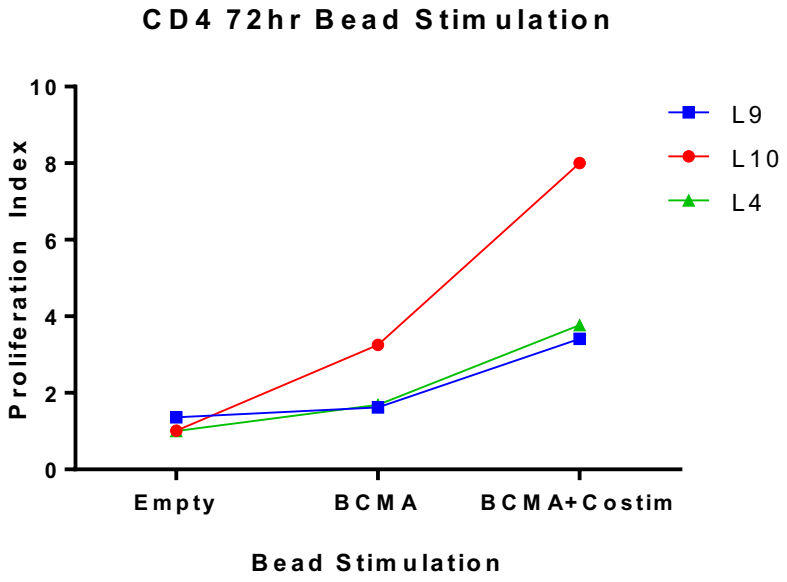

B.

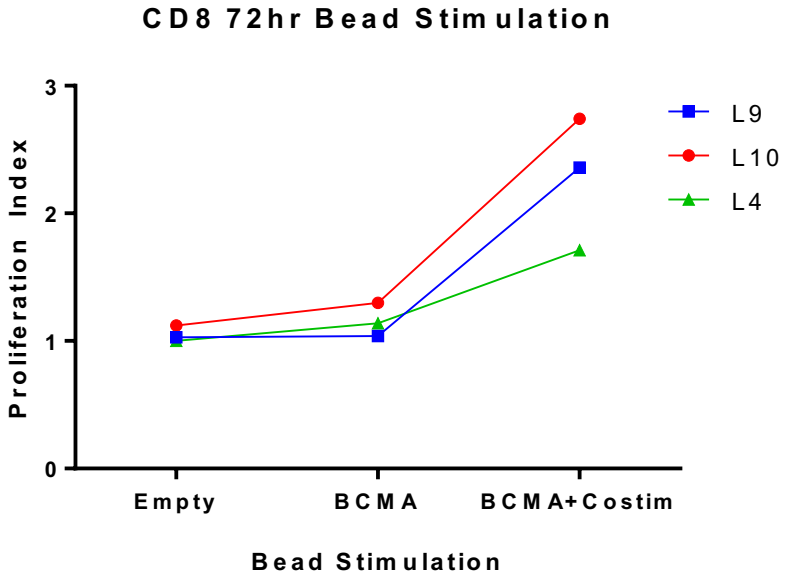

Figure 6: Proliferation Index of sorted CD4 and CD8 TAC T cells stimulated for 72hours. Bead stimulations were performed for 72 hours at a 1:1 effector: target ratio with uncoated, BCMA-coated, or BCMA+CD86+LFA3-coated beads in **A)** $CD4^+$, and **B)** $CD8^+$ sorted populations, across 3 biological replicates (n=3). Proliferation index was derived from the MFI dilution of CTV dye, captured by flow cytometry and analyzed on FCS Express software.

3.2 RNAseq computational analysis

3.2.1 RNAseq results

RNAseq results from the HiSeq run were analyzed by Anna Dvorkin (McMaster University). The principal component analysis (PCA) plots in figure 7 illustrate the sample distribution from bulk RNA. Our results displayed clustering of samples by timepoint and stimulation conditions. These samples clustered according to bead stimulation, similar to the results observed in the validation experiments in section 3.1.2 (figure 6). These effects were more pronounced in $CD4^+$ samples. There is a slight donor effect observed, as the samples do not overlap completely. However, the direction of change for each donor is similar across both timepoint and stimulation conditions. Further analysis will investigate meaningful differences between RNA transcripts, and will be used to perform a connectivity map to identify drugs which result in similar biological changes.

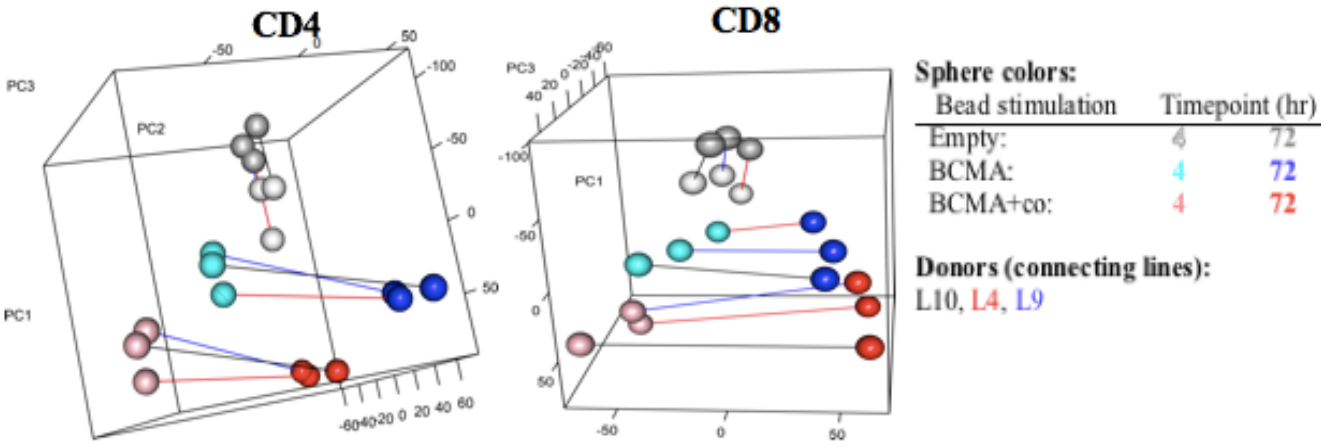

Figure 7: PCA plot displaying sample distribution from bulk RNAseq data. Data obtained from RNA samples as described in section 3.1.2. The coloured spheres represent the three empty (grey), BCMA (blue), BCMA+costim (red) bead stimulation conditions across 4hr (light) and 72hr (dark colour) timepoints. The coloured lines represent the three different donors, L10 (black), L4 (red), L9 (blue).

3.2.2 Differentially expressed genes and gene ontology pathway analysis

We investigated transcriptional differences specific to our antigen + costimulation condition by investigating differentially expressed genes and performing pathway analysis using the biological network gene ontology (BiNGO) analysis tool. To identify transcription changes associated with costimulation, we performed the analysis comparing our antigen + costimulation condition minus antigen stimulation alone. $CD4^+$ TAC T cell samples exhibited the greatest transcriptional changes at both 4 and 72 hour timepoints, representative of low p-values in figure 8A and 8C. The $CD8^+$ samples displayed few significantly differentially expressed genes, with p-values much larger than the $CD4^+$ comparison. The top upregulated biological processes for $CD8^+$ TAC T cells at 4 hours was similar to CD4s, with the main category being ribosomal metabolic processes. At 72 hours, cell cycle regulation was the highest upregulated biological process for both subsets. The top differentially expressed genes specific to the CD86 and LFA-3 costimulation condition for $CD4^+$ TAC T cells are annotated in red in figure 8A/C for both timepoints. The corresponding gene ontology pathway analysis for biological processes with adjusted p-values higher than $1x10^{-8}$ for the costimulation condition are illustrated in figure 8B/D. Differentially expressed genes which fall under individual biological processes contribute to their p-value and significance. In the $CD4^+$ 4 hour samples, ribosomal RNA processing and regulation of immune processes, such as T cell activation, was the greatest upregulated biological process (figure 8B). These suggest that early (4 hour) transcriptional changes as a result of costimulation occur on a ribosomal level, and are specific to T cell activation processes. In the $CD4^+$ 72 hour samples, gene transcription that was upregulated the most

were associated with metabolic, biosynthetic and catabolic processes. This suggests that late (72 hour) transcriptional changes as a result of costimulation are primarily metabolic modifications (figure 8D).

A.

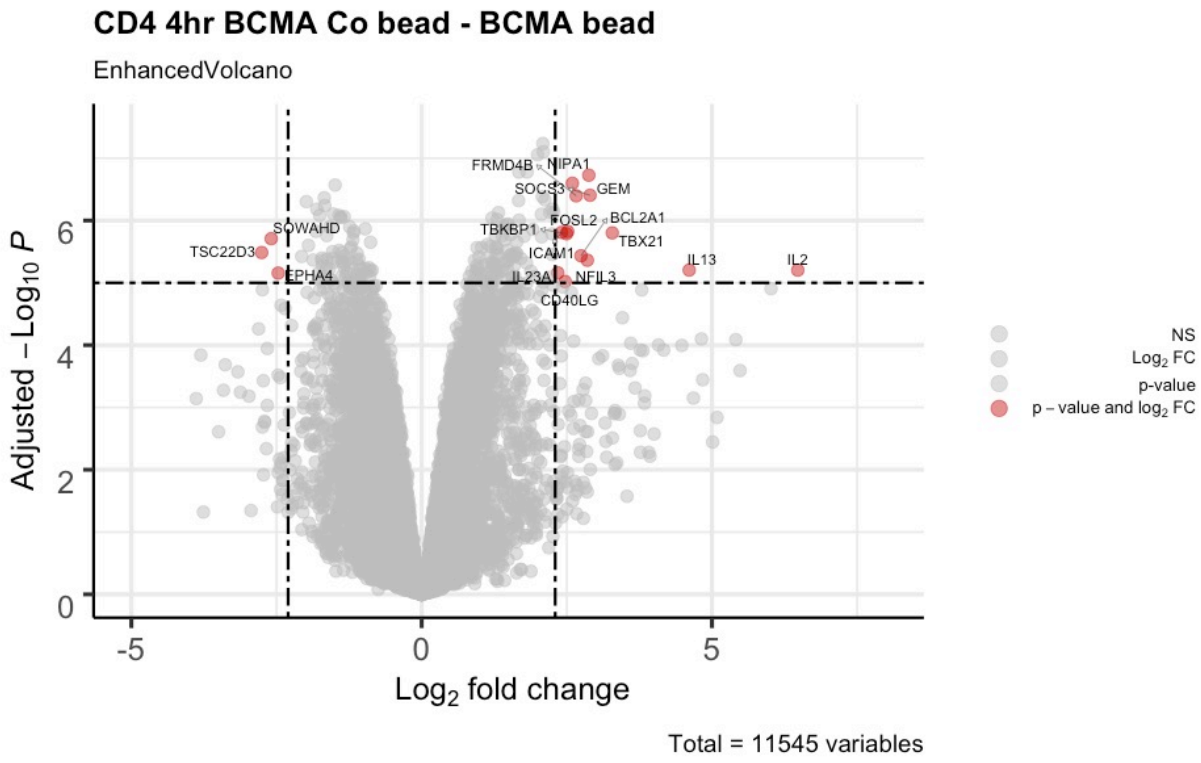

B.

Upregulated at 4hrs	GO biological process	Adj. p-value
rRNA processing	ribosome biogenesis	5.17E-20
	rRNA metabolic process	4.54E-15
	rRNA processing	1.11E-14
	ncRNA processing	7.93E-13
	ncRNA metabolic process	2.95E-12
Immune processes	ribonucleoprotein complex biogenesis	1.74E-15
	regulation of lymphocyte activation	1.80E-08
	regulation of cell activation	5.51E-08
	regulation of leukocyte activation	5.51E-08
	regulation of cell proliferation	6.06E-08
Response to stimulus	immune response	5.51E-08

C.

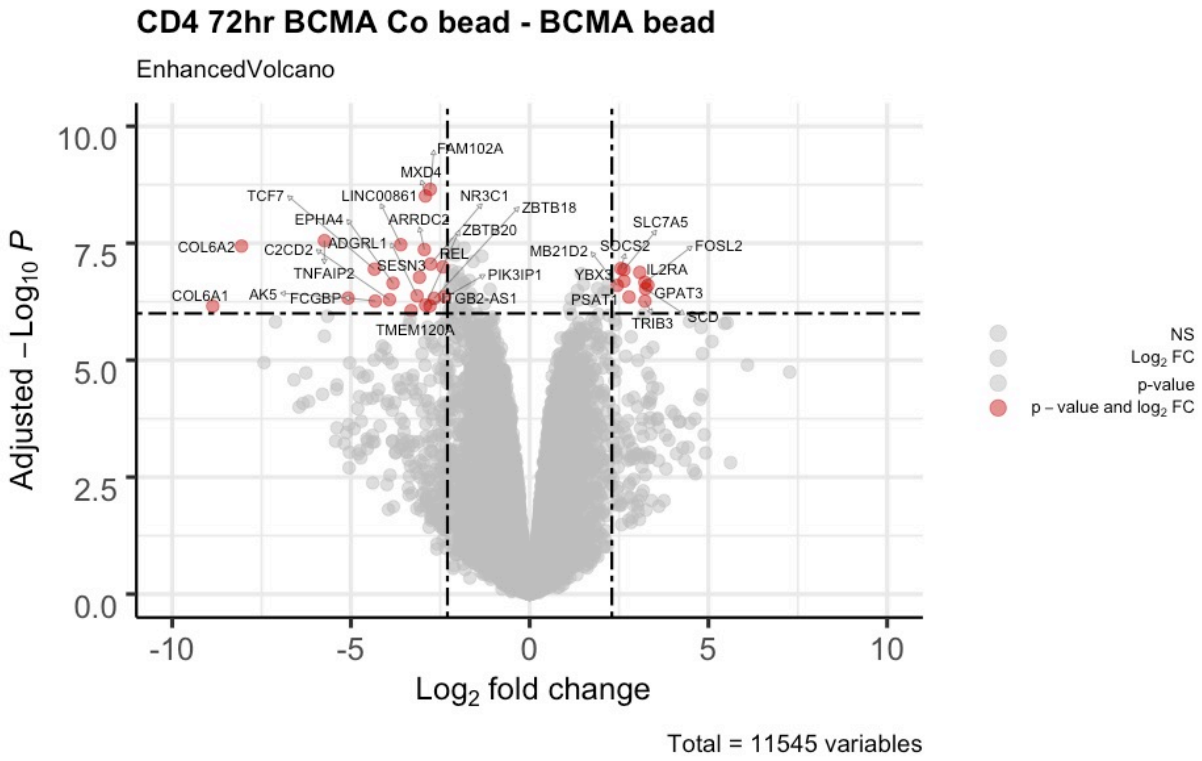

D.

Upregulated at 72hrs	GO biological process	Adj. p-value
Metabolic, biosynthetic, catabolic processes	small molecule metabolic process	1.99E-22
	metabolic process	1.11E-16
	primary metabolic process	1.11E-16
	biosynthetic process	1.12E-15
	cellular biosynthetic process	4.75E-14
	cellular metabolic process	4.75E-14
	cellular ketone metabolic process	5.30E-12
	organic acid metabolic process	2.39E-11
	carboxylic acid metabolic process	3.48E-11
	oxoacid metabolic process	3.48E-11
	small molecule biosynthetic process	1.22E-10
	alcohol metabolic process	1.52E-10
	nitrogen compound metabolic process	7.61E-10
	cellular amino acid and derivative metal	1.64E-08
	cellular nitrogen compound metabolic p	1.65E-08
Immune processes	cellular process	9.48E-12

Figure 8: TAC T cell costimulation-specific transcriptional changes and gene ontology pathway analysis. Differences in gene transcripts from $CD4^+$ TAC T cells stimulated with antigen (BCMA) + costimulation (CD86 and LFA-3) minus cells stimulated with antigen alone. A) and C) volcano plots illustrating differentially expressed genes for costimulated

$CD4^+$ TAC T cells at 4 and 72 hours post stimulation. B) and D) biological network gene ontology pathway analysis for biological processes with p-values less than $1x10^{-8}$ for TAC T cells costimulated for 4 and 72 hours.

3.2.3 Choosing a reference database of known small molecule perturbations

We chose to explore the connectivity map (CMap) database, a publicly available database provided by the Broad Institute, for compounds that may elicit a transcriptional signature similar to costimulation. The Broad Institute offers the build 01, build 02, and the L1000 (clue.io) CMap databases, containing different sets of microarray experiments representing the transcriptional changes across cell lines as a result of drug treatment. These online tools provide the gene signatures of several cell lines treated with small molecule drugs, across several time points (Subramanian, 2017). Each drug signature is representative of the transcriptional changes recorded within a cell population as a result of treatment. To investigate compounds which elicited a gene signature similar to that of our costimulated TAC T cells, we compared our RNAseq results to the build 02 database in a process known as connectivity mapping. The result was a list of small molecule drugs and their corresponding connectivity scores, indicative of their similarity to our costimulated TAC T cell transcriptomes. A positive connectivity score demonstrates similarity between the transcriptional changes induced by costimulation and the compound of interest, with higher scores indicative of a better match. A connectivity score of 1 represents a high positive correlation between two signatures, based on the expression and rank of their top regulated genes. Figure 9 demonstrates the list of small molecule drugs we obtained from our analysis with connectivity scores greater than 0.4. This represents a 40% or higher correlation between the differentially expressed genes of both drug and costimulation samples.

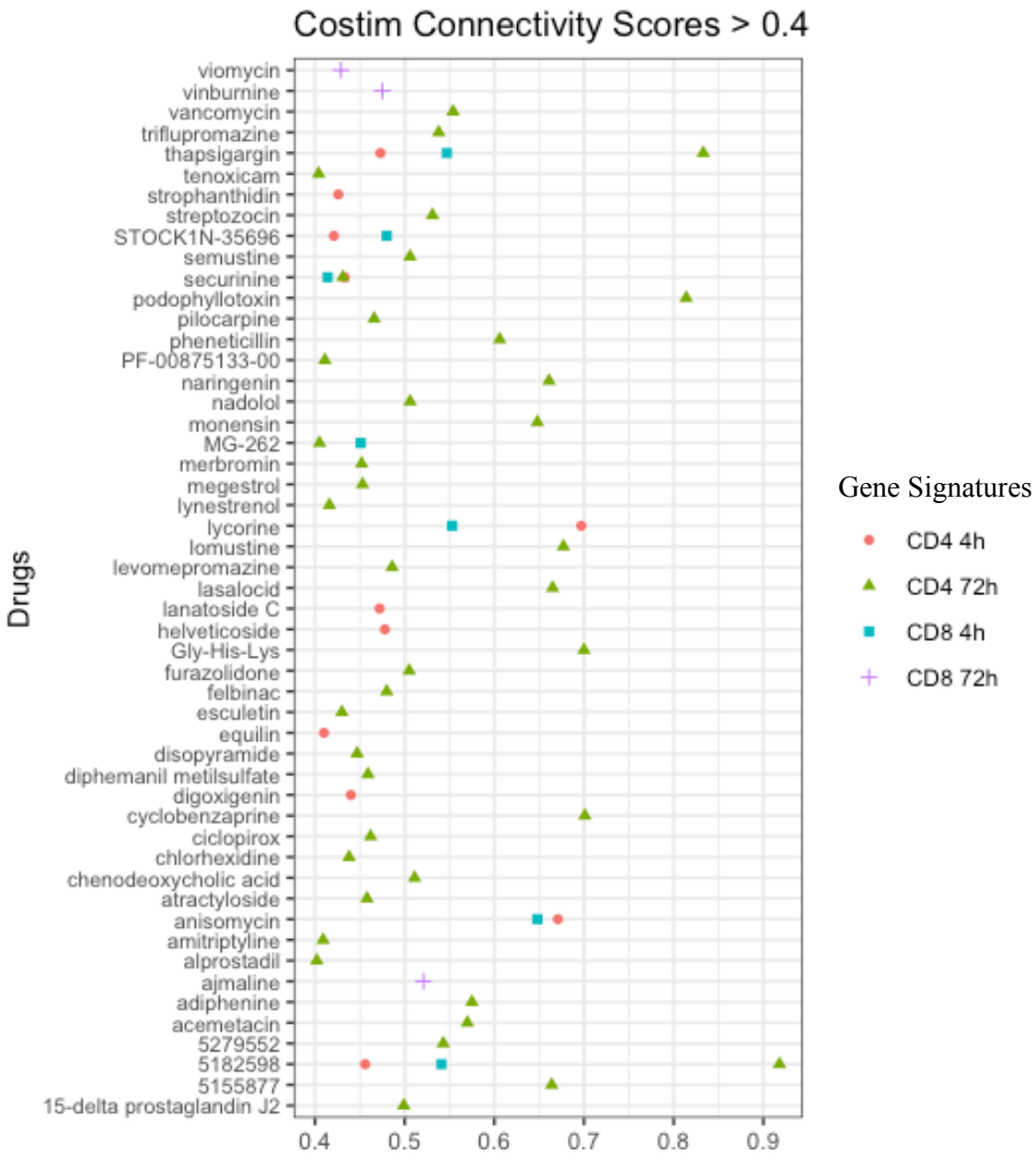

Figure 9: Connectivity map scores higher than 0.4 demonstrate positive similarity to gene signatures from costimulated TAC T cells. RNAseq data obtained from $CD4^+$ and $CD8^+$ TAC T cells stimulated with antigen + costimulation (as described in section 3.1.2) at 4hr and 72hr timepoints. Higher positive connectivity scores for a drug perturbation represents higher similarity to transcriptional differences found as a result of costimulation in each of our four RNAseq samples.

3.3 Characterization of top Connectivity Map compounds

Following the analysis of our connectivity mapping results, we narrowed down our compound list from figure 9 to only include drug perturbations that had two or more positive connectivity scores, with at least one score higher than 0.5. From this short list, we chose four compounds with the highest scores for *in vitro* studies. Figure 10 illustrates the connectivity scores of the four compounds selected: thapsigargin, securinine, podophyllotoxin, and lycorine. The compound '5182598', seen as having the highest connectivity score in figure 9, was not available for purchase and was therefore not evaluated.

All compounds except lycorine demonstrated positive connectivity scores for $CD4^+$ TAC T cell costimulation at 72 hours, and $CD4^+$ and $CD8^+$ costimulation at 4 hours (figure 10). Lycorine demonstrated positive connectivity only for the latter two. None of the compounds demonstrated connectivity for $CD8^+$ costimulation at 72 hours. However, the $CD8^+$ sorted cells did not proliferate well in response to stimulation, as seen in Section 3.1, and only resulted in a few significantly differentially expressed genes. Thapsigargin demonstrated the highest connectivity score at 0.85, followed closely by podophyllotoxin at 0.82, both for the $CD4^+$ costimulation transcriptome at 72 hours.

Thapsigargin is an endoplasmic reticulum calcium inhibitor and tumour promotor, that has been characterized to increase IL-2 production in T cells at low doses (Kim, 2018). Podophyllotoxin is used for the treatment of genital warts, and is a novel anticancer drug that binds tubulin to prevent cell division. At low concentrations, podophyllotoxin was reported to inhibit PD-1, a T cell coinhibitory receptor that suppresses T cell activation, by

destabilizing microtubules and mRNA translation (Franchini, 2019). Lycorine is an anticancer and anti-inflammatory drug that has been characterize to inhibit TNF-α production and NF-κB signaling (Roy, 2018). However, it has no known effect on T cell proliferation. Securinine is a γ-Aminobutyric acid type A ($GABA_A$) receptor agonist, reported to activate human macrophages and act as an innate immune adjuvant (Mendu, 2012). Securinine has not been linked to T cell proliferation.

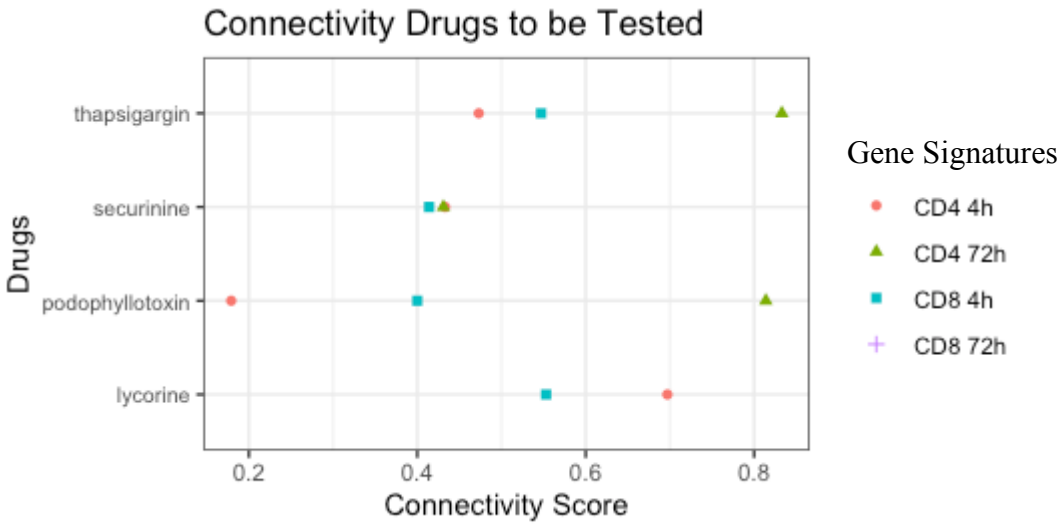

Figure 10: Connectivity scores the top four compounds of interest. Higher positive scores for each compound represent higher similarity to the differentially expressed genes found in the RNAseq data from our four costimulated TAC T cell samples. These four samples, under 'Gene Signatures", include $CD4^+$ and $CD8^+$ TAC T cells at 4 and 72 hour timepoints.

3.3.1 TAC T cell dose-response assays for top connectivity map drugs

To test the toxicity of each compound over a range of doses, we cultured engineered TAC T cells in cytokine supplemented media with each drug for 24 hours. We then counted TAC T cell number and viability in each sample using trypan blue to stain for dead cells. Figure 11 illustrates the change in TAC T cell viability following a 24hr incubation with

each compound over a 5-fold dilution experiment. Control cells treated with the highest concentration of DMSO, the carrier used to solubilize the test compounds (62µM), served as our vehicle control in these experiments. Over the 24-hour period, control DMSO treated cells maintained a similar cell density and viability as the starting population. The dotted lines on each line in figure 11 indicate the concentration of compound used in the build 02 CMap assay, from which the compound's transcriptional signature was derived. Only thapsigargin demonstrated toxicity in our TAC T cells. Following the results of the toxicity assay, we chose a smaller range of doses to test in an *in vitro* functional assay.

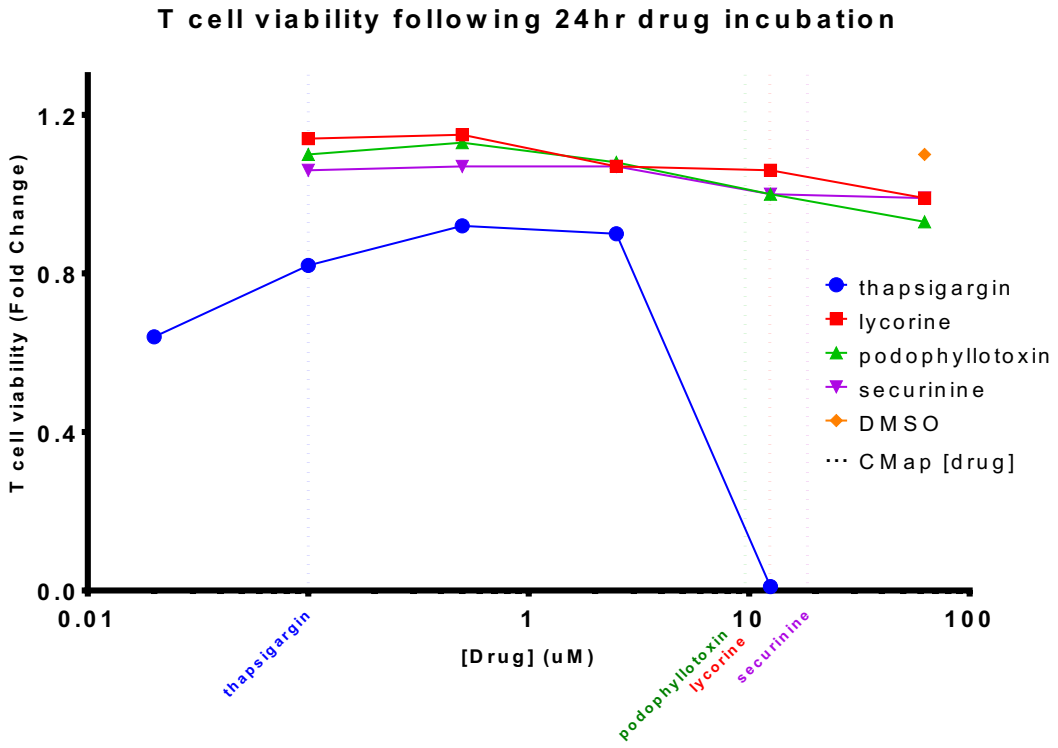

Figure 11: Toxicity of CMap compounds on TAC T cells over 24 hours. TAC T cells were cultured with drug in cytokine supplemented media for 24 hours, and counted using trypan blue to stain for dead cells. Compounds were tested in 5-fold dilutions at a highest dose of 62.5µM, with the exception of thapsigargin, with a highest dose of 12.5µM. DMSO treated cells (62.5µM) served as our vehicle control. Dotted lines indicate the concentration of drug used in the CMap experiments. (1 experiment, data representative of 2 experiments)

3.3.2 TAC T cell functional assays for top connectivity map drugs

Proliferation, in response to antigen stimulation, is a good measure of T cell function, as effector T cells must expand following tumour recognition in order to effectively kill their tumour targets. We chose a CellTrace Violet proliferation assay, as described in Section 3.1, to test the ability of the selected compounds to enhance the proliferation of TAC T cells. For these assays, we chose to use bulk engineered BCMA-specific TAC T cells containing both CD4+ and CD8+ T cells, as the chosen CMap compounds supposedly induced costimulation-like transcriptional changes in both T cell subtypes. TAC T cells were stimulated with antigen-coated beads in the presence of the test compounds or DMSO, and cells were collected and proliferation was assessed after 72 hours.

We tested each compound over a small range of doses to determine an optimal working concentration for further experiments. The optimal working concentration for each compound, determined by the highest proliferation indices after a 72-hour stimulation period, was 0.02μM for thapsigargin, 0.1μM podophyllotoxin, 0.5μM lycorine, and 2.5μM securinine. Figure 12 illustrates the total number of cells and the proliferation indices of TAC T cells re-exposed to the optimal CMap drug dose every 24 hours for a total of 72 hours, where the DMSO treated cells (at the highest dose, 2.5μM) represents the vehicle control. The proliferation and survival of TAC T cells treated with the CMap compounds was assessed by counting beads on the flow cytometer. The total number of TAC T cells at endpoint is illustrated in figure 12A. We saw no benefit to $CD4^+$ nor $CD8^+$ TAC T cell proliferation with any of the CMap drugs above that of the DMSO control with neither

single exposure (data not shown) nor repeat exposure (figure 12B). To compare the proliferation indices of TAC T cells re-exposed to drug every 24 hours to that of costimulated cells, we included a positive control treated with DMSO. Our positive control TAC T cells were stimulated with BCMA and costimulatory ligands (CD86 and LFA-3), termed 'Costim DMSO' in figure 12. Our positive control served as a reference point for previous experiments, as these cells were stimulated under the same conditions as our RNAseq experiment. While the positive connectivity scores infer a positive correlation between the gene signature elicited by costimulation and our four chosen CMap drugs, we did not see any benefits to TAC T cell proliferation in these *in vitro* proliferation assays.

A)

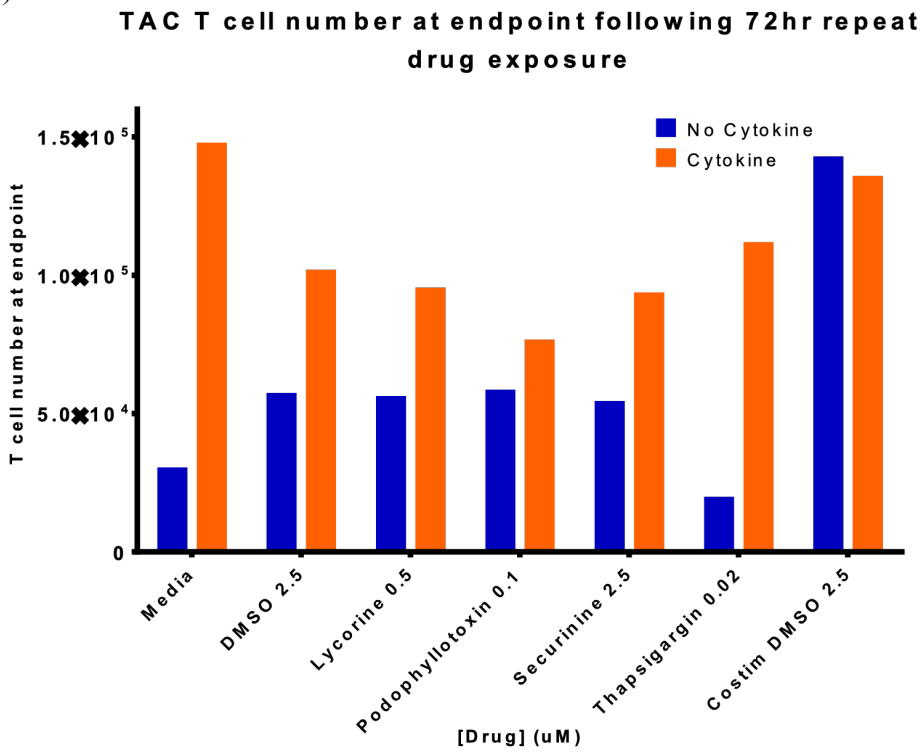

B)

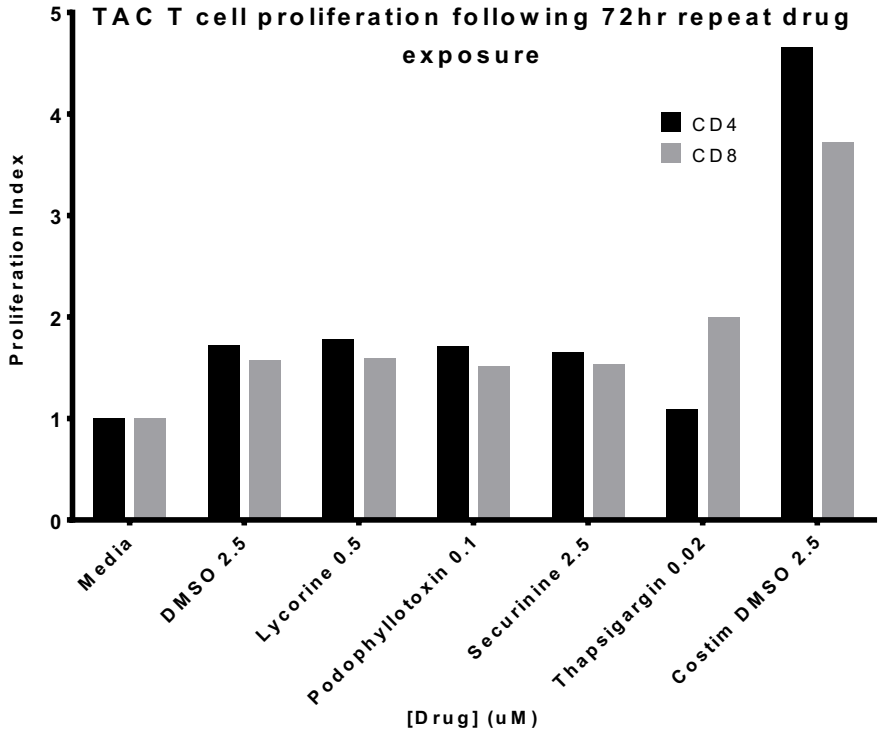

Figure 12: TAC T cells stimulated with antigen and repeat drug exposure over three days. TAC T cells were stained with CellTrace Violet and stimulated with antigen (BCMA)

loaded beads in the presence of drug or DMSO control (2.5μM) in non-supplemented or cytokine (IL-2, IL-7) supplemented media. Cells were washed every 24 hours and re-suspended in fresh media + drug, for a total of three drug exposure cycles. 'Costim DMSO' served as our positive control, where cells were stimulated with antigen (BCMA) and costimulatory ligands (CD86 and LFA-3) and re-exposed to DMSO (2.5μM) every 24 hours. Cells stained with live/dead, NGFR (transduction marker), and CD4/CD8 antibodies after 72 hours, and analyzed using Flow Cytometry. **A)** TAC T cell number at endpoint in cytokine vs. non-cytokine media. Cell number determined using counting beads. **B)** $CD4^+$ and $CD8^+$ proliferation indices of TAC T cells in non-supplemented media.

3.4 Development of a TAC T cell proliferation screen

As an alternate method to the *in silico* connectivity mapping prediction technique, we chose develop a proliferation assay that would be amenable to high throughput screening. We sought to screen the biologically active compounds library of ~4000 molecules, available at McMaster's Center for Microbial Chemical Biology. Two assays were chosen as possible screens: (i) live fluorescent imaging to quantify the number of TAC T cells following drug exposure (ii) TAC T cells engineered with a bioluminescent reporter, to indirectly evaluate TAC T cell number. Both screening methods employed the same stimulation conditions that were used to develop the costimulation transcriptional profiles as described above (polystyrene beads coated with antigen, with CD86 and LFA-3). Ultimately, we were interested in discovering drugs that enhanced T cell proliferation following stimulation with antigen loaded beads.

3.4.1 Live fluorescent imaging method

The live imaging assay comprised of a three-day stimulation period, as described in Section 3.1, as it revealed pronounced differences in TAC T cell proliferation between antigen and costimulation conditions. TAC T cells were then stained with calcein (nuclei stain) to identify the total number of cells in the sample, and Hoechst dye to identify dead

cells. Following the stain and washing process, the cells were imaged on a fluorescent microscope (see Appendix figure 1). We chose this method to both quantitatively and qualitatively distinguish differences between conditions, providing us with a measure of T cell number, viability, and visual characteristics. To evaluate the ability of our assay to accurately measure differences in proliferation, bead stimulations were set-up as described in Section 3.1, comparing TAC T cells stimulated with antigen to those stimulated with antigen + costimulation. TAC T cells were stimulated in a U-bottomed tissue culture plate and then transferred to a flat-bottomed plate for optical imaging after staining. During assay optimization, we found that our T cell media interfered with the catalytic activity of both calcein and hoechst dyes and caused the media to autofluoresce. To minimize autofluorescence, cells were washed prior to staining. Inconsistencies between repeats suggested that cells were being lost as a result of washing and transferring between plates, prior to staining and imaging. Due to these inconsistencies, we were not confident in the accuracy of this assay. To increase the accuracy of the assay and reduce complexity, we repeated these experiments in phenol red-free media, as recommended by a ThermoFisher representative to prevent media auto fluorescence. However, after optimization of cell number and dye concentration, the phenol-red free T cell media still exhibited a low level of auto fluorescence that interfered with spot analysis. Following a mock drug screen using a few in-house drug candidates, we saw large variability between replicates and little difference between drug or stimulation conditions (Appendix figure 2). As these results were not promising, we focused our efforts on developing an alternative high throughput assay.

3.4.2 Bioluminescent reporter system method

As an alternate to direct imaging of TAC T cells using optical microscopy, we elected for an indirect method of quantifying T cell proliferation using a reporter system. Reporter systems are a common high throughput screening method, as these plate-based assays use genetically engineered cells and do not require wash or staining steps. Unlike the optical imaging strategy in section 3.3.1, this no-wash, one-pot assay is better suited to a high throughput screening. TAC T cells were engineered to express firefly luciferase to indirectly measure cell density, where cell number was then evaluated by luciferase-activity. T cells were obtained from healthy donor PBMCs and infected with a bicistronic retrovirus encoding both a HER2-specific TAC receptor and firefly luciferase. Cells were enumerated by adding D-luciferin directly to each well, where luciferase signal intensity was then measured on a plate reader. To reduce batch-effects, I manufactured a large population of HER2-TAC/luciferase-expressing T cells (referred to as TAC-LUC T cells) and cryopreserved multiple aliquots. An aliquot of these cells was then thawed and transduction was quantified by Flow Cytometry based on HER2-Fc surface expression (indicative of TAC-LUC expression), and was reported as 75% transduced (figure 13).

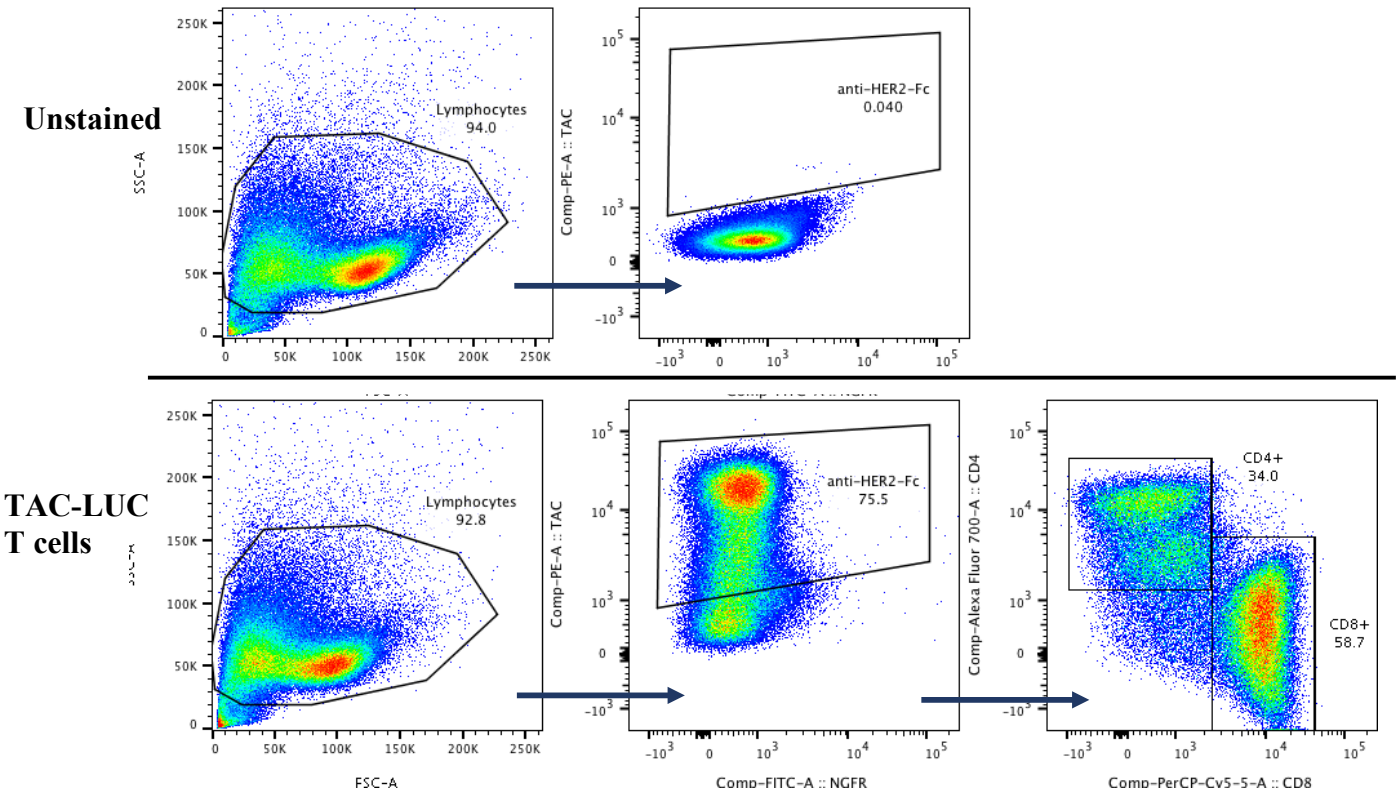

Figure 13: TAC-LUC T cell transduction quantified by anti-HER2-Fc. Surface expression of the HER2-TAC was quantified by flow cytometry, and gated on using an unstained population in FlowJo software. Our gating strategy used was: single cells (not shown) → lymphocytes → TAC → CD4 and CD8.

To validate the accuracy of the bioluminescent reporter system in measuring TAC-LUC T cell number, we plated a known number of cells and performed a dilution series to capture a wide range of cell densities. D-luciferin was added to each well and incubated for ~10 minutes before measuring luminescence. The relationship between TAC-LUC T cell number and luciferase signal intensity in our screen was linear with an R^2 value of 0.9865 (figure 14A). In our initial stimulation experiments, we saw up to a 13-fold increase in cell number in TAC T cells stimulated with antigen + costim coated beads (data not shown). Therefore, we chose a plating density of $5x10^4$ for our optimization experiments to ensure

sufficient dynamic range of the assay. To test if the relationship between signal intensity and TAC-LUC T cell number held true in a multi-day assay, we stimulated cells under different bead conditions for 72 hours and measured luminescence. Cells from each well were then mixed and counted using the Countess by Life Technologies and trypan blue to determine the number of live cells in each well. Similarly, the relationship between signal intensity and live cell number exhibited a high R^2 value of 0.9670 (figure 14B).

A.

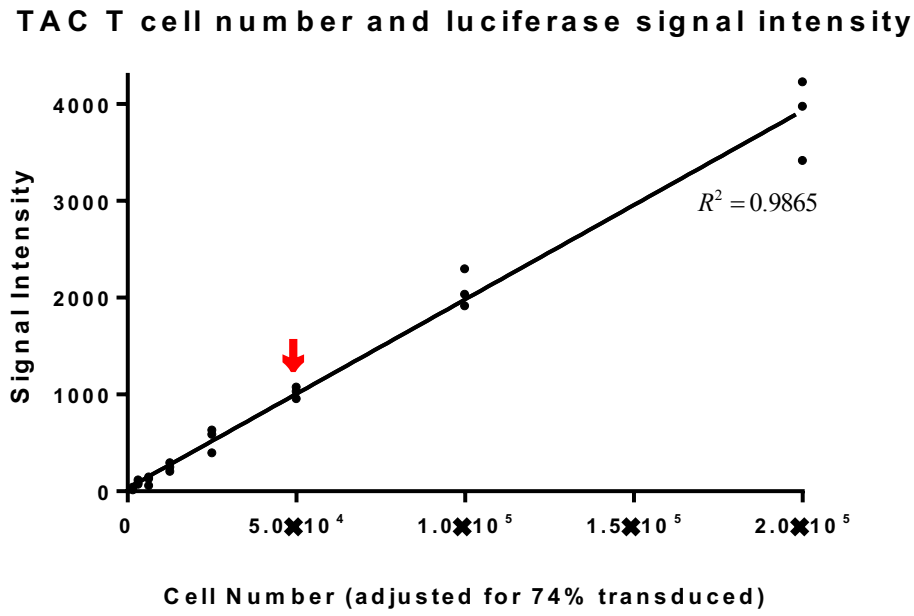

B.

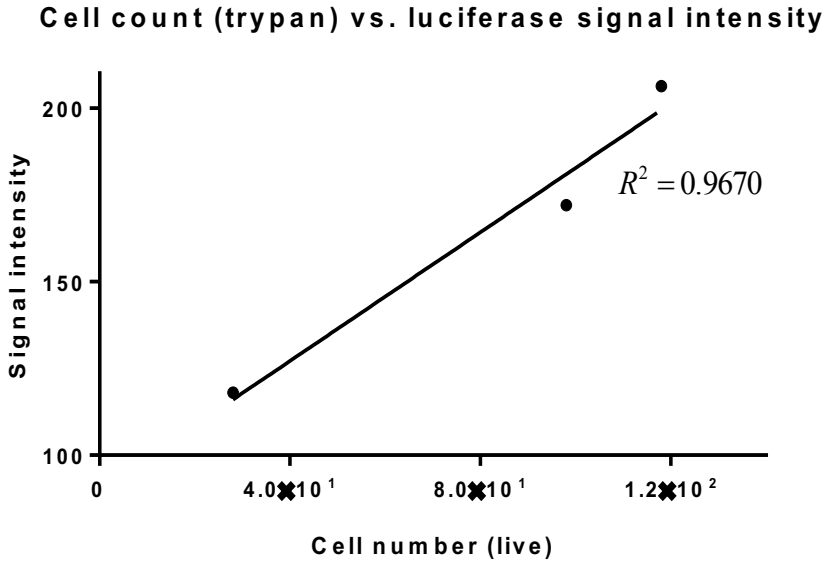

Figure 14: Luciferase signal intensity correlates with cell density of TAC-LUC T cells. Luciferase intensity measured following a 10-minute incubation with D-luciferin. **A)** TAC-LUC T cells were plated at $4x10^5$ per well in triplicate, and diluted two-fold six times over (n=3). **B)** TAC-LUC T cells were stimulated for 72hours with beads. Following luminance measurement on the plate reader, the same wells were counted using Trypan blue (n=1).

The use of bioluminescence as an indirect measure of live cell number demonstrated a strong positive relationship with the number of cells in each well over our 3-day assay. Given that luminescence appeared to be a reliable measure of cell number, we tested a range of effector: target bead ratios to optimize the separation between non-specific antigen (negative control), and antigen + costimulation (positive control) conditions. We performed a 72-hour proliferation assay with TAC-LUC T cells stimulated at four different effector: target ratios, from 0.125 to 1. Similar to our BCMA-specific TAC model in section 3.1, we saw that the addition of costimulatory ligands CD86 and LFA-3 increased the signal from TAC-LUC T cells after 72hours of stimulation (figure 15). This relationship was dependent on the number of beads available for stimulation, where an equal effector: target ratio of 1:1 was seen to correlate with a higher luminance signal.

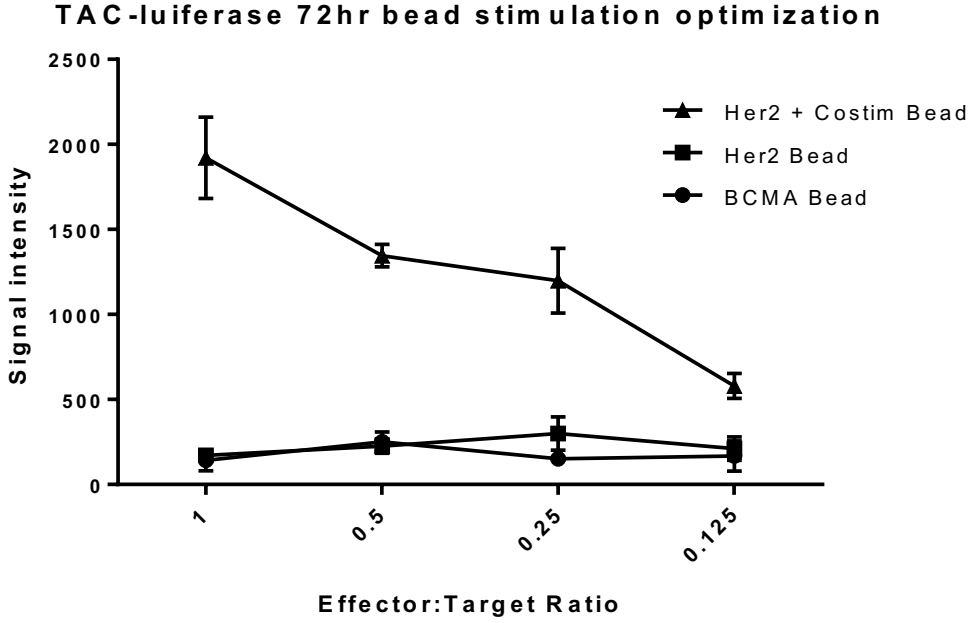

Figure 15: HER2-specific TAC-LUC T cells stimulated with different effector: target ratios for 72hours. Luminance of luciferase demonstrated as signal intensity. TAC-LUC T cells stimulated with protein coated polystyrene beads at a 1:0.125 to 1:1 effector: target

ratios in triplicate, with non-specific antigen (BCMA), HER2, or HER2+CD86+LFA3 coated beads. Error bars represent standard deviation (n=3).

3.5 Optimization of a high throughput screen

We sought to optimize our assay in a 384-well plate format, amenable to screening the whole biologically active compounds library from the CMCB at McMaster. To manage the scale of this library, we chose to use a robotics liquid handler (the Tempest and Multidrop Combi nL) and Echo Acoustic Dispenser to automate the volume of cells, beads, and drugs dispensed across each plate. With the use of these automated dispensers at the CMCB, we are able to plate the whole library (over 4000 compounds) in duplicate, in one day. The screen was performed in 13, 384-well plates, screened in duplicate for a total of 26 plates. To normalize luminescence signal within each plate, we included our previously optimized negative (HER2 bead stim + DMSO) and positive (HER2+ costim + DMSO) controls from Section 3.4 to reduce the effects of variation across plates. To recapitulate our 96-well assay, we chose to stimulate TAC-LUC T cells in the presence of drug for three days, add luciferase reagent, incubate for 40 minutes, and then read luminescence signal on the Neo2 plate reader with stackers. This schematic is visualized in figure 16. The compound library plates were thawed 1 hour before screen set-up and centrifuged to collect the volume at the bottom of each well. The compound volume was transferred from the library plates to our receiver plates by the Echo Acoustic Dispenser. We chose a standard screening concentration of 10μM to capture the effects of each drug on cell growth. We automated our screening method by dispensing 10μM of drug or DMSO in each well, followed by HER2 or HER+costim coated beads, and TAC-LUC T cells.

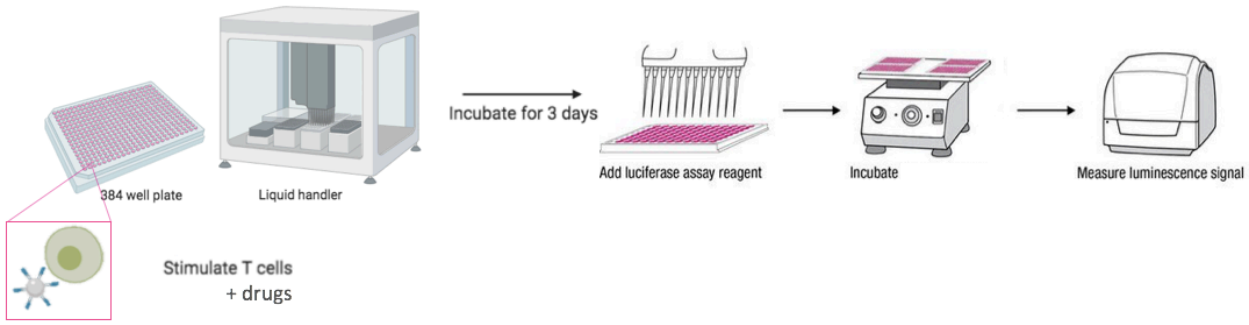

Figure 16: 384-well plate screen schematic. 10µM DMSO and compounds were plated, followed by HER2 or HER2+costim coated beads, then TAC-LUC T cells. Plates were incubated for three days. All plates received luciferase reagent, were incubated for 40 minutes, then signal intensity was read by the plate reader using stackers.

3.5.1 Comparison between flat and round-bottom plates

For 384-well tissue culture treated plates, we investigated two plate options amenable to our screening methods. We assessed flat-bottom plates, with a maximum volume of 50µL, and round-bottom plates, with a maximum volume of 15µL. The best signal resolution was observed at higher cell densities in the flat-bottom plates (figure 17). The 15µL working volume was associated with a larger range of error between replicates (n=3) at higher cell densities in the round-bottom plates. The vertical lines on figure 17 represent a cell density of $1x10^6$ T cells/mL, the optimal cell density for T cell growth. We selected flat-bottom plates for our screen, as we saw signal intensity was more accurately captured at higher cell densities. This is an important factor to consider in a proliferation screen, as we want a more accurate measure of signal intensity at higher cell concentrations due to cell expansion.

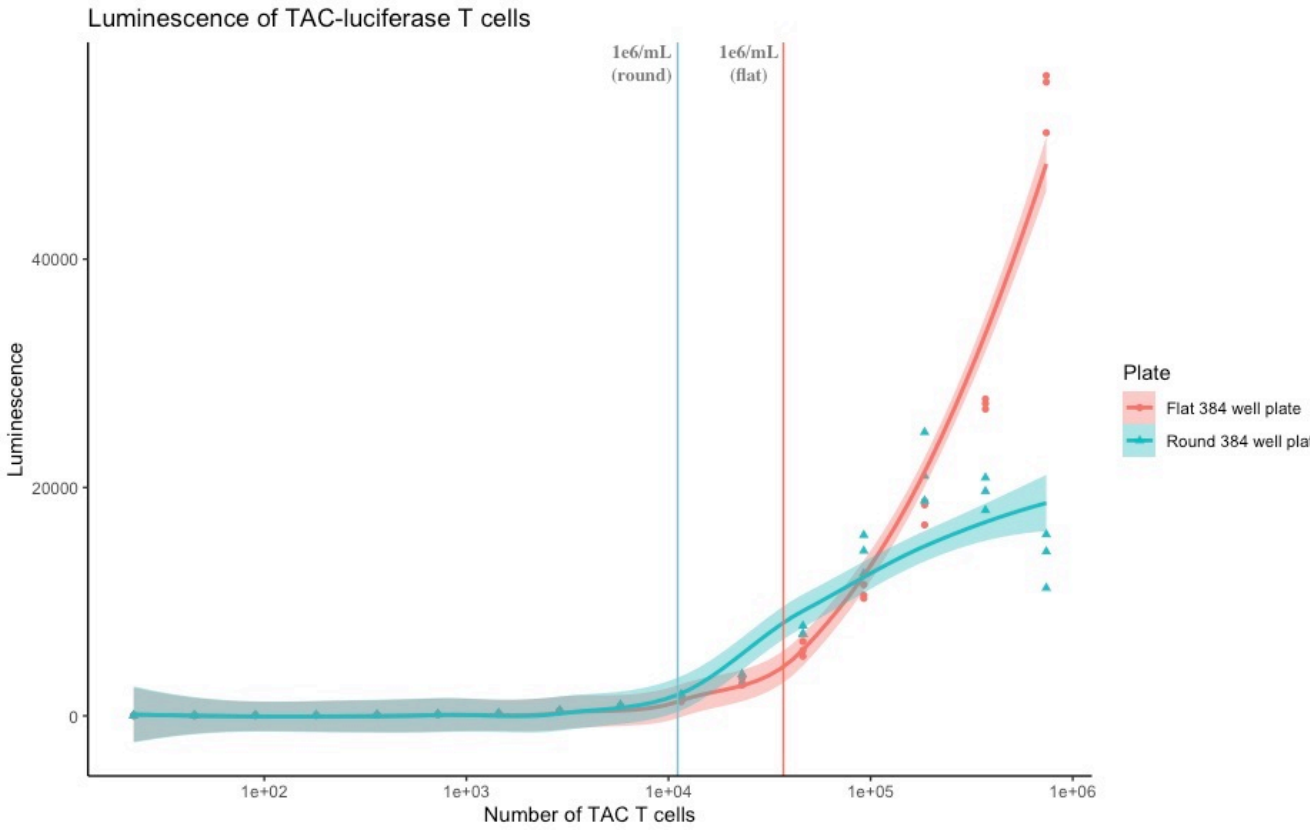

Figure 17: Comparison of TAC-LUC T cell luminescence in flat and round-bottom 384-well plates. TAC-LUC T cells were plated and diluted two-fold down each 384-well plate in triplicate (n=3). Luciferase agent was added to all wells, and signal intensity was read on a plate reader. Vertical lines represent a cell density of $1x10^6$ T cells/mL, an optimal working TAC-LUC T cell density.

3.5.2 Screen cell density optimization

Moving forward with optimizing our screening conditions in the flat-bottom 384-well plates, we next established a TAC-LUC T cell plating density that would be result in clear signal differences between our positive and negative controls. We plated TAC-LUC T cells in a dilution series, and stimulated these cells with antigen (HER2) and antigen + costimulation (CD86 and LFA-3) protein-coated beads at a 1:1 ratio to represent our positive and negative controls. As additional controls, we included beads loaded with non-specific antigen stimulation ('BCMA'), and beads loaded with only CD28/LFA-3

('Costim') (figure 18). We saw the greatest difference between negative and positive controls above the threshold of $3x10^4$ TAC-LUC T cells/well indicated by the red arrow on figure 18. In order to resolve differences at higher cell densities, we chose a plating density of $3x10^4$ TAC-LUC T cells/well to resolve luciferase signal intensity well above that of the positive control, should any compounds significantly increase cell growth. This consisted of $3x10^4$ protein-coated beads and $3x10^4$ TAC-LUC T cells/well, to achieve a 1:1 ratio as explained in Section 3.4.

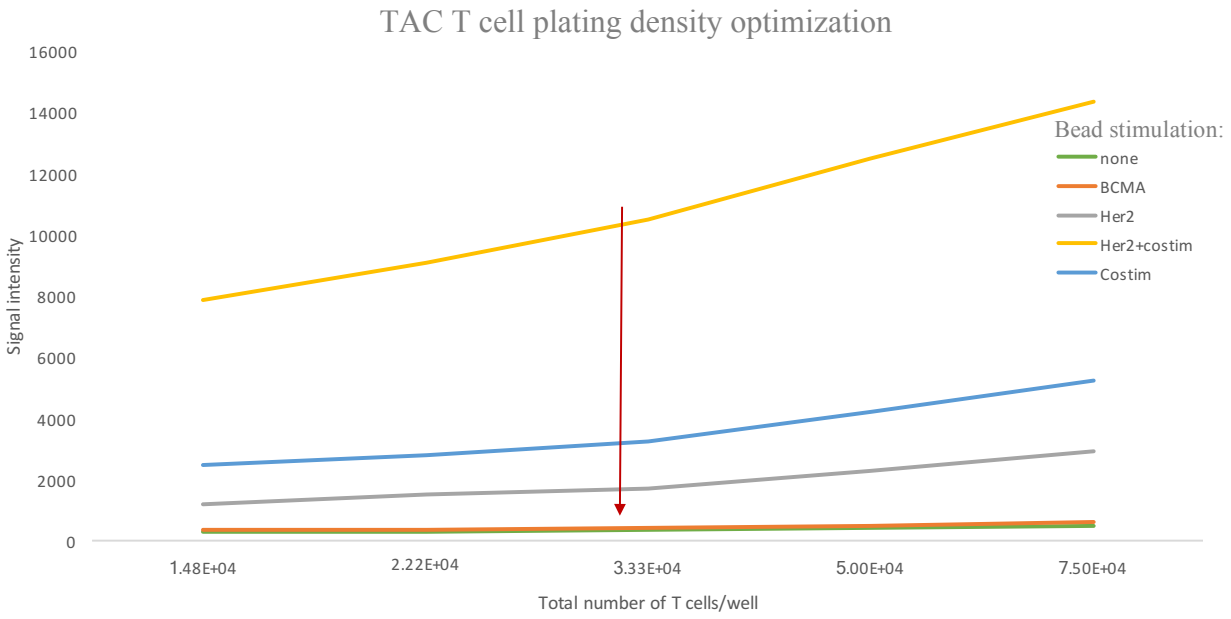

Figure 18: TAC T cell plating density optimization. HER2-specific TAC-LUC T cells plated at a series of cell densities and stimulated with protein-coated beads for three days. Indicative of cell number, luminescence of TAC-LUC T cells was measured following the addition of luciferase reagent and read on a plate reader. HER2 + costim bead stimulation was used as our positive control, and HER2 bead stimulation as our negative control. The unstimulated and non-specific (BCMA) bead stimulation conditions represent our non-proliferating controls.

With each plate containing its own set of both positive and negative controls, we sought to ensure that these conditions were repeatable and had low variation between

replicates. We repeated our optimized three-day proliferation screen, using a plating density of $3x10^4$ TAC-LUC T cells/well in the flat-bottom plates with a high number of replicates. Figure 19 illustrates the 10-fold difference we see between our negative and positive controls. This provided confidence that we would be able to resolve differences in luciferase signal in the spectrum between our high and low controls. We repeated this assay with a number of replicates for each condition (n=192) to obtain a Z-score for our controls, and found similar results (figure 19).

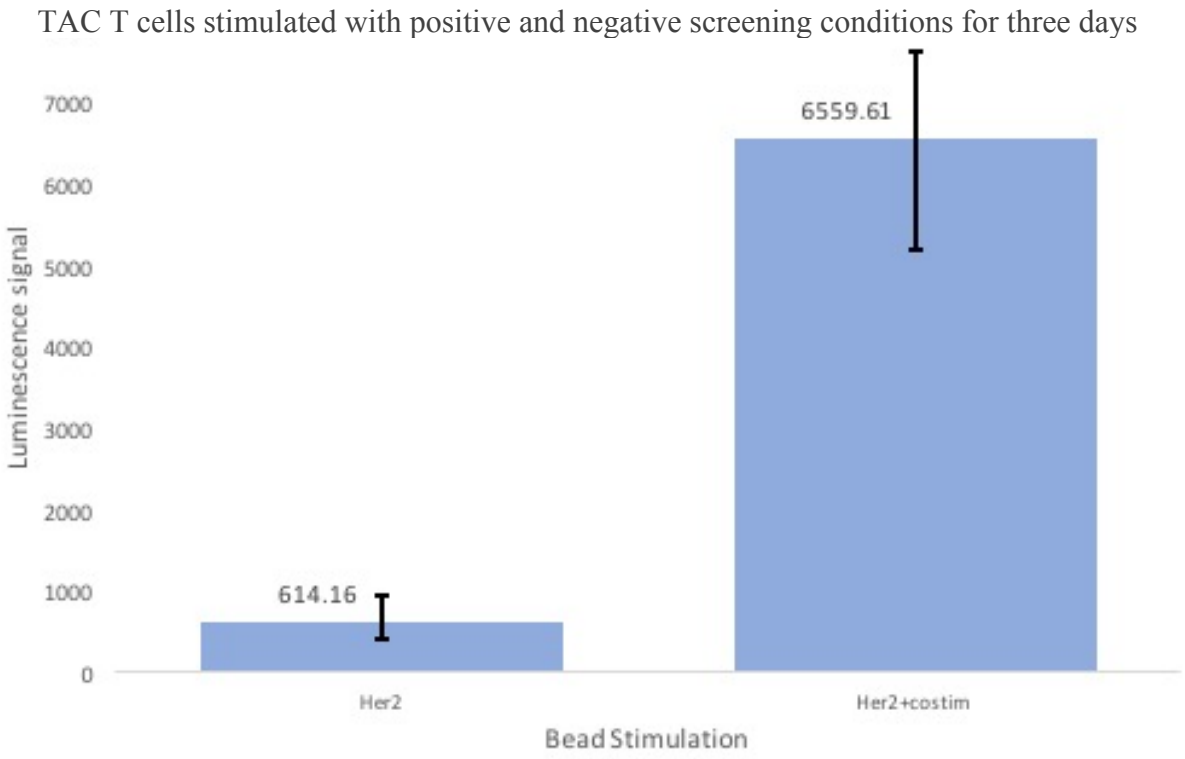

Figure 19: High replicate of TAC-LUC T cells stimulated with protein-coated beads for three days. Luminescence of TAC-LUC T cells was measured after three days, following the addition of luciferase reagent. Signal intensity was read on a plate reader. HER2 bead stimulation was used as our negative control, and HER2 + costim (CD86 + LFA-3) as our positive control (n= 192).

3.6 High Throughput Screen Results

With our screening method optimized, we then manufactured a second large batch of dual expressing TAC-LUC T cells with 48% transduction for screening purposes. While the transduction efficiency was lower on the second batch, functional assays revealed no differences in TAC-LUC efficacy. To control intra-donor differences, we used the same PBMC donor for all manufacturing batches. The first run of the screen utilized both the original batch of TAC-LUC T cells (75% transduced) and the second batch (48% transduced), with screening duplicates matched to the same manufacturing batch. We chose to screen the full compound library as our first run/ pilot screen as we had enough cells to do so. We then repeated the screen with a third large-scale batch of TAC-LUC T cells with 41% transduction. All manufacturing batches were tested for TAC-LUC function prior to setting up the screen. Within each plate, we included a high number of replicates of positive and negative controls to accurately normalized luciferase signal within each plate. Columns 1-2 contained our negative control (n=32), columns 3-22 contained library compounds, and column 24 contained our positive control wells (n=16). We elected to leave column 22 empty to reduce the luminescence spillover from our positive control wells into adjacent drug wells.

3.6.1 Results from the first screen

Although we didn't have enough T cells from a single manufacturing run to perform the entire screen, we elected to proceed with T cells from the first two batches. We screened the entire compound library in duplicate, with replicates matched to respective manufacturing batch. The last 2-3 plates in the first screen (library plates 11-13) were

deemed unreliable, as we ran into problems with low volume of cells and beads. This was corrected in the second screen, as we increased the dead volume needed to prime the automated liquid handlers.

Following the results of the screen, we normalized luciferase signal across each plate to the plate controls and analyzed the results from each replicate separately using the interquartile mean method. Most hits were significant in both replicates, giving confidence to the screen. Figure 20 illustrates the results for each compound (circle), coloured by plate. The hit compounds from both replicates lie in the upper right quadrant, with the cutoff at three standard deviations from the mean. Compounds with similar biological activity are clustered by plate in the compounds library, where we see most hits from our upper right quadrant resulting from library plate 1. The top hit compound annotated on the far upper right of the replica plot (figure 20) was isorhamnetine-3-glucoside. We sought to repeat the screen to confirm these hit compounds and to address the issues experienced with the last compound plates.

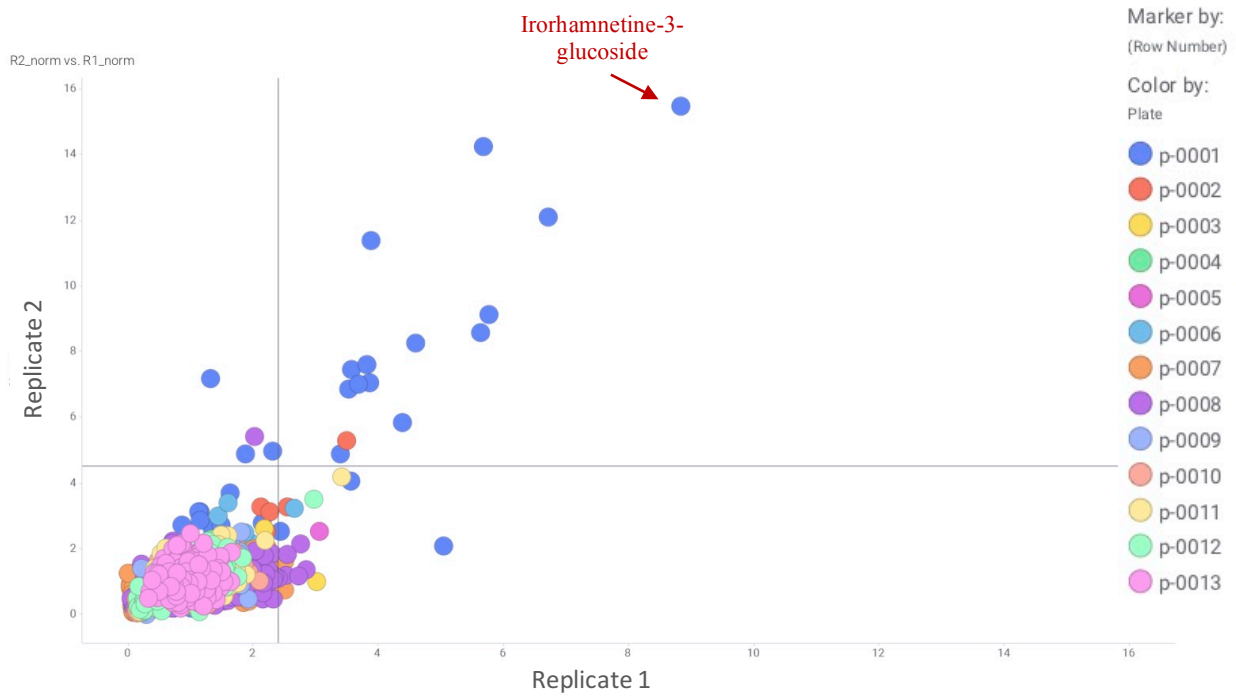

Figure 20: Pilot screen replica plot results. Each dot represents a compound, where each dot colour represents a compound library plate (13 total). The x and y-axis represent normalized signal intensity. Values are normalized to the negative and positive controls within each plate. The horizontal and vertical lines represent the cutoff of 3 standard deviations from the mean for each replicate. Hit compounds are illustrated in the upper right quadrant. The top compound is annotated in red. (1 experiment, 2 replicates)

3.6.2 Results from the repeat screen

We performed a second screen with a third batch of TAC T cells, with 41% transduction. Figure 21, a heat map, illustrates the signal intensity from plate 1 (replicate 1), where hit compounds are seen to elicit a similar signal intensity to that of the positive control (column 24). The compound in well B8 with the highest signal is isohametine-3-glucoside, previously described as our top hit in the first screen. Similar to our pilot screen, we normalized luciferase signals within each plate and set the cutoff for hit compounds at three standard deviations from the mean (figure 22). Our second screen recapitulated all the hits identified in our first screen, where the top hit compound was isorhamnetine-3-

glucoside (figure 22). The repeat screen identified 15 new compounds that demonstrated significance.

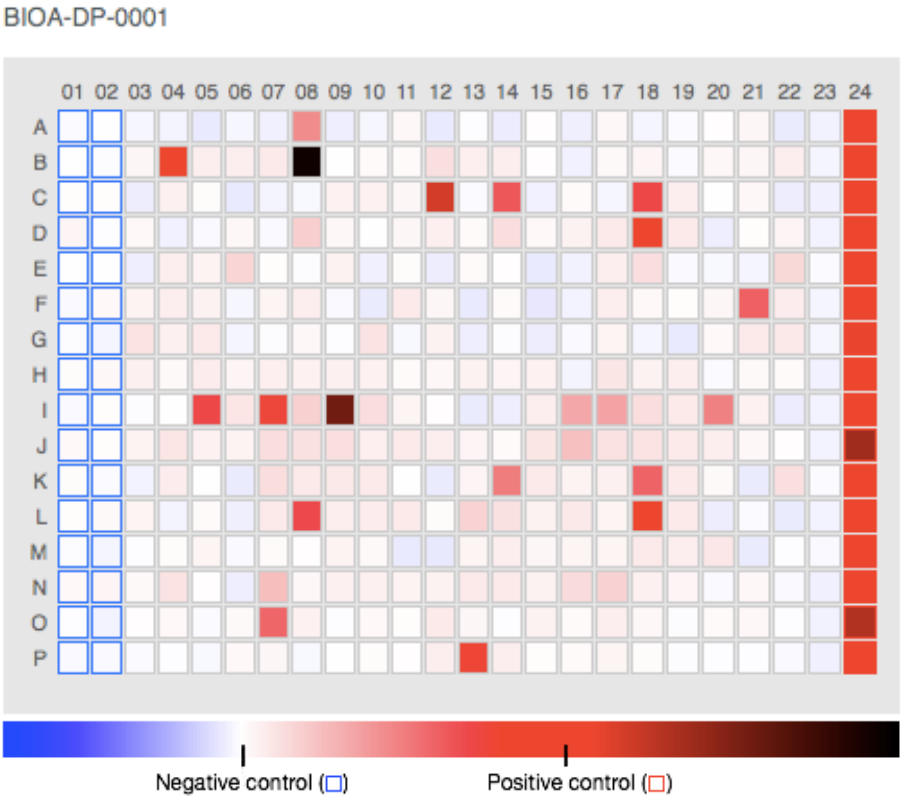

Figure 21: Heat map of luciferase signal intensity from plate 1 of screen. Raw signal intensity from plate 1, replicate 1 is mapped by colour, with red/black representative of a high luciferase signal. Compound wells lie in columns 3-22. Column 24 represents our positive control, with antigen (HER2) + costim (CD86 and LFA-3) bead stimulation (n = 16). Columns 1-2 represent our negative control with antigen only bead stimulation (n = 32). Hit compounds with high signal intensity are illustrated here in red. (representative of two experiments, each with two replicates)

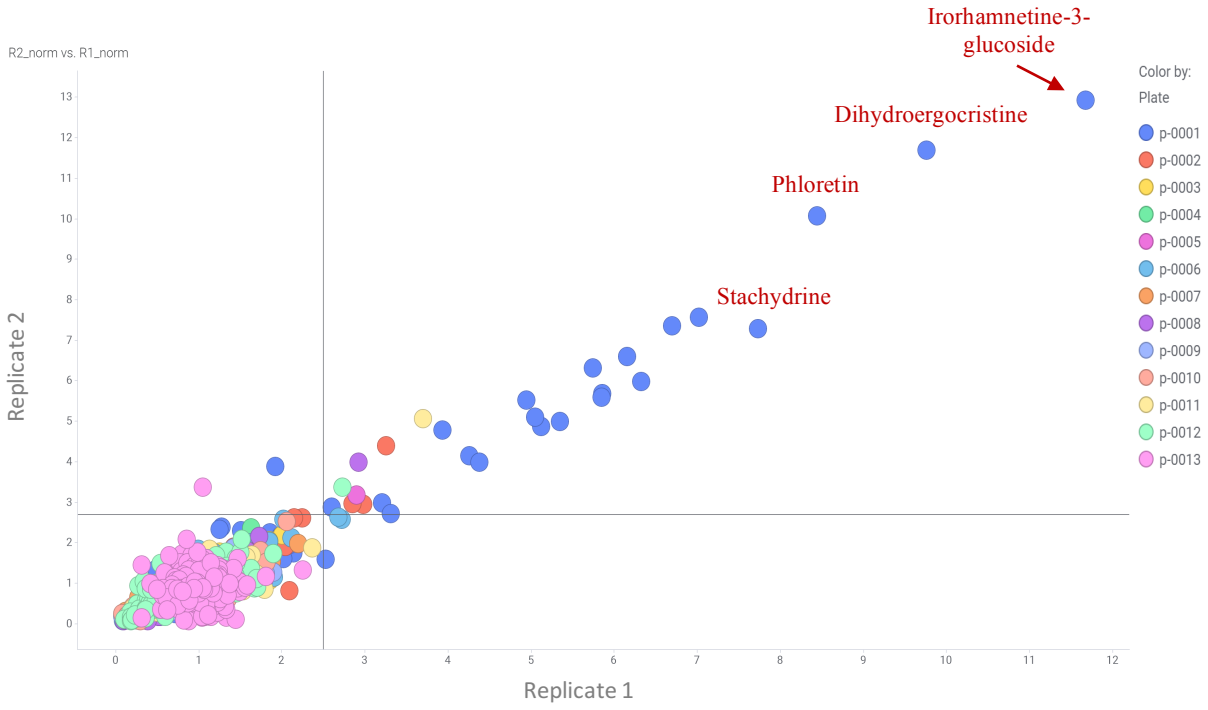

Figure 22: Screen replica plot results. Each dot represents a compound, where each dot colour represents a compound library plate (13 total). The x and y-axis represent normalized signal intensity. Values are normalized to the negative and positive controls within each plate. The horizontal and vertical lines represent the cutoff of 3 standard deviations from the mean for each replicate. Hit compounds are illustrated in the upper right quadrant. The top four compounds are annotated in red. (1 experiment, 2 replicates)

3.6.3 Hit compound chemical classes

We classified most of our 30 hit compounds into three chemical groups based on their core chemical structures: flavaones, cardenolides, and phorbol esters. Flavanones include our top hit, isohmetinine-3-glucoside, and erocitrin, which also elicited a strong signal in our screen (figure 23A). Flavanones belong to the class of flavanoids, which are known to be anti-cancer and anti-inflammatory (Martinez, 2019). However, flavanones specifically have not been explored for their effects on T cells. The second group we identified was cardenolides (figure 23B). Cardenolides have been characterized to have anti-cancer effects in humans by inducing immunogenic cell death through innate immune

cell activation (Calderón-Montaño, 2014), but their effects on T cell proliferation have also yet to be explored. The last of the three classes, PKC activators, have been widely characterized to enhance T cell proliferation and survival through the CD28 costimulatory pathway. These include our most potent phorbol ester, phorbol 12,13-dibutyrate (PdBu), and PKC activator, mezerein (figure 23C). TCR activation and costimulation by the native CD28 receptor triggers PKC-θ catalytic activation and translocation to the immunological synapse (figure 23D). These events initiate downstream signals to increase proliferation, including the activation of NF-κB, AP-1 and NFAT pathways (Wang, 2012). Phorbol ester compounds function to activate PKC- θ directly, and bypass the need for CD28 receptor stimulation.

A.

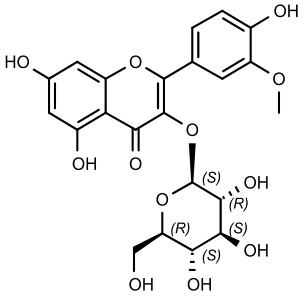

ISORHAMNETINE-3-GLUCOSIDE

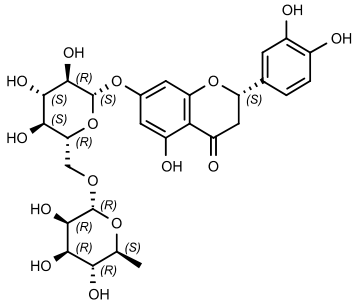

EROCITRIN

B.

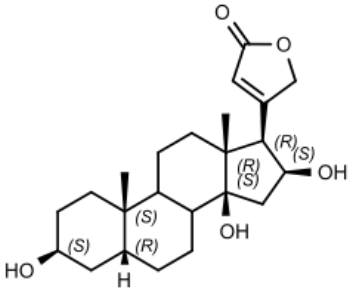

GITOXIGENIN

C.

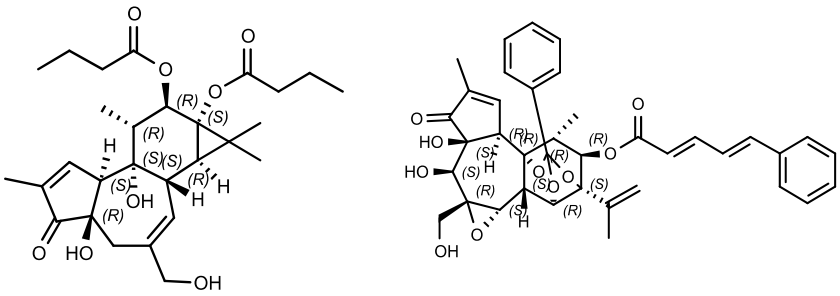

PHORBOL 12,13-DIBUTYRATE MEZEREIN

D.

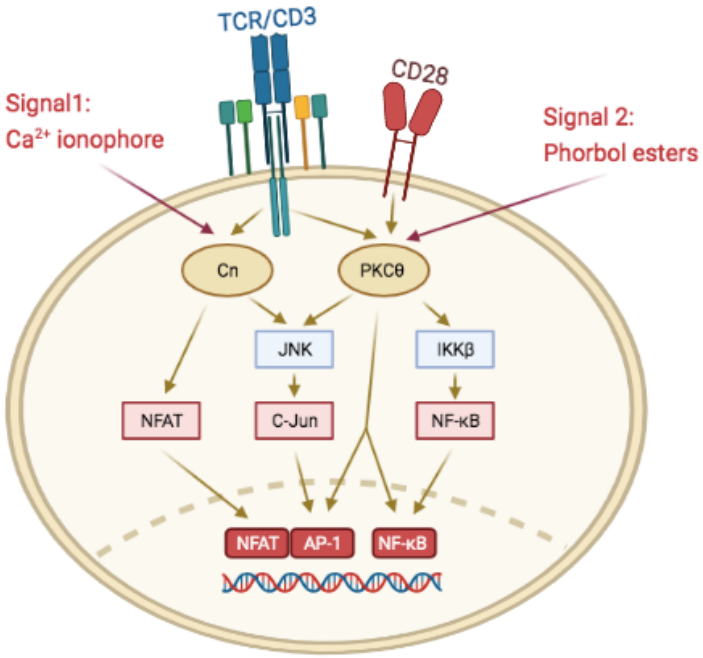

Figure 23: HTS compounds can be classified into three groups by chemical structure. A) The flavavones chemical class included compounds isorhamnetine-3-glucoside, the top hit compound from both runs of the screen, and erocitrin. B) The cardenolides chemical class included gitoxigenin. C) PKC activators made up the third class, including phorbol 12,13-dibutyrate (PdBu), 3 other phorbol ester compounds, and mezerein. D) The mechanism of action of phorbol ester compounds in combination with TCR activation is shown here. Figure made with Biorender.

3.7 Secondary Screening

To validate our hit compounds, we chose to pursue two consecutive secondary screening strategies. In Stage I of our secondary screen, we assessed the capacity of the hit compounds to augment in luciferase signal independent of TCR signaling. Our intention was to include compounds that increased cell growth and resulted in increased luciferase expression, but were only active in the presence of TCR activation. This served to exclude compounds that resulted in an increase in proliferation in the absence of TCR stimulation, that were then removed from further testing. Stage II of our secondary screen employed a direct measure of T cell proliferation by flow cytometry, using a CellTrace Violet dilution assay to confirm the ability of the hit compounds to enhance T cell proliferation.

3.7.1 Stage I secondary screen

Stage I of our secondary screen compared luciferase activity of TAC T cells treated with drug in the presence or absence of HER2 antigen stimulation. Given that our assay employs an indirect measure of T cell proliferation (luciferase expression), it is possible that some compounds may produce antigen-independent increases in luciferase activity as a consequence of effect on luciferase expression/activity or non-specific effects on T cell proliferation. To rule out compounds that increase signal in the absence of HER2 stimulation, we repeated our high throughput assay with both antigen stimulated and unstimulated bead conditions and the 30 hit compounds identified in our screen. The secondary screen was performed in duplicate, using the previously optimized high throughput screening protocol. TAC T cells were treated with drug in the presence of uncoated or HER2 protein-coated beads for 3 days. We used antigen (HER2) +

costimulation (CD86 and LFA-3) coasted-beads as our positive control in this assay. Luciferase signal for each sample was normalized to the unstimulated and antigen stimulated controls within each plate, by calculating % luciferase activity (as described in Section 5.6.2). This equation normalizes the luciferase signal of a given sample to the positive and negative controls for that plate; where 0% is the luciferase signal of the negative control, and 100% is that of the positive control. Samples exceeding %100 luciferase activity demonstrate luciferase activity above that of the costimulated positive control. The results from stage I of our secondary screen revealed several compounds that increased luciferase signal in both antigen stimulated and unstimulated conditions (figure 24A). The dotted horizontal line in figure 24A represents 100% luciferase activity, or signal equal to that of the positive control. Compounds with high signal in both conditions increased TAC-LUC cell number regardless of HER2 stimulation, and were therefore removed from further testing. Several of these compounds elicited luciferase signal above that of our positive control, and gave confidence to our primary screen (figure 24A). However, our strongest hit compound, isorhamnetine-3-glucoside, failed to demonstrate any enhancement in luciferase expression. This was contradictory to the results from both runs of our original screen. Isorhamnetine-3-glucoside was included in the following dose-response assay for further study. Figure 24B demonstrates the difference between antigen stimulated and unstimulated conditions, where the compounds with luciferase activity above 50% were selected for further testing. Of these compounds, three were phorbol esters with % activity of 72, 74, and 96. As a result of the likeness between these phorbol esters,

we chose to pursue only the highest performing compound, PdBu (96% activity) for further analysis. This left 13 of the initial 30 hit compounds for further investigation.

A.

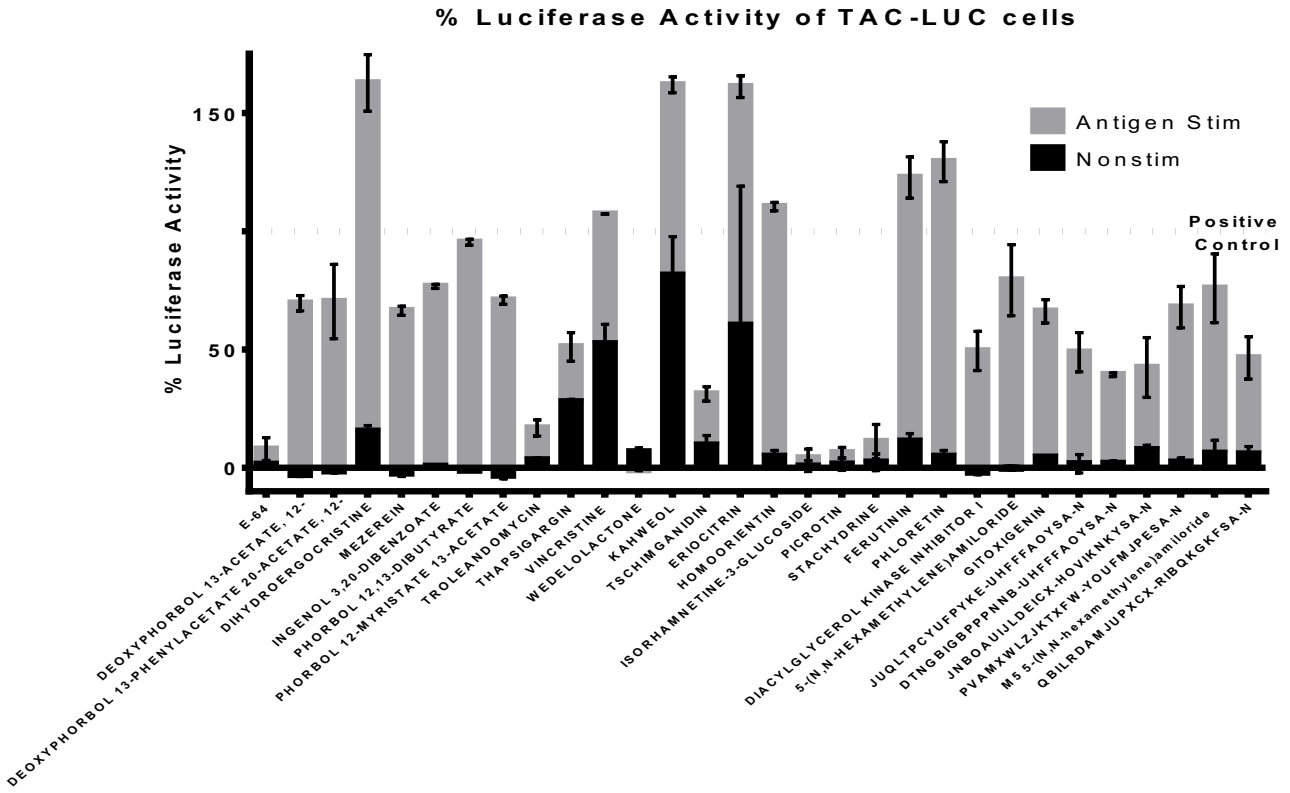
% Luciferase Activity of TAC-LUC cells
% Luciferase Activity
150
50
0
Antigen Stim
Nonstim
Positive Control
E-64
DEOXYPHORBOL 13-ACETATE, 12-
DEOXYPHORBOL 13-PHENYLACETATE 20-ACETATE, 12-
DIHYDROERGOCRISTINE
MEZEREIN
INGENOL 3,20-DIBENZOATE
PHORBOL 12,13-DIBUTYRATE
PHORBOL 12-MYRISTATE 13-ACETATE
TROLEANDOMYCIN
THAPSIGARGIN
VINCRISTINE
WEDELOLACTONE
KAHWEOL
TSCHIMGANIDIN
ERIOCITRIN
HOMOORIENTIN
ISORHAMNETINE-3-GLUCOSIDE
PICROTIN
STACHYDRINE
FERUTININ
PHLORETIN
DIACYLGLYCEROL KINASE INHIBITOR I
5-(N,N-HEXAMETHYLENE)AMILORIDE
GITOXIGENIN
JUQLTPCYUFPYKE-UHFFFAOYSA-N
DTNGBIGBPPPNNB-UHFFFAOYSA-N
JNBOAUIJLDEICX-HOVIKNKYSA-N
PVAMXWLZJKTXFW-YOUFMJPESA-N
M5 5-(N,N-hexamethylene)amiloride
QBILRDAMJUPXCX-RIBQKGKFSA-N

B.

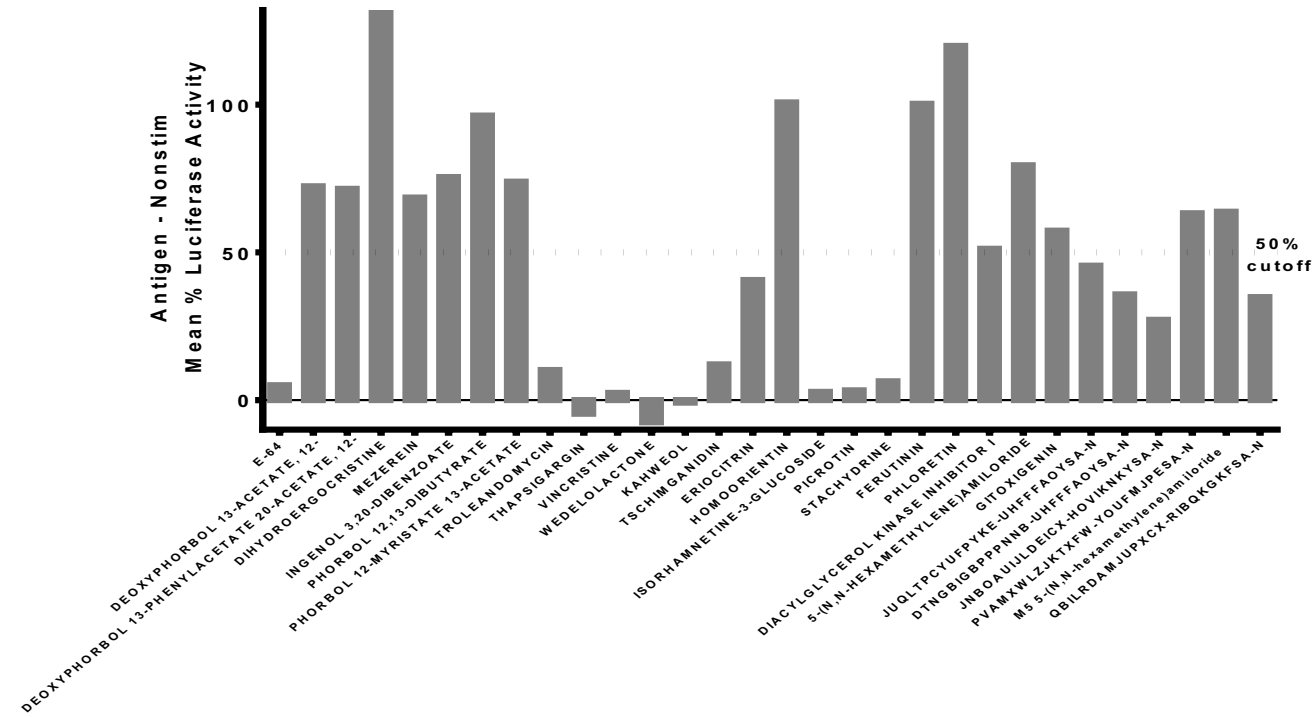
% Luciferase Activity of [Antigen Stim - Nonstim] TAC-LUC cells
Antigen - Nonstim
Mean % Luciferase Activity
100
50
0
50% cutoff
E-64
DEOXYPHORBOL 13-ACETATE, 12-
DEOXYPHORBOL 13-PHENYLACETATE 20-ACETATE, 12-
DIHYDROERGOCRISTINE
MEZEREIN
INGENOL 3,20-DIBENZOATE
PHORBOL 12,13-DIBUTYRATE
PHORBOL 12-MYRISTATE 13-ACETATE
TROLEANDOMYCIN
THAPSIGARGIN
VINCRISTINE
WEDELOLACTONE
KAHWEOL
TSCHIMGANIDIN
ERIOCITRIN
HOMOORIENTIN
ISORHAMNETINE-3-GLUCOSIDE
PICROTIN
STACHYDRINE
FERUTININ
PHLORETIN
DIACYLGLYCEROL KINASE INHIBITOR I
5-(N,N-HEXAMETHYLENE)AMILORIDE
GITOXIGENIN
JUQLTPCYUFPYKE-UHFFFAOYSA-N
DTNGBIGBPPPNNB-UHFFFAOYSA-N
JNBOAUIJLDEICX-HOVIKNKYSA-N
PVAMXWLZJKTXFW-YOUFMJPESA-N
M5 5-(N,N-hexamethylene)amiloride
QBILRDAMJUPXCX-RIBQKGKFSA-N

Figure 24: % luciferase activity of the 30 hit compounds in the absence of TCR stimulation. TAC T cells were treated with drug for 3 days in both antigen stimulated and unstimulated conditions according to the HTS screening protocol. On day 3, cells were incubated with D-luciferin and luciferase intensity was measured by plate reader. A) TAC T cell % luciferase activity as a result of drug intervention in antigen stimulated (orange bars) and unstimulated (blue bars) conditions. The positive control (normalized as 100% luciferase activity) is indicated by a line on the graph. Error bars are SD. B) The difference between antigen stimulated and unstimulated conditions are shown. The 50% cutoff value (line on graph) determined which compounds proceeded to the next phase of testing. (1 experiment, 2 replicates)

The results from stage I of our secondary screen ruled out compounds that led to an antigen-independent increase in luciferase signal. We selected 13 compounds that had displayed over 50% luciferase activity in Stage I of our secondary screen (figure 24B) for further evaluation. We performed a dose-response assay to investigate the effects of these compounds on luciferase activity over a range of 6 concentrations below our screening dose, with the highest concentration being 10μM, and the lowest concentration being 10nM. We performed a plate-based assay using the same high throughput protocol as previously described, and stimulated TAC T cells with beads over 3 days. We performed this assay with two replicates, where samples were normalized to plate controls using the % luciferase activity equation. The results from our dose response assay revealed that our PKC activating and phorbol ester compounds were more potent at lower concentrations (figure 25A). These included mezerein and PdBu, found to have an optimal dose of 100nM and 10nM respectively. Several compounds, including mezerein and PdBu demonstrated % luciferase activity well above the positive control. Figure 25B illustrates the optimal dose for each compound, which elicited the highest % luciferase activity in this assay. We set a cut-off value of 1 (equal to, or above the % activity of the positive control), and chose to move forward with 6 out of these 13 compounds. Compounds that were selected for Stage

II of our secondary screen included dihydroergocristine, mezerein, PdBu, erocitrin, homoorientin, and ferutinin. PdBu showed the highest % luciferase activity at a mean 306%, demonstrating a 3.06-fold increase from that of the positive control. Mezerein followed close behind at a mean of 248% activity. Again, isorhamnetine-3-glucoside failed to elicit signal above the negative control (mean 3% at 10μM). To understand if this was due to an error in the library sample, we sourced the compound for an alternate source, and repeated the assay using both the original and the alternatively-sourced isorhamnetine-3-glucoside compounds (data not shown), which confirmed the results of the secondary screen. It is unknown why isorhamnetine-3-glucoside demonstrated the highest luciferase signal in both runs of the screen, but had little to no activity in follow up experiments. Despite these results, we moved forward with this compound in the preliminary stage II secondary assays in hope of better understanding its effect on TAC T cells. Apart from mezerein, which was not available for synthesis, the 6 remaining compounds were obtained from alternate sources and reconstituted in DMSO for further secondary experiments. An aliquot of mezerein was obtained from the biologically active compounds library at McMaster for further studies.

A.

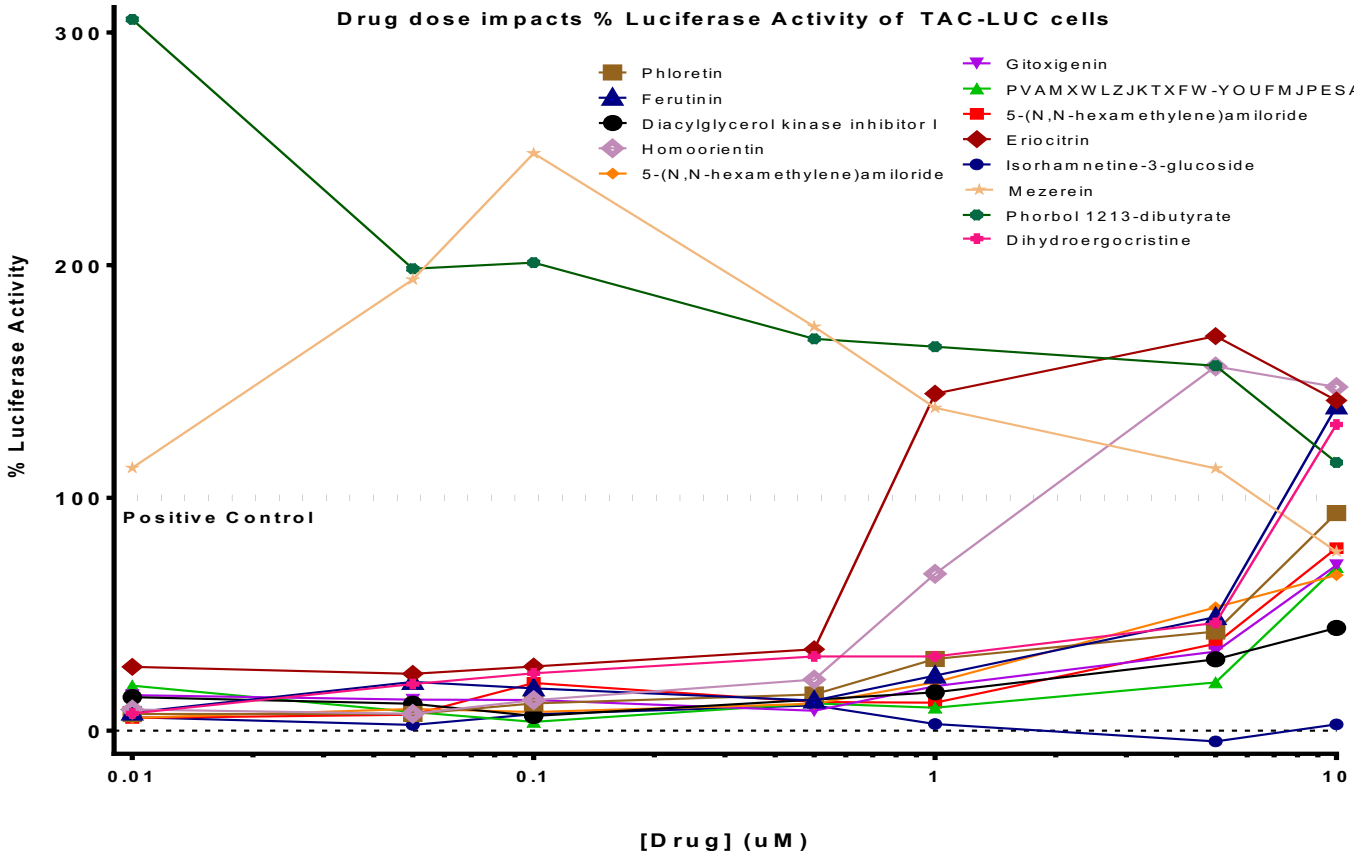
Drug dose impacts % Luciferase Activity of TAC-LUC cells
% Luciferase Activity
300
200
100
0
Positive Control
0.01
0.1
1
10
[Drug] (uM)
Phloretin
Ferutinin
Diacylglycerol kinase inhibitor I
Homoorientin
5-(N,N-hexamethylene)amiloride
Gitoxigenin
PVAMXWLZJKTXFW-YOUFMJPESA
5-(N,N-hexamethylene)amiloride
Eriocitrin
Isorhamnetine-3-glucoside
Mezerein
Phorbol 1213-dibutyrate
Dihydroergocristine

B.

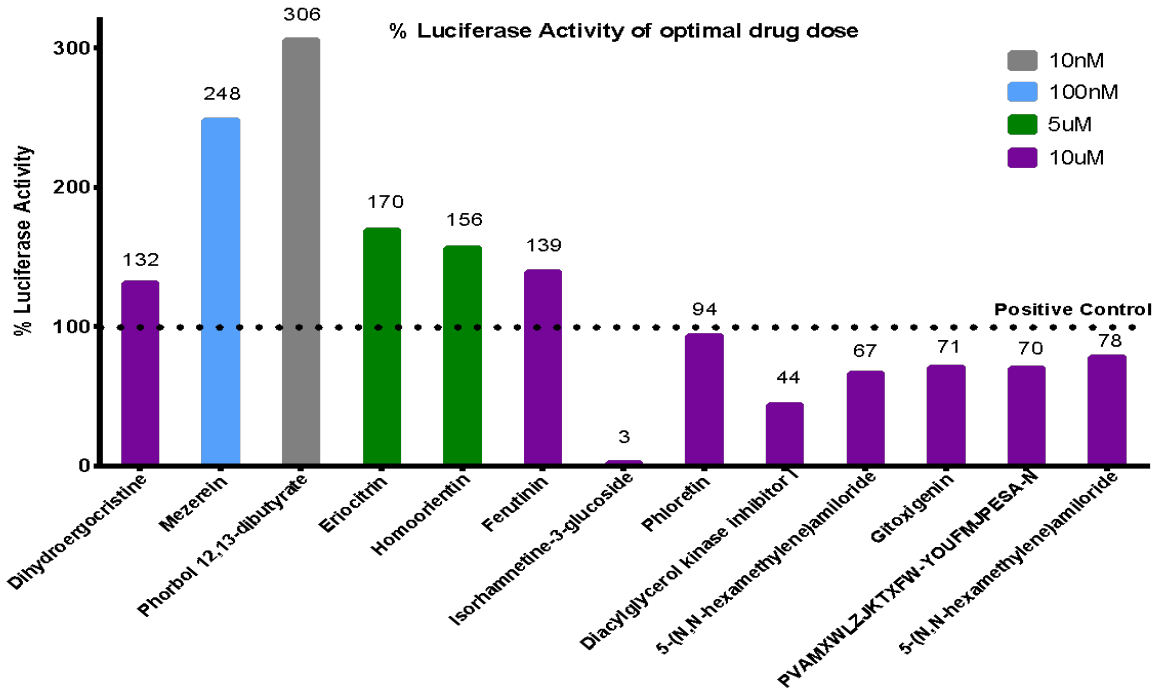
% Luciferase Activity of optimal drug dose
% Luciferase Activity
300
200
100
0
10nM
100nM
5uM
10uM
Positive Control
132
248
306
170
156
139
3
94
44
67
71
70
78
Dihydroergocristine
Mezerein
Phorbol 12,13-dibutyrate
Eriocitrin
Homoorientin
Fenutinin
Isorhamnetine-3-glucoside
Phloretin
Diacylglycerol kinase inhibitor I
5-(N,N-hexamethylene)amiloride
Gitoxigenin
PVAMXWLZJKTXFW-YOUFMJPESA-N
5-(N,N-hexamethylene)amiloride

Figure 25: % luciferase dose response assay for the 13 TCR-dependent compounds. TAC T cells stimulated with antigen (HER2) for 3 days at a range of drug concentrations (10nM to 10μM) according to the HTS screening protocol. On day 3, cells were incubated with D-luciferin and luciferase intensity was measured by plate reader. A) TAC T cell % luciferase activity as a result of 10nM, 50nM, 100nM, 500nM, 1μM, 5μM, 10μM drug intervention conditions. The positive control (normalized as 1) is indicated by a line on the graph. B) The % luciferase activity for the optimal working dose of each compound, values are annotated above each bar. The positive control (normalized as 1) is indicated by a line on the graph, with the negative control at 0. The 1 cutoff value (line on graph) determined which compounds proceeded to the next phase of testing. (1 experiment, 2 replicates)

3.7.2 Stage II secondary screen

All of the work to this point employed luciferase expression as an indirect measure of cell proliferation. In Stage II of our secondary screen, we directly examined the impact of the hit compounds on T cell proliferation using a flow cytometry-based assay. T cells were stained with Cell Trace Violet (CTV) tracker dye and stimulated with antigen in the presence/absence of the hit compounds for 3 days. Flow cytometry allows us to monitor survival/proliferation on a single cell basis and evaluate the impact of drug treatment on $CD4^+$ and $CD8^+$ cell subtypes. FCS proliferation modelling software produces statistics such as proliferation index, providing information on the number of division cycles an average cell in that sample has undergone. We first sought to validate the flow cytometry secondary screen using the previous TAC-LUC T cells. To confirm that the CTV assay demonstrated results comparable to the luciferase-based assay, we stained the cells with CTV and stimulated cells in the presence of drug for 3 days.

We also included the addition of a new compound, Bryostatin-1, a PKC activator recently characterized in literature to improve T cell proliferation (Hardman, 2020). Optimal *in vitro* dosing for Bryostatin-1 was indicated to be ~40nM. We performed a dose response assay with our TAC-LUC T cells ranging from 8nM to 1μM Bryostatin-1 (data

not down). The proliferation indices of Bryostatin-1 treated cells fell within a range of 0.10 for all concentrations 8nM to 200nM, with 40nM demonstrating the greatest benefit. Bryostatin-1 treated cells demonstrated a decrease in viability with increasing concentration, suggesting that the compound is toxic to cells at higher concentrations. The viability across most hit compounds was quite low as a result of the small TAC^+ population, and was not reproduced in experiments using sorted TAC T cells.

To better understand the effect of these compounds on TAC T cell proliferation and validate the screen results, we chose to use a BCMA-specific TAC construct for the flow cytometry based secondary assays. This construct provided a different antigen binder (BCMA) than what was used in the original screen (HER2), confirming that the effect of the compounds was not limited by the design of the original screen. The BCMA-TAC construct contains a NGFR transduction marker that can be positively selected for during cell culture. Three distinct PBMC donors were used to manufacture 3 batches of lentiviral engineered BCMA-TAC T cells. TAC T cells were positively selected for by their NGFR transduction marker, resulting in 85%+ pure TAC populations. The BCMA-TAC construct also provided an advantage when performing single cell analysis as the sorted TAC population allowed for better resolution between control and drug conditions.

Using the BCMA-TAC construct, we performed a second dose response experiment to investigate the efficacy of the remaining compounds at higher doses, above 10μM. As PKC activators are known to be more potent at lower concentrations, we did not test these at higher concentrations, and included PdBu and mezerein at their optimal dose of 10nM and 100nM respectively. Bryostatin-1 dosing was repeated at a lower concentration range

in this assay (0.1nM to 10nM), as the compound had previously demonstrated a reduction in viability at concentrations above 40nM. As there was no observable benefit to luciferase signal in any of the follow-up studies, isorhamnetine-3-glucoside compound was excluded from further investigation.

TAC T cells were stained with CTV tacker dye, stimulated in the presence of drug for three days, and were stained and analyzed by flow cytometry. Similar to our HTS assays, negative and positive controls were included. The negative control consists of cells stimulated with antigen (BCMA) coated beads in the presence of DMSO, matched to the highest drug concentration in the assay. For the positive control, cells were stimulated in the presence of DMSO with antigen and costimulatory protein (LFA-3 and CD86) coated beads. To better understand the effect of these compounds on proliferation, we included counting beads in our flow cytometry analysis to determine the total number of cells in each sample at endpoint. The total number of live NGFR+ gated cells is shown in figure 26A, where the horizontal lines indicate cell number for the negative and positive controls. $CD4^+$ and $CD8^+$ proliferation indices for each drug treatment is shown in figure 26B. Each drug condition shown in blue (figure 26) was performed at 1x, 2x, and 3x the initial chosen concentration from stage I of our secondary assay (figure 25). Compound dose was capped at 25μM to keep DMSO concentrations to less than 0.5% sample volume and limit DMSO toxicity and cell death.

The PdBu treated cells demonstrated the highest total cell number at endpoint, and was the only sample that displayed a TAC T cell number above that of the positive control (figure 26A). 10μM ferutinin displayed the second highest cell number, similar to that of

the positive control. None of the compounds were found to perform significantly better at higher concentrations, therefore the original dosing was kept for further experiments. Bryostatin-1 demonstrated the greatest benefit to cell number at a concentration of 0.1nM, where cell number decreased linearly in response to higher concentrations, and was chosen for further studies. The proliferation indices for the $CD4^+$ and $CD8^+$ subsets provide us with supporting information about the proliferative capacity of each subtype as a result of drug treatment (figure 26B). While PdBu and dihydroercocristine preferentially supported $CD4^+$ proliferation, the other 5 compounds provided equal or greater benefit to $CD8^+$ subtypes. The stars at the bottom of each figure indicate the chosen concentration moving forward into following experiments (figure 26). As dihydroergocristine did not provide a benefit to cell number above that of the negative control at any of the concentrations tested, we chose not to pursue this compound further.

A.

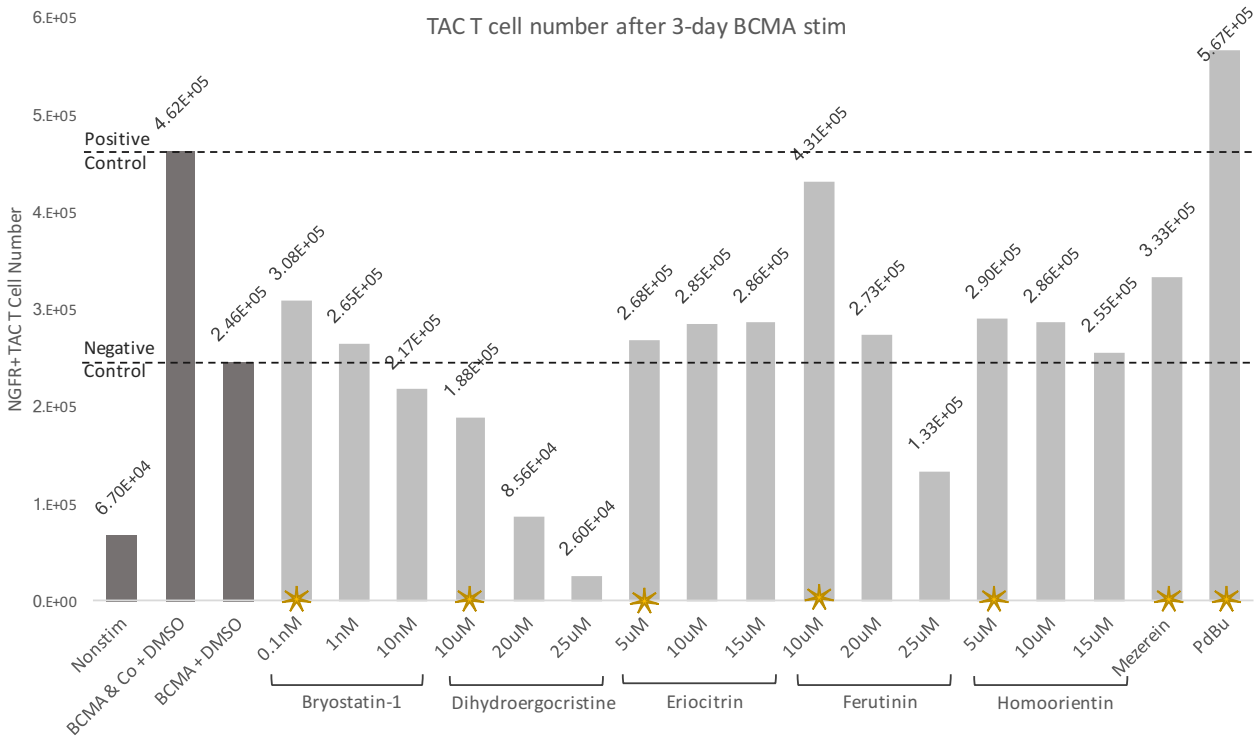
TAC T cell number after 3-day BCMA stim
NGFR+TAC T Cell Number
6.E+05
5.E+05
4.E+05
3.E+05
2.E+05
1.E+05
0.E+00
Positive Control
Negative Control
6.70E+04
4.62E+05
2.46E+05
3.08E+05
2.65E+05
2.17E+05
1.88E+05
8.56E+04
2.60E+04
2.68E+05
2.85E+05
2.86E+05
4.31E+05
2.73E+05
1.33E+05
2.90E+05
2.86E+05
2.55E+05
3.33E+05
5.67E+05
Nonstim
BCMA & Co + DMSO
BCMA + DMSO
0.1nM
1nM
10nM
10uM
20uM
25uM
5uM
10uM
15uM
10uM
20uM
25uM
5uM
10uM
15uM
Mezerein
PdBu
Bryostatin-1
Dihydroergocristine
Eriocitrin
Ferutinin
Homoorientin

B.

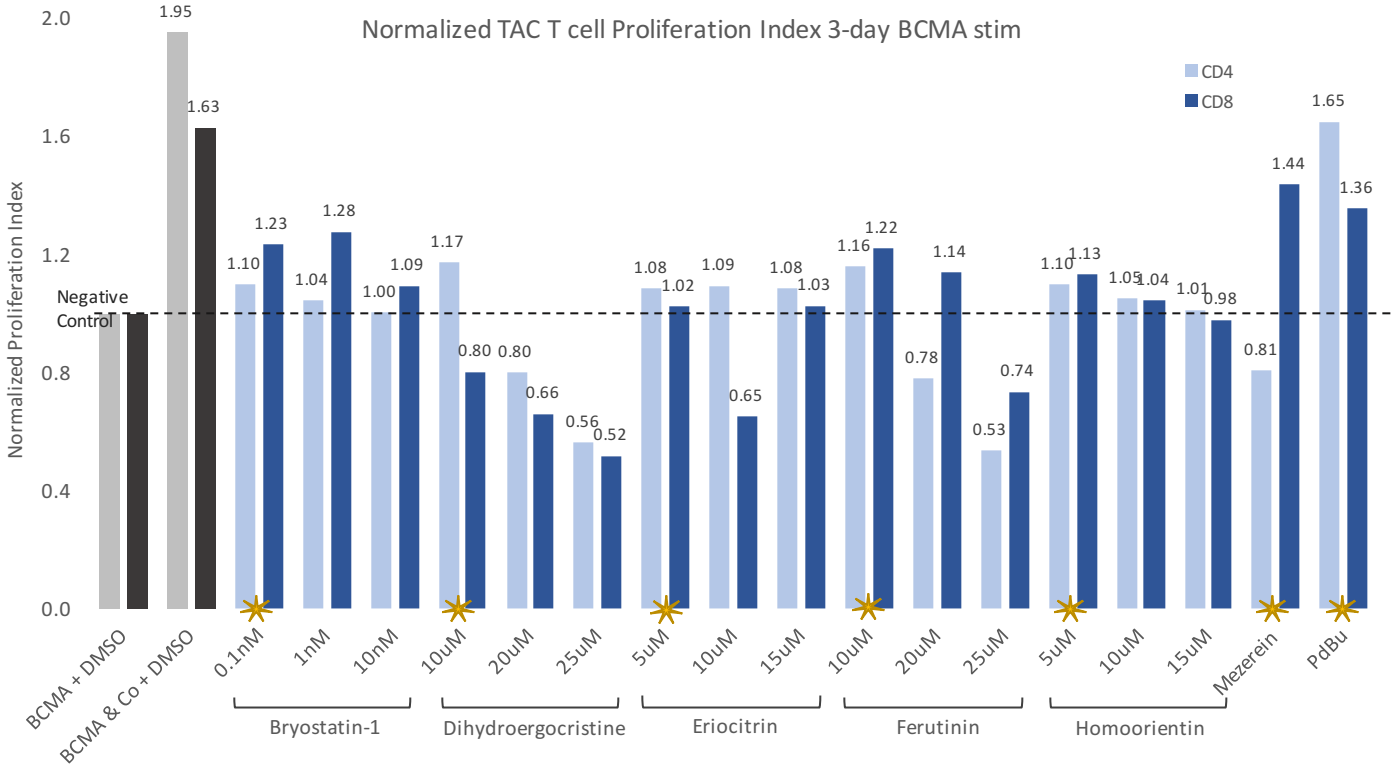
Normalized TAC T cell Proliferation Index 3-day BCMA stim
Normalized Proliferation Index
2.0
1.6
1.2
0.8
0.4
0.0
CD4
CD8
Negative Control
1.95
1.63
1.10
1.23
1.04
1.28
1.00
1.09
1.17
0.80
0.80
0.66
0.56
0.52
1.08
1.02
1.09
0.65
1.08
1.03
1.16
1.22
0.78
1.14
0.53
0.74
1.10
1.13
1.05
1.04
1.01
0.98
0.81
1.44
1.65
1.36
BCMA + DMSO
BCMA & Co + DMSO
0.1nM
1nM
10nM
10uM
20uM
25uM
5uM
10uM
15uM
10uM
20uM
25uM
5uM
10uM
15uM
Mezerein
PdBu
Bryostatin-1
Dihydroergocristine
Eriocitrin
Ferutinin
Homoorientin

Figure 26: Proliferation tracker dye assay of BCMA-TAC T cells treated with dosing range of remaining compounds. TAC T cells stained with CTV tracker dye, stimulated with antigen (BCMA) and drug for 3 days. On day 3, cells were stained and analyzed by flow cytometry. The stars at the bottom of the graph determined which compound doses were chosen for the next phase of testing. Blue bars represent drug conditions, grey bars show unstimulated, positive (antigen & costim + DMSO vehicle), and negative (antigen + DMSO vehicle) controls. DMSO vehicle matched to the highest drug concentration (25μM)). A) The number of live TAC NGFR+ T cells at endpoint, calculated using the ratio of counting beads: cells. The positive and negative controls are indicated by horizontal lines on the graph. B) $CD4^+$ (light blue/grey bars) and $CD8^+$ (dark blue/grey bars) show the proliferation indices for each compound, normalized to the negative control. Blue bars indicate drug treatment, where grey bars represent controls. Horizontal line shows the negative control. (1 experiment)

To validate these results, we repeated the CTV tracker dye assay as described above, across 3 donors (donors 1, 2, and 3) at each optimal compound dose. Figure 27A illustrates the number of BCMA-TAC T cells in each sample at endpoint, calculated by the ratio of cells: counting beads. Samples were normalized to their donor-specific negative control to account for differences in proliferation between donors. PdBu displayed the highest number of TAC T cells at endpoint, above that of the positive control for all three donors. Ferutinin resulted in cell number similar to that of the positive control across all three donors. Mezerein displayed a benefit to proliferation above that of the negative control, but was not as potent as PdBu or ferutinin. Bryostatin-1, eriocitrin, and homoorientin did not result in cell number above the negative control in any of the three donors. These rankings differed slightly with regards to proliferation index. Bryostatin-1 treatment resulted in the highest $CD8^+$ proliferation indices for all three donors, and a benefit to $CD4^+$s (figure 27B & C). PdBu and ferutinin provided a benefit to both $CD4^+$ and $CD8^+$ proliferation indices above that of the negative control. Eriocitrin, homoorientin and mezerein treatment resulted in proliferation indices similar or lower than the negative control.

A.

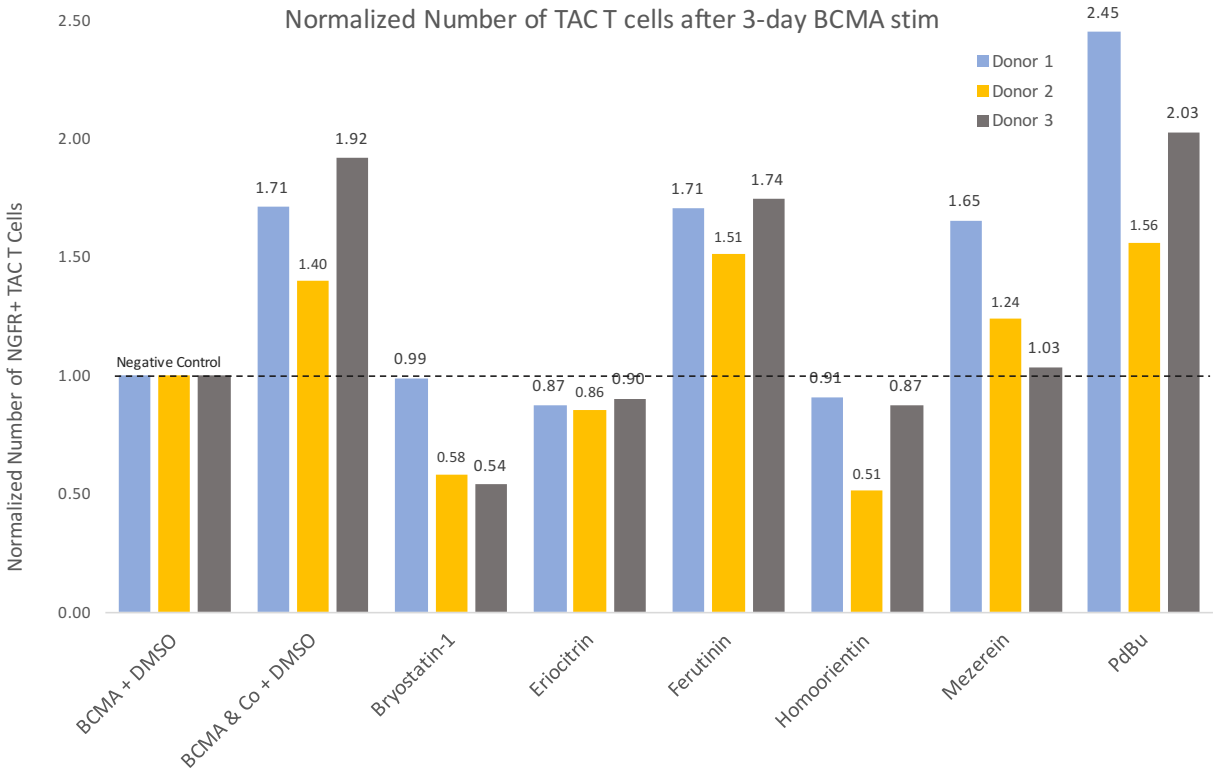
Normalized Number of TAC T cells after 3-day BCMA stim
Normalized Number of NGFR+ TAC T Cells
Donor 1
Donor 2
Donor 3
Negative Control
2.50
2.00
1.50
1.00
0.50
0.00
1.71
1.40
1.92
0.99
0.58
0.54
0.87
0.86
0.90
1.71
1.51
1.74
0.91
0.51
0.87
1.65
1.24
1.03
2.45
1.56
2.03
BCMA + DMSO
BCMA & Co + DMSO
Bryostatin-1
Eriocitrin
Ferutinin
Homoorientin
Mezerein
PdBu

B.

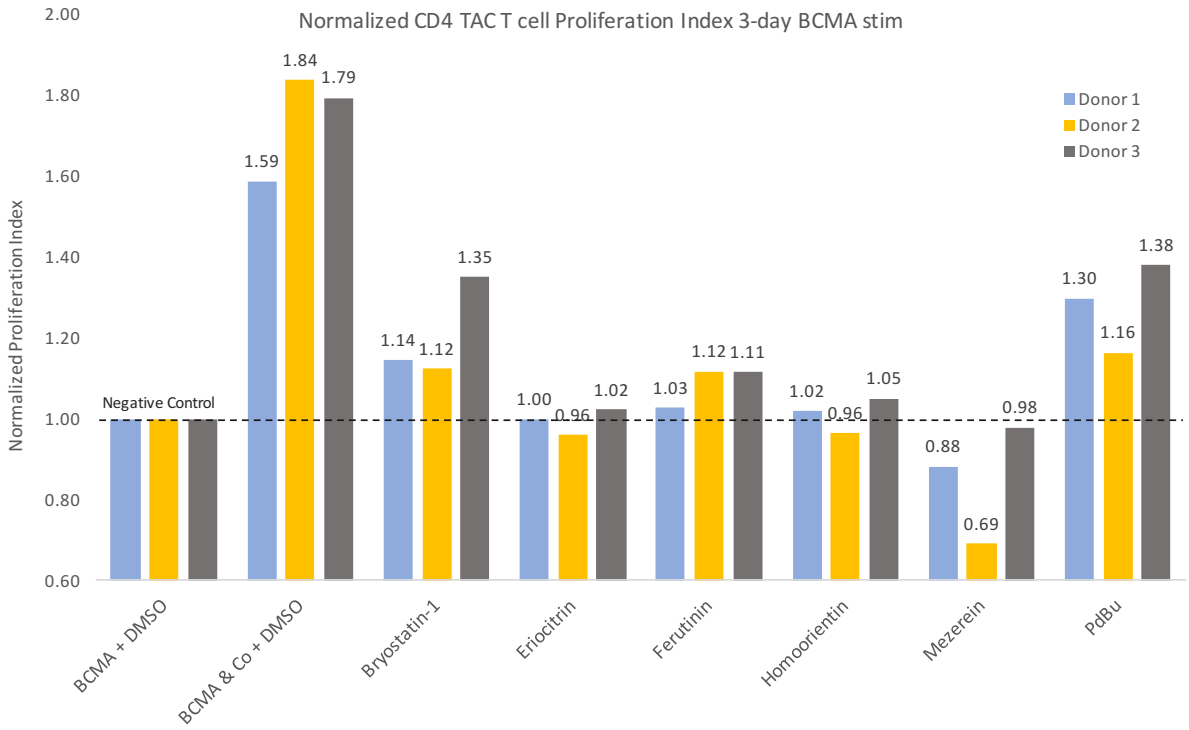
Normalized CD4 TAC T cell Proliferation Index 3-day BCMA stim
Normalized Proliferation Index
Donor 1
Donor 2
Donor 3
Negative Control
2.00
1.80
1.60
1.40
1.20
1.00
0.80
0.60
1.59
1.84
1.79
1.14
1.12
1.35
1.00
0.96
1.02
1.03
1.12
1.11
1.02
0.96
1.05
0.88
0.69
0.98
1.30
1.16
1.38
BCMA + DMSO
BCMA & Co + DMSO
Bryostatin-1
Eriocitrin
Ferutinin
Homoorientin
Mezerein
PdBu

C.

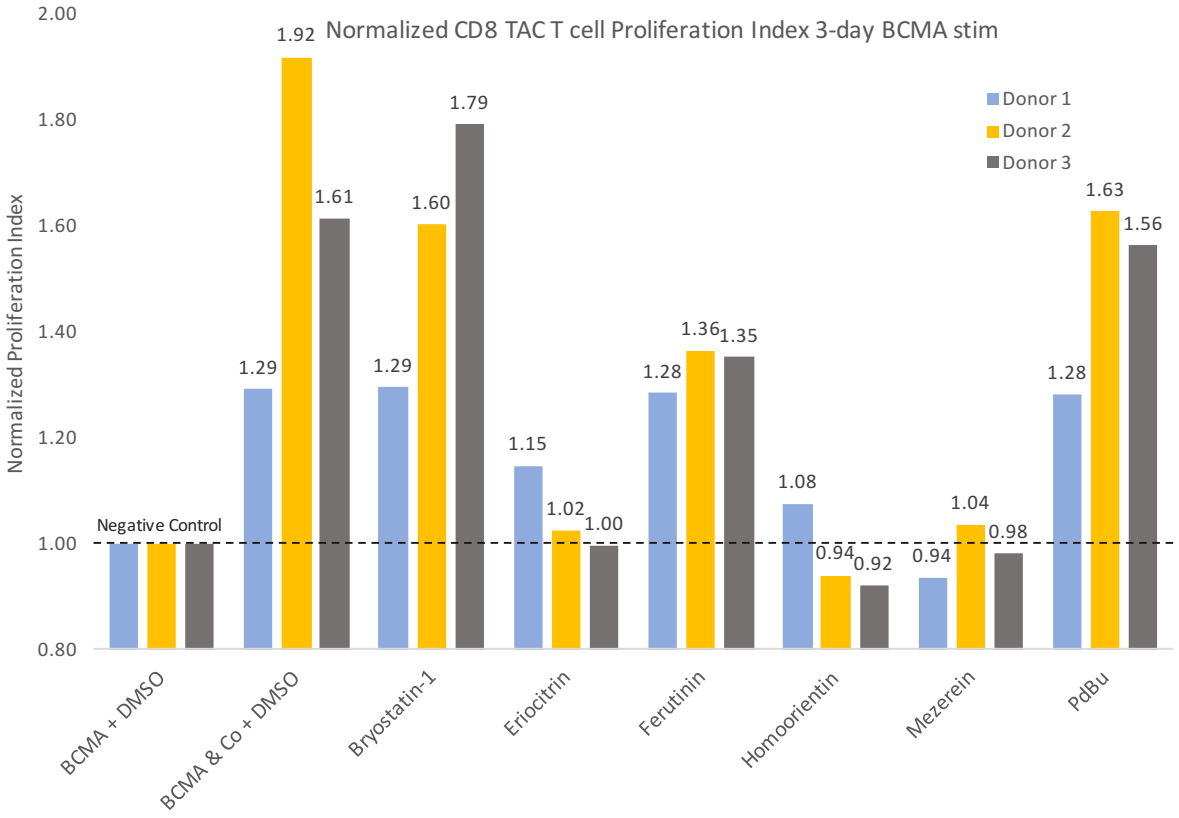

Figure 27: Proliferation statistics for BCMA-TAC T cells treated with drug across 3 donors. Three TAC T cell donors stained with CTV tracker dye, stimulated with antigen (BCMA) and drug for 3 days. On day 3, cells were stained and analyzed by flow cytometry. Coloured bars represent the three donors, where each sample is normalized to the negative control (antigen + DMSO stimulated cells). The negative control is indicated by a horizontal line on each graph. DMSO vehicle matched to the highest drug concentration (10µM). A) The number of live TAC NGFR+ T cells at endpoint, calculated using the ratio of counting beads: cells. B) $CD4^+$ and C) $CD8^+$ proliferation indices for each compound, normalized to the negative control. (1 experiment)

3.8 RNAseq computational analysis of selected compounds

To better understand whether the top hits from the secondary screen (PdBu, mezerein, ferutinin) were affecting similar biological pathways, we performed RNA sequencing on cells stimulated with antigen in the presence of three drug for 24 hours.

Based on the data from the previous experiments, we elected to treat cells with PdBu at 10nM, mezerein at 100nM, and ferutinin at 10μM.

A 24 hour timepoint was chosen to capture transcriptional changes as a result of T cell activation in the presence of drug. This timepoint was chosen based on the activity of transcription factors upregulated following T cell stimulation, where AP-1 activity peaks at 8 hours, and NF-κB peaks at 24 hours-post activation (Jutz, 2016). In our previous RNA sequencing data (Section 3.2), we saw genes specific to ribosomal metabolic changes upregulated as a result of T cell activation processes at an early timepoint (4 hours). By a late timepoint (72 hours), transcriptional changes of these proliferating cells were primarily modifications to metabolic, biosynthetic and catabolic processes. Cells stimulated in the presence of costimulatory compounds for 24 hours were expected to produce a unique transcriptional profile reflective of the biological pathways targeted by these compounds.

BCMA-TAC T cells were thawed, rested, and dead cells were removed using the Miltenyl dead cell removal kit prior to bead stimulation. Cells were stimulated with BCMA-coated beads in the presence of PdBu, ferutinin, and mezerein. Controls included unstimulated cells, antigen stimulated cells, and antigen + costimulation stimulated cells in the presence of 10μM DMSO, matched to the highest drug concentration (10μM ferutinin). RNA was collected from the cells 24 hours later and subjected to sequencing.

3.8.1 Principal Component Analysis

The principal component analysis (PCA) plot illustrates the sample distribution from the bulk RNAseq dataset (figure 28). These data displayed a minimal and consistent donor effect, where the direction of change between donors was very similar across all

stimulation conditions. Samples clustered according to either bead or drug stimulation, where three distinct clusters were identified on the PCA plot. Control unstimulated cells, and cells stimulated in the presence of PKC activating compounds (PdBu and mezerein) formed two distinct clusters. The third cluster consisted of control antigen stimulated and costimulated cells, and cells stimulated in the presence of ferutinin. Costimulated cells clustered closely to antigen stimulated cells, suggesting that the result of costimulation did not have as pronounced of an effect as seen in our previous RNAseq PCA plots (Section 3.2). This may be a result of differences in the way the T cells were engineered (as sorted populations in Section 3.2, or whole PBMC in Section 3.8). The ferutinin stimulated cells displayed little distinction from control, where the distribution of these samples almost overlapped the antigen stimulated control cells. Further analysis will investigate meaningful differences between RNA transcripts, to identify the biological processed upregulated as a result of pharmacological costimulation.

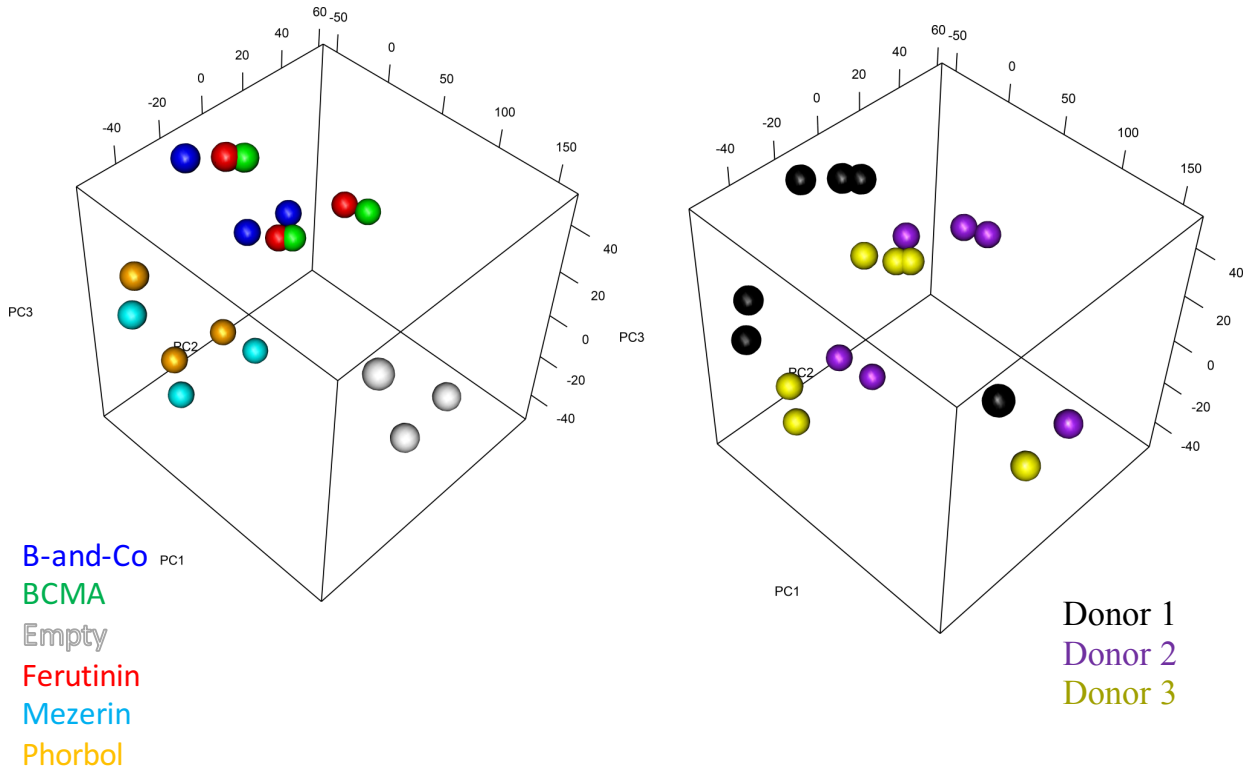

Figure 28: Principal component analysis of RNAseq samples. Data obtained from RNA samples as described in section 3.8. The coloured spheres on the left represent the six bead and drug stimulation conditions across 24 hours: DMSO + empty bead (grey), DMSO + BCMA bead (green), DMSO + BCMA+costim (dark blue), ferutinin + BCMA bead (red), mezerein + BCMA bead (light blue), and PdBu + BCMA bead (gold). The directional change of each sample relative to the control represents the similarity/dissimilarity of its bulk transcriptional profile. The coloured spheres on the right represent the distribution of the three T cell donors, donor 1 (black), donor 2 (purple), and donor 3 (yellow).

3.8.2 Differentially expressed genes and gene ontology pathway analysis

We investigated the transcriptional differences specific to costimulation and drug intervention, by examining differentially expressed genes and performing biological network gene ontology (BiNGO) pathway analysis. To isolate the costimulation-specific transcriptional differences, we performed our analysis comparing our antigen + costimulation condition minus antigen alone stimulation. The volcano plots demonstrate the comparison between each sample, to the DMSO antigen stimulated control. Our

analysis did not demonstrate many differentially expressed genes for the costimulation – antigen stimulation comparison (figure 29A), consistent with how similar these samples clustered in our PCA plot. The top differentially expressed genes specific to costimulation are annotated in red in figure 29A, where genes with positive $\log_2$ fold change are upregulated, and negative $\log_2$ fold change genes are downregulated as a result of costimulation. CALD1, an upregulated differentially expressed gene found specific to costimulation, was also upregulated to a similar degree in mezerein and PdBu stimulated cells. Corresponding gene ontology pathway analysis for upregulated biological processes with adjusted p-values higher than $1x10^{-4}$ for the costimulation condition are illustrated in figure 29B. Differentially expressed genes that fall under individual biological processes contribute to their p-values and significance. The top upregulated biological processes specific to costimulation was positive regulation of the JAK-STAT signaling pathway. The JAK-STAT pathway has broad applications in T cells, but is known to be involved in T cell growth, survival and cytokine signaling.

As mezerein and PdBu samples clustered together in the PCA plot, we expected our analysis to reveal that these compounds modified similar biological processes. Indeed, both mezerein and PdBu volcano plots demonstrate similar differentially expressed gene profiles, with the top genes being CALD1, PLAUR, and GJB2. This was also apparent in the biological processes analysis, as both displayed immune system process and response, and cell development as their top processes. Mezerein revealed transcriptional changes the most dissimilar from the DMSO stimulated control, and displayed the highest p-values. This is consistent with the distribution of the data in the PCA plot, as mezerein stimulated

cells demonstrated the furthest distribution from the control stimulated cells. The ferutinin comparison revealed the two significant upregulated genes, GLI1 and LOC652276 (figure 29G). The top annotated genes in red in figure 29G show differentially expressed genes with p-values less than $1x10^{-2}$. The BiNGO analysis for the ferutinin comparison revealed only a few significant upregulated biological processes, and no significant downregulated biological processes.

A.

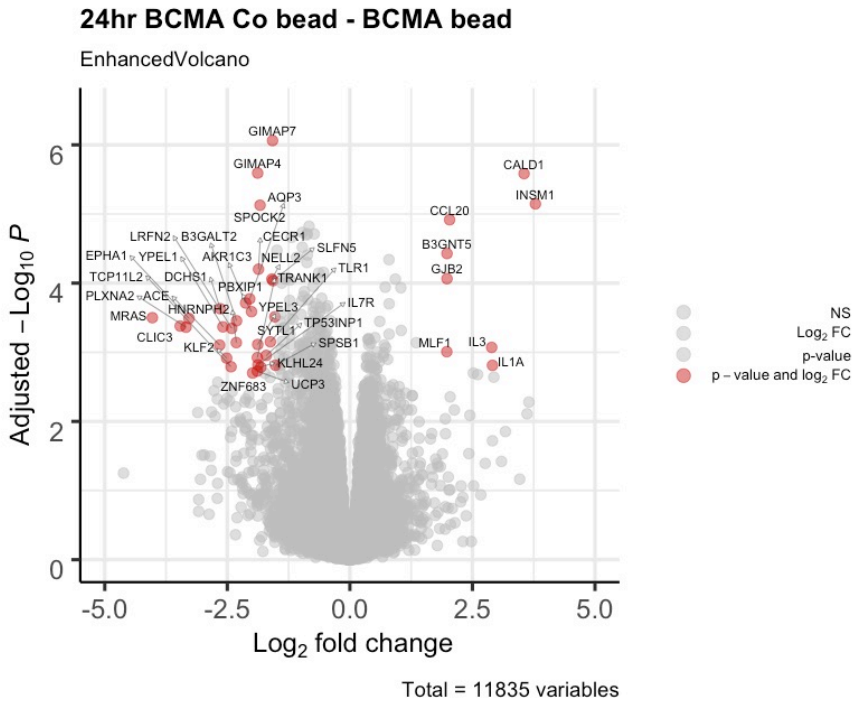

B.

Upregulated at 24hrs: GO biological process	Adj. p-value	Genes in test set
positive regulation of JAK-STAT cascade	1.97E-05	IL3|CSF2|IL5|LIF|IL2
regulation of JAK-STAT cascade	4.50E-05	IL3|CSF2|IL5|LIF|IL2
inflammatory response	1.26E-04	NDST1|IL1A|HRH1|IL
positive regulation of tyrosine phosphorylation of STAT protein	1.52E-04	IL3|CSF2|LIF|IL2
positive regulation of peptidyl-tyrosine phosphorylation	1.73E-04	IL3|CSF2|IL5|LIF|IL2
regulation of cell communication	1.86E-04	CSF2|SPHK1|NEK6|SF
positive regulation of protein amino acid phosphorylation	2.51E-04	IL3|CSF2|IL5|SPHK1|
regulation of tyrosine phosphorylation of STAT protein	2.55E-04	IL3|CSF2|LIF|IL2
regulation of signal transduction	2.55E-04	IL1A|IL3|CSF2|IL5|TB
positive regulation of phosphorylation	2.55E-04	IL3|CSF2|IL5|SPHK1|
regulation of signaling process	2.55E-04	IL1A|IL3|CSF2|IL5|TB
positive regulation of tyrosine phosphorylation of Stat5 protein	2.55E-04	IL3|CSF2|IL2
positive regulation of phosphorus metabolic process	2.55E-04	IL3|CSF2|IL5|SPHK1|
positive regulation of phosphate metabolic process	2.55E-04	IL3|CSF2|IL5|SPHK1|
regulation of peptidyl-tyrosine phosphorylation	2.68E-04	IL3|CSF2|IL5|LIF|IL2
immune system process	2.69E-04	CSF2|IL1R1|CCL20|LI
response to wounding	2.84E-04	NDST1|IL1A|HRH1|IL
positive regulation of cellular metabolic process	2.84E-04	CSF2|SPHK1|ACSL6|L
positive regulation of intracellular protein kinase cascade	2.84E-04	IL1A|IL3|CSF2|IL5|NE
regulation of tyrosine phosphorylation of Stat5 protein	3.13E-04	IL3|CSF2|IL2
regulation of signaling pathway	3.86E-04	CSF2|SPHK1|NEK6|SF
positive regulation of metabolic process	4.34E-04	CSF2|SPHK1|ACSL6|L
positive regulation of cellular biosynthetic process	4.49E-04	IL1A|IL3|HRH1|CSF2|
cell-cell signaling	4.57E-04	IL3|HRH1|GJB2|MAO
positive regulation of biosynthetic process	4.78E-04	IL1A|IL3|HRH1|CSF2|
defense response	6.82E-04	NDST1|IL1A|HRH1|IL
positive regulation of signal transduction	8.37E-04	IL1A|IL3|CSF2|IL5|NE
positive regulation of signaling process	9.07E-04	IL1A|IL3|CSF2|IL5|NE

C.

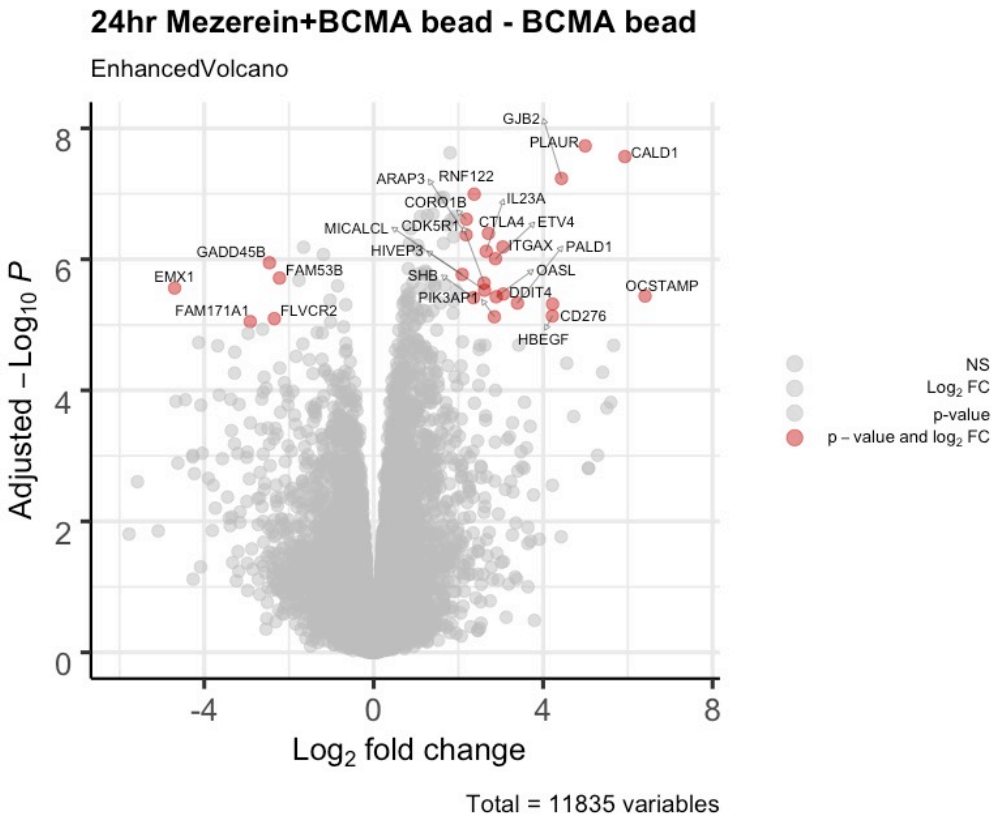

D.

Upregulated at 24hrs: GO biological process	Adj. p-value	Genes in test set
immune system process	2.91E-13	CSF2|ITGAM|IFITM2|CSF1|
immune response	4.71E-10	CEBPB|CSF2|NOTCH1|IFITM
regulation of cell communication	2.47E-07	RAB3A|CSF2|CSF1|CITED2|
positive regulation of biological process	9.61E-07	NRP1|CSF2|CSF1|CITED2|G
regulation of signal transduction	9.61E-07	CSF2|RGS19|CSF1|RGS14|C
cell differentiation	9.61E-07	CLIC5|NRP1|RAB3A|CSF2|C
regulation of signaling process	9.61E-07	CSF2|RGS19|CSF1|RGS14|C
developmental process	9.62E-07	RAB3A|CSF2|CSF1|GPR65|
response to wounding	9.62E-07	NRP1|CEBPB|NOTCH1|STXI
regulation of multicellular organismal process	1.70E-06	NRP1|RAB3A|CSF1|PPP3CA
cellular developmental process	1.76E-06	CLIC5|NRP1|RAB3A|CSF2|C
system development	1.76E-06	CLIC5|NRP1|RAB3A|CSF2|C
anatomical structure development	2.17E-06	RAB3A|CSF2|CSF1|KLHL35|
regulation of developmental process	2.39E-06	NRP1|CSF2|NOTCH1|CSF1|
multicellular organismal development	5.27E-06	RAB3A|CSF2|CSF1|GPR65|
regulation of signaling pathway	7.02E-06	CSF2|CSF1|CITED2|GPR65|
response to stimulus	9.22E-06	FCMR|RAB3A|CSF2|IFITM2

E.

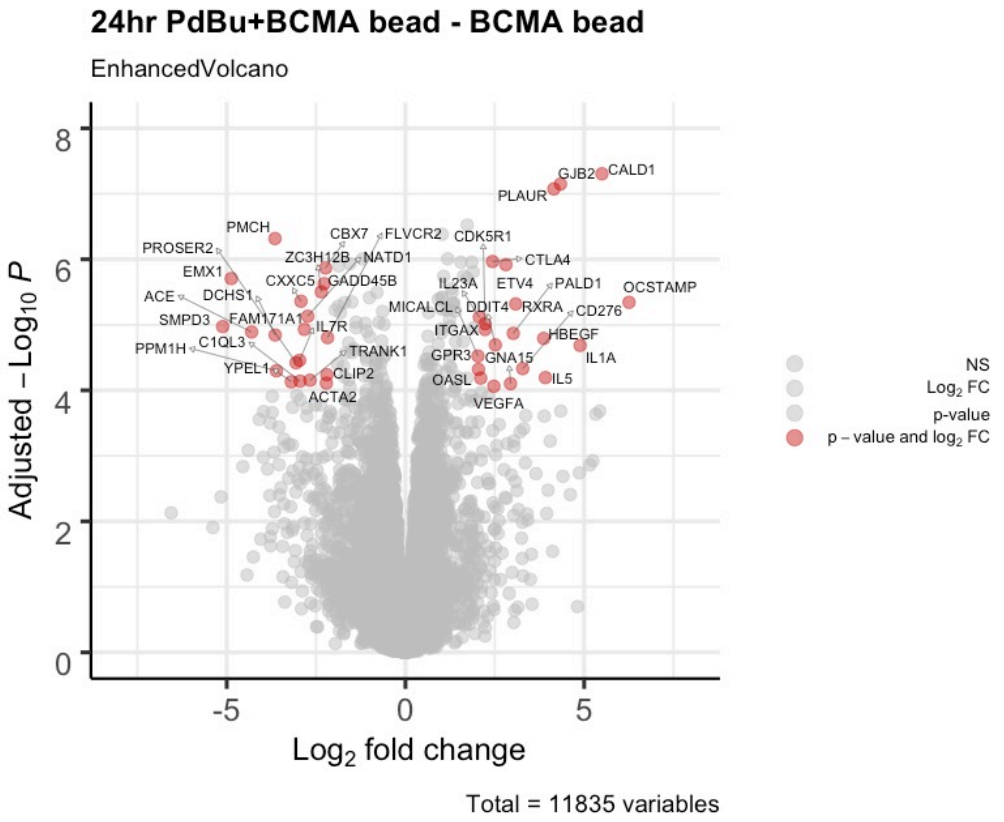

F.

Upregulated at 24hrs: GO biological process	Adj. p-value	Genes in test set
immune system process	6.83E-10	CEBPB|CSF2|NOTCH1|CSF1|
immune response	2.55E-08	CEBPB|CSF2|NOTCH1|CTSW
regulation of multicellular organismal process	4.25E-08	NRP1|CEBPB|RAB3A|NOTCH
developmental process	4.25E-08	CLIC5|NRP1|RAB3A|CSF2|CS
system development	8.11E-08	CLIC5|NRP1|RAB3A|CSF2|CS
regulation of developmental process	8.11E-08	NRP1|CSF2|NOTCH1|CSF1|K
organ development	8.11E-08	CLIC5|NRP1|RAB3A|CSF2|CS
anatomical structure development	8.11E-08	CLIC5|NRP1|RAB3A|CSF2|CS
multicellular organismal development	1.58E-07	CLIC5|NRP1|RAB3A|CSF2|CS
regulation of cell communication	1.92E-07	RAB3A|CSF2|NOTCH1|CSF1|
positive regulation of biological process	2.51E-07	NRP1|CSF2|CSF1|CITED2|AD
cell differentiation	6.64E-07	CLIC5|NRP1|RAB3A|CSF2|CS
cellular developmental process	1.62E-06	CLIC5|NRP1|RAB3A|CSF2|CS
positive regulation of cellular process	3.49E-06	NRP1|CSF2|CSF1|CITED2|AD
inflammatory response	5.60E-06	CCR1|IL10|CEBPB|SPHK1|F1
positive regulation of developmental process	5.60E-06	NRP1|CSF2|NOTCH1|TNFRSI
regulation of signaling pathway	6.43E-06	CSF2|NOTCH1|CSF1|CITED2
regulation of response to stimulus	6.43E-06	TMPRSS6|CD79A|SOCS3|NT

G.

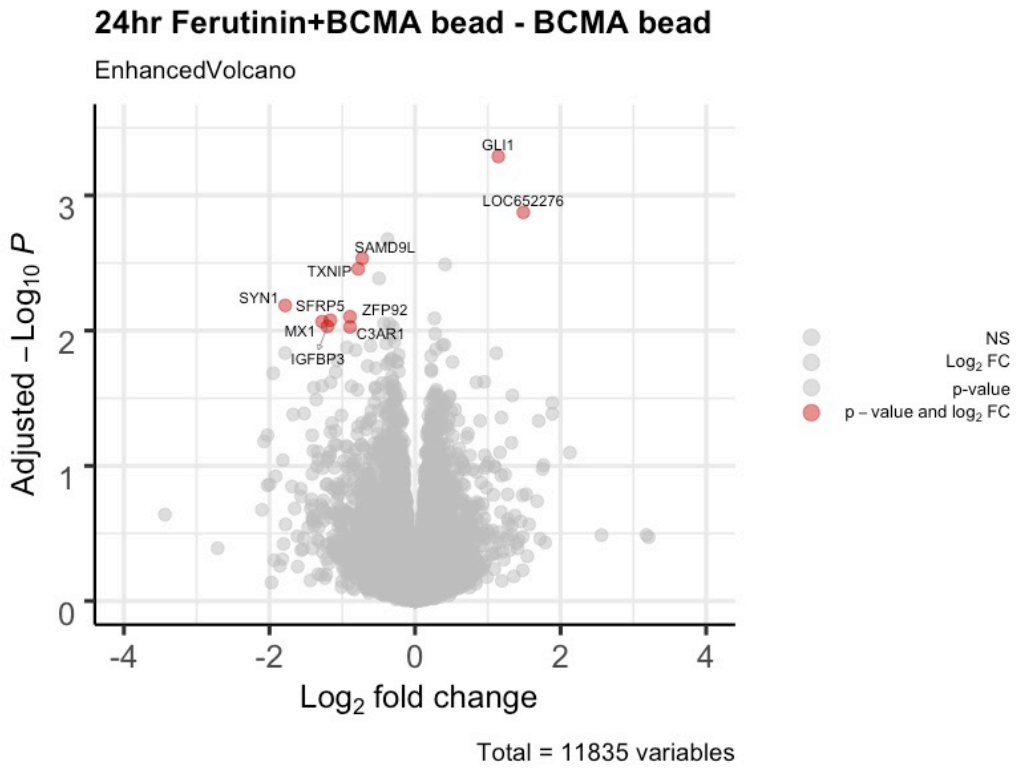

Figure 29: Differentially expressed genes and gene ontology pathway analysis relative to the antigen stimulated control. Differences in gene transcripts from TAC T cells stimulated with antigen (BCMA) + costimulation (CD86 and LFA-3) or drug (mezerein, PdBu, or ferutinin) minus cells stimulated with antigen alone. Volcano plots illustrating differentially expressed genes annotated in red for TAC T cells stimulated with drug + beads for 24 hours, with cutoff values of A) p-value $2x10^{-4}$ and FC 1.5; C) p-value $1x10^{-6}$ and FC 2; E) p-value $1x10^{-5}$ and FC 2; G) p-value $1x10^{-2}$ and FC 0.5. B) and D) and E) display the top biological processes from the biological network gene ontology pathway analysis, with B) p-values less than $1x10^{-3}$; D) and E) p-values less than $1x10^{-5}$.

The ferutinin samples clustered closely to the stimulated control in the PCA plot, and resulted in low differentially expressed gene p-values (figure 29G illustrates a p-value cutoff of 0.01 for annotated genes in red). As the effects of ferutinin were subtle in our analysis, we chose to pursue gene set enrichment analysis (GSEA) for the ferutinin + BCMA bead – DMSO + BCMA bead stimulation comparison. GSEA is useful in the case of a gene set of differentially expressed genes with low p-values, as it analyzes genes in the

gene set that move directionally as a cluster. We used ssGSEA to analyze the differentially expressed gene sets from all three donor samples in the ferutinin comparisons. This analysis is more specific than BiNGO analysis, as it compares transcriptional changes across an entire gene set to similar changes found in other publically available gene sets. GSEA can be used to discover new transcriptional profiles, rather than limiting the analysis to known biological pathways. In our analysis, we used to the Hallmark and Canonical pathway gene sets to analyze our data, which contains the directional transcriptional changes for most standard 'Hallmark' and 'Canonical' immunological events. Gene clusters in our ferutinin comparison were formed by sets of genes that were upregulated in a similar fashion, with specific GSEA clusters determined by the 'Hallmark' or 'Canonical' pathway gene sets. In our analysis, only one publically available data set was found to have significant overlap with our transcriptional data set. A data set for 'Wildtype – SAP knockout' in $CD4^+$ follicular helper T cells was found to have significant overlap with many gene clusters significant to ferutinin treatment in our TAC T cells ($p<0.05$). These overlapping gene clusters, with clusters determined by the hallmark gene set, are seen in figure 30. These overlapping gene clusters are specific to ferutinin treatment of TAC T cells (k) and SAP expression in $CD4^+$ T cells (K). In both hallmark and canonical pathway gene sets, 100 upregulated clusters were found to overlap. An exhaustive list of the 100 overlapping gene clusters between these two data sets is included in the appendix (figure A3). The 'Wildtype – SAP knockout' data set explored genes upregulated in $CD4^+$ follicular helper T cells with SH2D1A knockout (KO) versus wildtype cells. RNA was collected from $CD4^+$ T follicular helper cells 8 days after LCMV infection (Yusuf, 2010). This sequencing experiment

investigated the role of SAP protein on cytokine production and the generation and maintenance of germinal cells by $CD4^+$ T follicular helper cells. This comparison revealed genes that are upregulated specifically when SAP protein or SH2D1A gene expression is present. SH2D1A encodes SAP protein, which is a signaling lymphocyte activation molecule (SLAM) associated protein. SAP, consisting of a single SH2 domain, binds with high affinity to co-receptor SLAM (CD150), a transmembrane protein, to deliver costimulatory signals to mature T cells (Nichols, 2001). SLAM is a T cell costimulatory receptor and member of the Ig superfamily of receptors, under the CD2 subset. The CD2 T cell receptor does not use SAP directly, however the CD2-related SLAM receptors do. CD2 ligation to LFA-3 is the costimulatory event that is used throughout this project to boost proliferation in our TAC T cells.

Gene Set	Gene Set Name	Description	# Genes in Gene Set (K)	# Genes in Overlap (k)	k/K	p-value	FDR q-value
HALLMARK	INTERFERON GAMMA RESPONSE	Genes up-regulated in response to IFNG [GeneID=3458].	200	19	0.095	1.71E-13	5.08E-10
HALLMARK	ALLOGRAFT REJECTION	Genes up-regulated during transplant rejection.	200	15	0.075	1.71E-09	1.02E-06
HALLMARK	APOPTOSIS	Genes mediating programmed cell death (apoptosis) by activation of caspases.	161	12	0.0745	7.86E-08	2.92E-05
HALLMARK	IL2 STAT5 SIGNALING	Genes up-regulated by STAT5 in response to IL2 stimulation.	199	12	0.0603	7.76E-07	1.52E-04
HALLMARK	APICAL JUNCTION	Genes encoding components of apical junction complex.	200	12	0.06	8.19E-07	1.52E-04
HALLMARK	UV RESPONSE DN	Genes down-regulated in response to ultraviolet (UV) radiation.	144	10	0.0694	1.82E-06	3.09E-04
HALLMARK	COAGULATION	Genes encoding components of blood coagulation system; also up-regulated in platelets.	138	9	0.0652	9.98E-06	1.14E-03
HALLMARK	HEDGEHOG SIGNALING	Genes up-regulated by activation of hedgehog signaling.	36	5	0.1389	2.65E-05	2.39E-03
HALLMARK	INFLAMMATORY RESPONSE	Genes defining inflammatory response.	200	10	0.05	3.28E-05	2.79E-03
HALLMARK	KRAS SIGNALING UP	Genes up-regulated by KRAS activation.	200	10	0.05	3.28E-05	2.79E-03
HALLMARK	MITOTIC SPINDLE	Genes important for mitotic spindle assembly.	199	9	0.0452	1.73E-04	9.61E-03
HALLMARK	COMPLEMENT	Genes encoding components of the complement system, which is part of the innate immune system.	200	9	0.045	1.80E-04	9.61E-03
HALLMARK	MYOGENESIS	Genes involved in development of skeletal muscle (myogenesis).	200	9	0.045	1.80E-04	9.61E-03
HALLMARK	EPITHELIAL MESENCHYMAL TRANSITION	Genes defining epithelial-mesenchymal transition, as in wound healing, fibrosis and metastasis.	200	8	0.04	8.82E-04	2.82E-02
HALLMARK	ESTROGEN RESPONSE EARLY	Genes defining early response to estrogen.	200	8	0.04	8.82E-04	2.82E-02
HALLMARK	TNFA SIGNALING VIA NFKB	Genes regulated by NF-kB in response to TNF [GeneID=7124].	200	8	0.04	8.82E-04	2.82E-02
HALLMARK	XENOBIOTIC METABOLISM	Genes encoding proteins involved in processing of drugs and other xenobiotics.	200	8	0.04	8.82E-04	2.82E-02

Figure 30: ssGSEA revealed overlap of upregulated genes between ferutinin + BCMA– BCMA comparison and WT – SAP KO TFH CD4$^+$ T cells. Significant overlap is illustrated here between genes specific to ferutinin treatment in TAC T cells (k) and SAP expression in CD4$^+$ T cells (K), using the Hallmark gene set. Q value is indicative of the false positive discovery rate. ($p<0.05$).

4. DISCUSSION

4.1 Costimulation of $CD4^+$ and $CD8^+$ sorted T cells

As $CD4^+$ and $CD8^+$ T cell subtypes are known to differ in their anti-tumour functions, we sought to separate $CD4^+$ and $CD8^+$ costimulation induced transcriptional changes in our initial RNA sequencing experiment. In addition, it was our intention to identify compounds through connectivity mapping that preferentially targeted either $CD4^+$ or $CD8^+$ T cells. Through separating these transcriptional profiles, we first investigated drugs that benefitted both $CD4^+$ and $CD8^+$ proliferation. We chose this strategy in the hope of discovering a compound that can transiently induce costimulation in both $CD4^+$ and $CD8^+$ T cells.

$CD4^+$ and $CD8^+$ TAC T cells were found to demonstrate different proliferative capacities in response to costimulation, depending on their culture conditions. When TAC T cells were separated by $CD4^+$ or $CD8^+$ receptor expression on day 0 of culture, these cells were found to proliferate better in response to both antigen stimulation and costimulation. Sorted $CD4^+$ and $CD8^+$ cells were found to behave differently, where the absence of signaling between these two populations altered their phenotype. The effector T cell response of helper $CD4^+$ cells have been reported to depend on the cytokine environment in culture, where cytokine exposure in the environment dictates the $CD4^+$ response (Cano-Gamez, 2020). In our cultures, sorted $CD4^+$ T cells displayed increased proliferation and viability, presumably due to the lack of competition for resources from $CD8^+$ T cells. In contrast, $CD8^+$ T cells have been reported to demonstrate reduced clonal expansion upon stimulation in the absence of $CD4^+$s (Janssen, 2005). However, in our results we saw that

both $CD4^+$ and $CD8^+$ sorted TAC T cell populations displayed more robust proliferation when cultured separately as sorted populations, compared to the proliferation of $CD4^+$ and $CD8^+$ TAC T cells when cultured together. Albeit there being differences in sorted $CD4^+/CD8^+$ cultures, we chose to pursue RNA sequencing studies with sorted cells, to elucidate differences between $CD4^+$ and $CD8^+$ response to costimulation.

4.2 $CD4^+$ and $CD8^+$ sorted TAC T cell RNAseq results and pathway analysis

Our RNA sequencing analysis demonstrated many differentially expressed genes (figure 8A, C) in $CD4^+$ TAC T cells, representative of the transcriptional changes resulting from costimulation. Similar to our *in vitro* proliferation assay in Section 3.1, $CD4^+$ TAC T cells demonstrated the most robust response and the greatest number of differentially expressed genes. The pathway analysis for the $CD4^+$ TAC T cells revealed that at 4 hours most of the upregulated biological processes contribute to ribosomal RNA processing and T cell activation, which is consistent with previous reports demonstrating that costimulation of $CD4^+$ T cells results in an increase in ribosomal RNA expression to accommodate a higher level of cytokine production (Asmal, 2003). This is dependent on ERK-MAPK signaling as a result of costimulation. Our analysis revealed that at 4 hours post-stimulation, the transcription of cytokines IL-2 and IL-13 was upregulated as a result of costimulation, with high fold change values. IL-2 is a classical T cell growth factor that drives the proliferation response as a result of activation and costimulation. Among others, IL-13 is an early differentiation marker that drives a Th2 inflammatory response (Asmal, 2003). At 72 hours post-stimulation, metabolic, biosynthetic and catabolic processes are upregulated in our TAC T cells. This supports the observation that TAC T cells receiving costimulation

undergo specific metabolic changes to accommodate a robust proliferative phenotype. These metabolic changes are sustained after 72 hours, and may be contributing to the costimulation-induced increase in TAC T cell growth that we see *in vitro*.

Using the set of costimulation-specific differentially expressed genes for each of our $CD4^+$ and $CD8^+$ conditions, we compared these transcriptomes to compounds from the connectivity map database to discover compounds that may elicit a costimulatory-like response in our TAC T cells. Using this database, we performed connectivity mapping to computationally compare our desired costimulatory gene signature to the gene signatures produced by hundreds of drugs, and found several compounds of interest with high connectivity scores (figure 9). Using this method, our aim was to identify compounds that target costimulation signaling pathways and induce robust proliferation in our TAC T cells.

4.3 Characterization of Connectivity Map compounds

The connectivity mapping results revealed several compounds with high positive connectivity scores for the transcriptomes of our costimulated $CD4^+$ and $CD8^+$ cells. We investigated four of the top compounds, all with two or more positive scores. We sought to investigate the compounds that induced costimulatory-like changes in our TAC T cells, representative of CD28 and LFA-3 costimulation. While none of the compounds improved proliferation over that of our vehicle control in the re-exposure experiments, they could be targeting other T cell costimulatory pathways such as cytokine production or survival pathways. Other CD28 and LFA-3 costimulatory-like changes would not have been captured by the proliferation assay.

The connectivity map demonstrated thapisgargin and podophyllotoxin had the highest scores for $CD4^+$ costimulation at 72 hours, and positive scores for $CD4^+$ and $CD8^+$ costimulation at 4 hours. A high positive connectivity score for thapsigargin is supported by its known biological activity as an endoplasmic reticulum calcium pump inhibitor, where treatment has been characterized to induce IL-2 production in T cells (Kim, 2018). None of the compounds exhibited toxicity except thapsigargin, which has been characterized to induce necrosis at high concentrations (Collins, 2015). Although IL-2 exposure is expected to promote proliferation and rescue T cell exhaustion, we saw no benefit to TAC T cell proliferation in our assays with 20nM thapsigargin treatment. Further investigation is required to understand the effect of thapsigargin on TAC T cell cytokine production and proliferation.

Podophyllotoxin on the other hand, was not expected to induce proliferation based on its known activity to inhibit cell division. Podophyllotoxin's connectivity to our costimulated transcriptomes may be a result of costimulation gene pathways unrelated to proliferation. Podophyllotoxin has been characterized to bind tubulin and inhibit cell growth by arresting the cell cycle in S phase (Franchini, 2019). Based on its mechanism of action, podophyllotoxin treatment should decrease TAC T cell proliferation. However, T cells treated with a low dose have been reported to display a reduction in PD-1 surface expression, a coinhibitory receptor on T cells (Franchini, 2019). PD-1 inhibits T cell activation and proliferation, where a decrease in PD-1 expression allows the T cell to regain effector-like function. Therefore, it is possible that podophyllotoxin's high positive connectivity score for $CD4^+$ costimulation at 72 hours may be linked to a non-proliferative

costimulation-induced T cell response. Further characterization of the effects of podophyllotoxin on TAC T cells is required to understand it's mechanism of action.

Additional functional assays may give us more information on which pathways these compounds are targeting, and how they may resemble costimulated $CD4^+$ or $CD8^+$ sorted cells. It is also possible that these drug-induced costimulatory-like changes are specific to sorted $CD4^+$ and $CD8^+$ TAC T cells, where the treatment of bulk TAC T cells may result in more modest effects. Given the many caveats with the connectivity mapping approach and the lack of any obvious hits from our initial drug screen, we elected to pursue an alternate method of discovering compounds that boost proliferation in TAC T cells, through a high throughput functional screen.

4.4 Development of a bioluminescent TAC T cell proliferation screen

We sought to develop a high throughput functional screening assay to measure the proliferation of TAC T cells following antigen stimulation in the presence of drug treatment over 3 days. We compared a live fluorescent imaging assay and a luciferase reporter plate-based assay, and chose to pursue the latter. Due to the inconsistency of the live fluorescent imaging assay, and the number of time-consuming wash steps, we determined that it was not amenable to high throughput screening. In contrast, the reporter system validation assays revealed that cell number highly correlated with luciferase signal intensity, making the bioluminescent reporter system an attractive choice as a high throughput screen. These results were consistent across several plating densities and in a 3-day proliferation assay using our previous bead stimulation conditions. We determined that the difference in signal intensity between our negative and positive controls was sufficient enough to capture differences in cell number. The large delta between these controls increases the sensitivity of our assay, where small increases in TAC-LUC T cell number resulting from drug treatment will be captured by luciferase signal intensity.

Between our two proposed methods, the bioluminescent reporter system was an obvious choice for a high throughput assay. Following this decision, we sought to optimize our screening conditions and produce a reliable screening method to investigate the library of biologically active compounds at McMaster.

4.5 Optimization of a high throughput proliferation screen

Following several optimization experiments, we chose a plate type and plating density that resulted in the highest resolution of luciferase signal at higher cell densities.

Flat-bottom 384-well plates were chosen for our screen, with a working volume of 50µL. This consisted of 100nL drug or DMSO, 25µL of protein-coated beads, and 25µL TAC-LUC T cells, all dispensed using an automated liquid handler. The luminescence signal was then read on a plate reader using lumi fibers to measure total luminescence, resulting in a lower range of error than the standard absorbance filters. To be confident in our screening method, we sought to maximize the difference between our positive and negative controls in order to capture differences in signal intensity as a result of drug intervention. A low plating density of $3x10^4$ TAC-LUC T cells/well was chosen to resolve signal intensity from wells with cell numbers above that of the positive control, should a compound stimulate robust TAC-LUC T cell growth. Our screening assay demonstrated sensitivity to changes in TAC-LUC T cell signal intensity as a result of different bead stimulation conditions, and low variation in our controls across a high number of replicates. These results gave confidence that our screening assay would indirectly measure differences in TAC-LUC T cell proliferation through luciferase signal, and provide a means to screen a large library of compounds for costimulatory activity.

4.6 High Throughput Screen Results

Through our high throughput screen, we identified a total of 30 hit compounds to characterize further. The reproducibility of the results across two screening runs gave confidence to these results. Both runs of the screen revealed similar hit compounds, with the repeat screen identifying an additional 15 compounds. There were two groups of chemical structure and similarity that emerged in our analysis of the hit compounds from our first screen, phorbol esters/ PKC activators and flavanones. The top hit compound

emerging from both screens was isorhamnetine-3-glucoside, a flavanone. In our second screen, we saw the emergence of a third chemical group, cardenolides. Both flavanones and cardenolides are described as anti-inflammatory, but have not been explored for their costimulatory effects in T cells.

The emergence of phorbol esters as a chemical class provided confidence in our screen as a reliable tool to identify costimulatory compounds, as phorbol esters are known in the literature to activate PKC theta (Wang, 2012). PKC activators synergize with TCR engagement in T cells to increase intracellular calcium and induce activation, proliferation, and cytokine production (Kim, 2018). This activity recapitulates CD28 costimulatory signaling, providing T cells with signal 2 via chemical costimulation. Five out of our 30 hit compounds were PKC activators. These results were promising, as we know from the literature that these drugs target pathways downstream of CD28 costimulation.

4.7 Secondary screening results

Following the screen results, we selected 30 hit compounds for further evaluation. To confirm that these compounds were boosting TAC-LUC T cell proliferation as a result of targeting costimulatory signaling pathways, we chose to validate these compounds using a series of secondary screens.

Our secondary assays served to narrow down the 30 hit compounds from the screen, to a list of 15 compounds that increased TAC-LUC T cell signal only in the presence of antigen stimulation. Of these compounds, 6 were seen to increase luciferase signal above that of our positive control at their optimal working concentration. These results were

validated in stage II of our secondary assays using a second TAC construct, containing a BCMA antigen-binder instead of the HER2 binder on TAC-LUC cells.

Three phorbol esters were found to increase luciferase signal in our stage I secondary assay. The best performing of these, PdBu, was chosen to represent this chemical group in stage II of our secondary assays. A concentration between 10-100 nM of PdBu and other PKC activating molecules was found to produce a stronger luciferase signal than observed at 10μM, which was used in the screen. High concentrations of PKC activating molecules can negatively regulate PKC activity through inhibition of PKC-θ translocation and downstream signaling cascades. As a result, a 10 and 100nM dose was chosen for PKC activators PdBu, and mezerein respectively.

Bryostatin-1 was added to our compound list as a result of its known activity on PKC. Bryostatin-1 is a PKC activator recently characterized in literature to provide benefit to T cell proliferation. Bryostatin-1 can regulate cell activation, growth, and differentiation by modulating the activities of protein kinase C isoenzymes. Inhibition of tumour growth and activation of T lymphocytes *in vitro* are the most recognized consequences of drug treatment (Ramakrishna, 2019). The effect of bryostatin-1 on T cells was reported to range from induction of apoptotic cell death to T cell activation, expansion, and increased antigen-specific effector functions (Ramakrishna, 2019). While we did not choose bryostatin-1 for our following RNA sequencing studies, we did see a benefit to TAC T cell proliferation with the addition of this drug, as we anticipated from the literature.

While cell number provides a big picture understanding of proliferation and viability of the T cell population at endpoint, proliferation statistics provide a summary of

cell division on a cell by cell basis. Ferutinin treatment resulted in TAC T cell numbers at endpoint similar to the number of cells in the positive control stimulations for all three BCMA TAC T cell donors (figure 27A). While the impact of ferutinin on proliferation statistics were not as robust as the PKC activators, we did note that the $CD8^+$ proliferation indices exceeded the baseline control (figure 27C). Ferutinin is as a naturally occurring non-steroidal phytoestrogen and a strong agonist for estrogen receptor (ER) α and an agonist/antagonist for ER β. Ferutinin treatment has been shown to increase calcium permeability in the lipid bilayer and is being investigated as an anti-cancer agent (Macrì, 2020). High doses of ferutinin is described to cause mitochondrial dysfunction, leading to preferential cancer cell death (Macrì, 2020). With respect to T cells, ERα activation has been shown to promote T cell activation and proliferation and contribute to T cell–mediated autoimmune inflammation (Mohammad, 2018). ERβ signaling in $CD8^+$ T cells has been reported to boost T cell receptor activation and antitumor immunity through a phosphotyrosine switch (Yuan, 2021). Based on the literature, it is possible that ferutinin is increasing Ca^{2+} in TAC T cells, to amplify TCR activation. Ferutinin's phytoestrogen properties may be also contribute to the increased proliferative phenotype we see *in vitro*.

Our top hit from the high throughput screens, isorhamnetine-3-glucoside, did not demonstrate any activity in our secondary assays and was abandoned in favor of more promising drugs. The reason for the discrepancy between the results in our high throughput screen and the secondary screens is unknown but serves as a reminder of the importance of secondary assays and counter screens.

Dihydroercocristine was eliminated from our compound list in early stages of our Stage II secondary assays. This compound did not demonstrate consistent TAC T cell proliferation above that of the negative control, and may be targeting T cell signaling pathways indirectly related to T cell proliferation. Following the results from Stage II of our secondary assays, we also eliminated erocitrin and homoorientin from further assays as they did not result in proliferation above that of the negative control across 3 donors. PdBu, mezerein, and ferutinin were the most promising agents as these compounds consistently increased TAC T cell proliferation over a 3-day period in all secondary assays, regardless of the TAC antigen-binder.

A possible limitation to our secondary assays, was the single focus on proliferation as a functional readout. While the primary goal of the screen was to identify compounds that enhance proliferation, additional parameters may have improved our understanding of how these compounds benefit TAC T cell function. In addition to proliferation, costimulation modulates the cytokine production and secretion profile, and anti-tumour function. To achieve a better understanding of how these compounds effect TAC T cells, a cytokine analysis using the supernatant from these secondary assays would have contributed to our understanding. Compounds that emerged from our screen may have altered other aspects of the T cell response not contingent on proliferation, such as cytokine expression. It is possible that a few of these compounds also induced the secretion of pro-inflammatory cytokines such as IFN-γ, or TNF-α in our TAC T cells, that enhance T cell anti-tumour function.

While PdBu and dihydroercocristine preferentially supported $CD4^+$ proliferation, the other 5 compounds provided equal or greater benefit to $CD8^+$ proliferation. Preference for a single subtype may be indicative that these compounds target signaling pathways specific to either $CD4^+$ or $CD8^+$ subtypes to a higher degree. Further investigation into the specific targets of each compound and their mechanism of action will help elucidate these differences.

PdBu, mezerein, and ferutinin were selected for RNA sequencing analysis to further understand the effects of drug treatment on modulating the TAC T cell response.

4.8 RNAseq computational analysis of PdBu, mezerein, and ferutinin

The RNA sequencing results provided additional information on the effect of the top three compounds on TAC T cell function during antigen stimulation. The similar transcriptional profiles of mezerein and PdBu offer assurance that these PKC activators are targeting similar pathways, resulting in proliferative phenotypes. Clustering of these samples in the PCA plot, with comparable donor-specific directional changes, provides confidence in the accuracy of the results generated.

In our costimulation comparison, regulation of the JAK-STAT pathway was identified as a top biological process due to CD28 and CD2 costimulation in our TAC T cells. Positive regulation of STAT5, revealed in the significantly upregulated biological processes in figure 29, is known to be involved in T cell growth, differentiation and a T_H1/ T_H2 cytokine response. STAT5 is phosphorylated by Janus kinase 3 (Jak3) in response to several cytokines, including IL-2. STAT5 phosphorylation (pSTAT5) has been used as a marker of T cell proliferation, where treatment with STAT5 inhibitors resulted in complete

suppression of proliferation (Bitar, 2019). Translocation of pSTAT5 into the nucleus regulates IL-2 receptor α transcription, and is critical for progression into G1 of the cell cycle. pSTAT5 and IL-2 are described to reach their peak values at 24 hours following CD3/CD28 T cell stimulation, and decline afterwards (Bitar, 2019). Upregulation of STAT5 in our costimulation-specific BiNGO analysis is likely one of the pathways targeted by CD2 and CD28 costimulation at 24 hours, contributing to the enhanced proliferative phenotype we see *in vitro*.

Costimulation, mezerein, and PdBu -specific conditions all upregulated the differentially expressed gene GJB2 (figure 29 A, C, E). GJB2 encodes a gap junction protein connexin 26 (Cx26). Connexins (Cx) are a family of small integral membrane proteins that modulate gap junction channels to establish cell-cell communication. Cx allow for cell-cell communication by mediating the passage of small molecules, and are crucial for immune response, migration, cell survival, and proliferation (Gleisner, 2017). Specifically, Cx allow for the passage of several immunologically relevant molecules between neighboring cells, including adenosine triphosphate (ATP), inositol triphosphate (IP_3), and Ca^{2+} (Gleisner, 2017). The role of Cx26 has yet to be defined in the T cell response, where most research has focused on Cx26 expression and cancer cell metastasis. These findings suggest a link between Cx26, GJB2 gene upregulation, and tumour progression (Gleisner, 2017). Validation of Cx26 expression in proliferating TAC T cells, and further investigation of the role of Cx26 will aid in our understanding of the influence of GJB2 gene upregulation in TAC T cell proliferation.

Both mezerein and PdBu volcano plots demonstrated similar differentially expressed gene profiles, with the top genes being GJB2, CALD1, and PLAUR. CALD1 encodes a calmodulin and actin binding protein that is known to mediate smooth muscle contraction. However, CALD1 expression in T cells has yet to be described. PLAUR encodes the surface receptor for urokinase plasminogen activator (uPAR) known to promote extracellular matrix degradation during tumorigenesis, and is a signaling receptor for the invasion and survival of tumour cells (Armor, 2020). Increased T cell surface expression of uPAR and elevated soluble uPAR are used as a biomarker for the senescence-associated secretory phenotype (SASP) in T cells. uPAR has also been targeted by uPAR-specific CAR T cells to successfully eliminate senescent cells *in vivo* mouse models (Amor, 2020). Therefore, it is possible that PKC activators mezerein and PdBu target signaling pathways leading to T cell senescence. PLAUR expression is induced by Fos-related antigen 1 (FRA-1), a member of the AP-1 transcription factor family, and is positively regulated by uPAR expression (Annis, 2018). PKC θ has been reported to phosphorylate FRA-1 to induce PLAUR expression (Annis, 2018). FRA-1 regulates proliferation, differentiation and apoptosis in cells, and has been investigated as a pro-tumour transcription target as it has been shown to support tumour proliferation and metastasis (Annis, 2018). Upregulation of PLAUR appears to be specific to their shared target, PKC, however, investigation into their mechanisms of action will aid in our understanding of this phenomenon. It is also of interest to note that CTLA4 gene expression was upregulated in both mezerein and PdBu (figure 29C, E). CTLA4 is a well-known marker of T cell exhaustion, where strong TCR stimulation can lead to the upregulation of CTLA4. Further

research into the long-term effects of PdBu and mezerein drug treatment on TAC T cells may aid in understanding the consequences of CTLA4 and uPAR upregulation.

The gene for IL-23A was commonly upregulated in both mezerein and PdBu comparisons as well, where IL-23 is known to promote T cell proliferation and survival following TCR and CD28 stimulation. IL-23 engineering in CAR T cells has been reported to improve expansion and anti-tumour function in solid tumour models (Ma, 2020). Upregulation of IL-23 in response to PdBu and mezerein treatment may be a factor contributing to the increased proliferative phenotype we see *in vitro*.

Relying on sequencing results from only one timepoint may have been a limitation to this experiment, and could have resulted in the modest transcriptional differences between costimulation and control conditions. This may have also contributed to the non-significant biological effects of ferutinin treatment on stimulated cells (BiNGO analysis revealed 0 upregulated processes, $p>0.05$). Further studies looking at a time course of the drug-induced effects of ferutinin on TAC T cells would be beneficial in understanding the mechanism of action of this compound.

The volcano plot for differentially expressed genes specific to ferutinin treatment revealed only two significantly upregulated genes, GLI1 and LOC652276 (figure 29G). GLI1 upregulation is involved in activation of the Hedgehog (Hh) signaling pathway, where Hh signaling has been linked to an increase in proliferation and IL-2 production in $CD4^+$ T cells (Stewart, 2002). GLI1 is both a transcription factor and a target gene of Hh signaling, where the expression of GLI1 is often used to confirm Hh pathway activation. The second significant differentially expressed gene was LOC652276, a human potassium

channel tetramerization domain containing 5 pseudogene, which has yet to be linked to T cell function.

The ssGSEA analysis revealed overlapping gene clusters between ferutinin treatment and SAP expression in $CD4^+$ follicular helper T cells. The 'Wildtype – SAP knockout' data set explored genes upregulated in $CD4^+$ follicular helper T cells with SH2D1A KO versus wildtype cells. In this experiment, RNA was collected from $CD4^+$ T follicular helper cells 8 days after LCMV infection (Yusuf, 2010). Therefore, it is reasonable to suggest that these $CD4^+$ T cells were still receiving antigen stimulation at the time of collection, where upregulated gene clusters may be telling of SAP-induced costimulatory changes in activated $CD4^+$ T cells. SH2D1A (SAP) mutations are known to cause X-linked lymphoproliferative disease, where SH2D1A KO in $CD8^+$ T cells has been reported to reduce proliferation and effector function upon stimulation with APCs that express SLAM family receptors (Huang, 2015). Costimulation by SAP has been described to drive the proliferation of $CD8^+$ T cells under weak antigen stimulation conditions, and signal through ERK and AKT pathways (Huang, 2015). TCR activation in cells costimulated by SAP/SLAM ligation resulted in an increase in proliferation and production of IL-2 and IFN-γ (Nichols, 2001). It has also been suggested that SAP regulates IFN-γ production in T cells during activation, where SAP KO leads to an increase in a T_H1 type cytokine response following activation (Nichols, 2001). T cell costimulation by the ligation of SAP to SLAM may be the pathway that is modified by ferutinin treatment.

From the ssGSEA analysis by the Hallmark gene set, we can make several assumptions about the state of our ferutinin treated TAC T cells. The highest overlapping

cluster was 'IFN-γ response' ($p=1.71x10^{-13}$), suggesting that fertuinin treated cells, and SAP expressing $CD4^+$ T cells both upregulate genes in response to IFN-γ. 'IL-2 STAT5 signaling' ($p=7.76x10^{-7}$) was also a significantly upregulated gene cluster, in response to IL-2 stimulation. It may be that ferutinin treatment stimulates the secretion of IFN-γ and IL-2 in our TAC T cells. In addition, TNF-α may be upregulated in these cells as 'TNFα signaling via NFκB', and 'Apoptosis' are also upregulated gene clusters ($p=8.82x10^{-4}$ and $7.86x10^{-8}$ respectively). Following up these results with a cytokine secretion analysis of TAC T cells treated with ferutinin during stimulation would aid in better understanding the cytokine secretion prolife of these cells. A cytokine profile may help us better understand fertuinin's effects on activated TAC T cells.

The gene cluster for 'Apical Junction' was also found to overlap between ferutinin treated and SAP expressing cells ($p=8.19x10^{-7}$). This cluster involves genes that encode components of the apical junction complex. Apical junctions are a type of tight junctions that allow for cell-cell adhesion, polarization and signaling, and are necessary for the mechanics of TCR activation. The gene cluster defined as 'KRAS Signaling Up' ($p=3.28x10^{-5}$), confirms that ferutinin treatment results in KRAS activation, necessary for the propagation of cell signaling pathways involved in cell growth. The 'Estrogen Response Early' ($p=8.82x10^{-4}$) gene cluster involves genes defining an early response to estrogen. Based on ferutinin in the literature (as described in Section 3.7), we had suspected that Ferutinin's phytoestrogen properties may be contributing to the increased proliferative phenotype we see *in vitro.* These results suggest that ER signaling activity is influenced by ferutinin treatment.

Another interesting result in the ssGSEA is the upregulation of 'Hedgehog Signaling' genes ($p=2.65x10^{-5}$), which corresponds with the top significant differentially expressed gene for ferutinin treatment, GLI1 (figure 29G). GLI1 is used as a marker for Hh pathway activation. Hh signaling by the Sonic Hh protein has been reported to attenuate T cell activation in $CD4^+$ T cells, leading to an increase in proliferation and IL-2 production (Stewart, 2002). Therefore, the Hh signaling pathway may also be a target of fertutinin treatment in TAC T cells, leading to increased T cell proliferation.

T cell culture conditions during the engineering process and resulting $CD4^+$: $CD8^+$ culture ratios may have had an impact on T cell activation and costimulation. We know from Section 3.2 that $CD4^+/CD8^+$ sorted T cell cultures behave differently than bulk cultures. For $CD8^+$ T cells, this may be due to a lack of $CD4^+$ support during cell culture. In our previous sequencing results, we saw that $CD4^+$ sorted T cell cultures displayed more robust proliferation and transcriptional changes as a result of costimulation. $CD8^+$ sorted T cell cultures did not proliferate well and produced little transcriptional differences in comparison to antigen stimulated cells. While $CD4^+$ and $CD8^+$ differences were amplified in sorted populations, we also saw observable differences between $CD4^+/CD8^+$ proliferation indices in co-cultured populations in Section 3.7. In the sequencing experiments with co-cultured populations, the bi-directional change in transcriptional responses between $CD4^+$ and $CD8^+$ subsets may have led to a reduction in the bulk transcriptional changes observed in our analysis. Therefore, the data analyzed in Section 3.8 is an average of the $CD4^+$ and $CD8^+$ TAC T cell response, dictated by the $CD4^+$:$CD8^+$ ratio in each donor-specific sample.

In Section 3.7, we saw that ferutinin preferentially supported $CD8^+$ proliferation (figure 27). It is possible that the subset of cells significantly affected by ferutinin treatment, those that persist after 72 hours of stimulation in our CellTrace Violet secondary assays, may be too small of a population to achieve significance in our bulk RNA sequencing analysis.

In addition, these RNA sequencing results describe TAC T cell transcriptional changes after 24 hours as a result of drug treatment during stimulation, but may have been too early to capture the robust proliferative phenotype seen in our secondary assays. RNA was collected at 24 hours to capture early transcriptional changes affecting AP-1 and NF-κB activity, however transcriptional events that occurred later than 24 hours were not captured. The single timepoint chosen, and the possibility of bi-directional transcriptional changes in $CD4^+$ and $CD8^+$ cells may have contributed to the minimal effect of costimulation on our control cells.

5. FUTURE APPLICATIONS

Following the completion of the small molecule screen, characterization of hit compounds, and RNA sequencing analysis of TAC T cells treated with drug, several research questions worth investigating have arisen relating to the mechanism of action of the top three compounds.

What role does the upregulation of GJB2 (Connexin 26) play in TAC T cell proliferation?

The transcription of GJB2 (more commonly known as connexin 26 or Cx26) was upregulated in three of the four costimulation conditions. These include TAC T cells stimulated with costimulatory ligands, and TAC T cells stimulated with PKC activating compounds mezerein and PdBu. As GJB2 was upregulated in all three of these highly proliferative TAC T cell populations, it may be important for proliferation or other related functions. Connexins allow for cell-cell communication by mediating the passage of small molecules, and are crucial for immune response, migration, cell survival, and proliferation (Gleisner, 2017). Specifically, connexins allow the passage of several immunologically relevant molecules including adenosine triphosphate (ATP), inositol triphosphate (IP_3), and Ca^{2+} (Gleisner, 2017). The role of Cx26 has yet to be defined in the T cell response. By investigating the role of connexins, specifically Cx26, we may understand the impact of gap junctions and cell-cell communication in the proliferation of T cells. Understanding the types of molecules passaged by Cx26 between T cells, and activity in response to a strong stimulus (costimulation or PKC activation) may reveal the importance of these additional molecules in T cell proliferation.

Other connexin family members, Cx40 and Cx43, have been described as important to facilitating communication to support lymphocyte proliferation (Ni, 2017). Cx43 channel inhibition was reported to significantly reduce proliferation in stimulated T cells and decrease pro-inflammatory cytokine production (Ni, 2017). In CD4+ T cells, Cx43 protein levels were found to increase in response to CD3 and CD28 stimulation, where Cx hemichannels were required to sustain clonal expansion (Oviedo-Orta, 2010). The consistent upregulation of GJB2 in three of our sequencing results suggest that Cx26 hemichannels may be involved in TAC T cell proliferation. It is tempting to speculate that Cx26 may be involved with transmission of secondary messengers (ex. IP_3, Ca^{2+}) between T cells and may contribute to the costimulatory effects of mezerein and PdBu treatment.

Validation of Cx26 expression in proliferating TAC T cells by western blot, and further investigation into the role of Cx26 will aid in our understanding of the influence of GJB2 gene upregulation in TAC T cell proliferation. Future assays quantifying the changes in Cx26, Cx40, and Cx43 protein levels following TAC T cell stimulation will reveal if these Cx are involved in the TAC T cell proliferative response. Studying the effects of Cx26 deletion in TAC T cells will aid in understanding the implications of blocking Cx26 activity for TAC T cell proliferation and function. Additionally, inducing Cx26 overexpression in TAC T cells by lentiviral delivery of GJB2 will reveal if proliferation or effector functions are directly enhanced by increased cell-cell communication by Cx26.

How does PLAUR upregulation impact mezerein and PdBu treated TAC T cells? Is PLAUR transcription a direct result of PKC activation and phosphorylation of FRA-1?

PKC θ phosphorylation of FRA-1 leads to upregulation of the PLAUR gene, more commonly known as the protein uPAR, in breast cancer cell lines (Annis, 2018). PLAUR upregulation seems to be more specific to PKC activation than T cell costimulation, as we do not see PLAUR upregulated in our costimulated control cells receiving CD2/CD28 costimulation. Research on the long-term effects through repeat-exposure and repeat-stimulation assays will assist in understanding the connection between drug treatment and PLAUR upregulation, relating to T cell dysfunction. As uPAR is a biomarker for SASP in T cells (as discussed in Section 4.8), investigation of uPAR levels following TAC T cell stimulation in the presence of several small molecule PKC activators, will reveal if uPAR expression is directly impacted by PKC activation.

Follow-up studies regarding the long-term effects of these compounds may be beneficial in understanding the effect of PLAUR gene expression on the TAC T cell phenotype. Specifically, repeated drug exposure would reveal the relationship between these compounds and T cell malfunction, where markers of senescence, such as uPAR, and markers of T cell exhaustion, such as CTLA4, can be evaluated by flow cytometry. uPAR positive T cells were reported to lack Ki67 expression, a marker for proliferation, consistent with a senescent phenotype (Amor, 2020). A repeated drug exposure assay, followed over multiple days, will reveal if TAC T cells develop a senescent phenotype following excessive exposure to small molecule PKC activators. It may be that the proliferation-

induced effects of these PKC activators are short term, and that long-term exposure reveals a different phenotype in these cells.

CRISPR/Cas9 gene editing to delete PLAUR transcription and uPAR expression in TAC T cells may also be of interest, to understand the implications of removing uPAR activity and potentially suppressing SASP in TAC T cells treated with these PKC activating compounds. Furthermore, uPAR deletion may reveal if this protein plays a role in TAC T cell proliferation and function, or if it is a byproduct of PKC activation by PdBu and mezerein, and other PKC activating molecules.

What is ferutinin's mechanism of action and target in TAC T cells?

Further studies investigating the targets of ferutinin, and the cytokine profile of ferutinin treated TAC T cells will improve our understanding of the drug's effects on T cell proliferation and function.

Ferutinin has been described as a naturally occurring non-steroidal phytoestrogen and a strong agonist for ERα and agonist/antagonist for ERβ. ERα activation has been shown to promote T cell activation and proliferation, and contribute to T cell-mediated inflammation (Mohammad, 2018). Additionally, ERβ signaling in $CD8^+$ T cells has been reported to boost T cell receptor activation and antitumor immunity through a phosphotyrosine switch (Yuan, 2021). While upregulation of the estrogen response gene cluster in the ssGSEA results confirms that ferutinin is demonstrating some phytoestrogen activity in our TAC T cells, the influence of ER signaling on TAC T cell function remains unclear. Further experiments investigating an increase in ERα- and ERβ-target genes following ferutinin treatment would confirm if ER signaling is involved in the observed

TAC T cell response. Furthermore, investigating TAC T cell proliferation by Flow Cytometry, comparing the proliferation of ferutinin treated cells in the presence of ERα and ERβ inhibitors (separately) would aid in determining if ERα or ERβ activation is involved in ferutinin-induced TAC T cell proliferation. If ERα or ERβ inhibitors are found to decrease the proliferative response in ferutinin treated TAC T cells, selective ERα or ERβ agonists could also be used as targets to induce proliferation in T cells.

TAC T cells treated with ferutinin revealed differential expression of the upregulated gene GLI1, and upregulation of hedgehog signaling in the ssGSEA analysis. GLI1 is commonly used as an indication of Hh activity, where Hh signaling by the Sonic Hh protein during $CD4^+$ TCR activation was reported to increase proliferation and IL-2 production in these cells (Stewart, 2002). Investigating Sonic Hh protein levels, indicative of Hh pathway activation, following ferutinin treatment in TAC T cells will aid in determining if Hh signaling is a target of ferutinin treatment. Hh pathway inhibitors could also be used in combination with ferutinin treatment in TAC T cells, to determine if Hh pathway inhibition abrogates TAC T cell proliferation and reveal the link between ferutinin-induced proliferation and Hh signaling.

Gene cluster overlap between SAP expression in CD4 follicular helper T cells and TAC T cells treated with ferutinin suggest possible involvement of SAP in response to ferutinin. T cell costimulation by the ligation of SAP to SLAM may also be the pathway that is modified by ferutinin treatment. An experiment investigating if SAP expression is enhanced following ferutinin treatment during TAC T cell stimulation will reveal if increased SAP expression is the target of ferutinin treatment. The ssGSEA analysis also

revealed that cytokines IL-2 and IFN-γ play a role in the proliferative TAC T cell phenotype we see following ferutinin treatment. Previous findings revealed that activation in T cells costimulated by SAP/SLAM ligation resulted in an increase in proliferation and production of IL-2 and IFN-γ (Nichols, 2001). Western blot analyses measuring elevated SAP expression and downstream pathway activation of ERK and AKT in ferutinin treated vs. control TAC T cells would also confirm these results. Additional assays investigating ferutinin treatment on T cell proliferation in the presence of SLAM or SAP inhibitors would reveal if increased SAP/SLAM interaction is the pathway leading to enhanced proliferation in our TAC T cells. As SAP is thought to regulate IFN-γ production in activated T cells, a cytokine analysis of ferutinin treated TAC T cells would validate the effect of IFN-γ on TAC T cell proliferation and function. Increased IFN-γ production by T cells enhances the anti-tumour response, where high doses of IFN-γ in the tumour microenvironment has been linked to tumour regression (Jorgovanovic, 2020). Future assays investigating the effect of ferutinin treatment on TAC T cells in the presence of tumour target would reveal if ferutinin provides a synergistic effect on TAC T cell proliferation and on anti-tumour function.

Could SAP/SLAM signaling be a new target of costimulation in TAC T cells?

Costimulation by SAP has been described to drive the proliferation of $CD8^+$ T cells under weak antigen stimulation conditions, and signal through ERK and AKT pathways (Huang, 2015). TCR activation in cells costimulated by SAP/SLAM ligation resulted in an increase in proliferation and production of IL-2 and IFN-γ (Nichols, 2001). Targeting SLAM with soluble anti-SLAM antibodies or soluble SAP antibodies in TAC T cells,

would reveal the impact of SAP/SLAM on TAC T cell proliferation. Costimulation by SLAM family receptors offer additional TAC T cell functional benefits, such as enhanced IL-2 and IFN-γ production, and potentially IFN-γ mediated anti-tumour function. Further investigation into this pathway will elucidate its effects on TAC T cells, and may reveal the mechanism of action by which ferutinin induces proliferation in our TAC T cells.

5. MATERIALS & METHODS

5.1 Manufacturing of Engineered T cells

5.1.1 Lentivirus production

Third-generation, self-inactivating and non-replicative lentivirus was produced by transfection of $12x10^6$ HEK293T cells cultured on 15cm diameter tissue culture- treated dishes (NUNC; Thermo Fisher Scientific) were transfected with the packaging plasmids pRSV-Rev (6.25 μg), pMD2.G (9 μg), pMDLg-pRRE (12.5 μg) and the transfer plasmid pCCL containing the TAC transgene (32 μg) using Opti-MEM (Gibco; Thermo Fisher Scientific) and Lipofectamine 2000 (Thermo Fisher Scientific; Cat#11668-019) according to manufacturer's guidelines. Ten to twelve hours after transfection, media was replaced with fresh media supplemented with sodium butyrate (Sigma-Aldrich; Cat#B5887) at a final concentration of 1 mM. Media containing lentivirus particles were collected 36-48 hours later and concentrated via Amicon filter concentration (EMD Millipore; Cat#UFC910024). Viral titer in TU/mL was determined by serial dilution and transduction of HEK293T cells, and %tNGFR+ was determined via flow cytometry using an anti-NGFR-VioBrightFITC antibody (Miltenyi).

5.1.2 Retrovirus production

For generating human retrovirus, a stable retrovirus expressing murine cell line PG13 was generated. Retroviral supernatants were generated by murine retrovirus transduction of PG13 cells. On day 0, $1x10^5$ PG13s were seeded into a T25 flask. On day 2,3, and 4, the media was replaced and 2ml DMEM CM + 2 ml murine retrovirus was added. On day 5, the virus was removed and the newly generated stable expressing PG13 line was expanded.

To generate human PG13 retrovirus, $2x10^6$ of the stably expressing PG13 cell line was seeded on day 0 in a T75 flask. On day 3, virus was collected from the supernatant from PG13s using a 0.45um filter. 1-2ml retrovirus was added to T cells on day 2 of activation.

5.1.3 Culture of Human Engineered T Cell Bank

Human peripheral blood mononuclear cells (PBMCs) were extracted from blood samples and isolated from healthy donors. Cells were cryopreserved in 10% DMSO in heat inactivated human AB serum (Corning). CD4 and CD8 sorted T cell cultures were obtained from PBMCs using EasySep Human CD4+ (Stemcell; Cat#17952) and CD8+ (Stemcell; Cat#17953) T cell isolation kits, following their associated protocols. PBMCs were transported on dry ice, and thawed in a 37°C water bath while constantly swirled to ensure an even distribution of heat. Thawed PBMCs were washed in 10x volume of standard T cell media (RPM1 1640 (Gibco), 10% heat-inactivated fetal bovine serum (Gibco), 2mM L-glutamine (BioShop), 10mM HEPES (Roche), 0.5 mM sodium pyruvate (Sigma Aldrich), 1x non-essential amino acids (Gibco), 55μM β-mercaptoethanol (Gibco), 100U/mL penicillin + 100μg/mL streptomycin (Gibco)). Cells were re-suspended with standard T cell media at a concentration of $1x10^6$ cells/mL containing recombinant human IL-2 (Peprotech) and IL-7 (Peprotech) at a final concentration of 100IU/mL and 10ng/mL, respectively. Human T-Activated αCD3/αCD28 Dynabeads (Life Technologies) were used at 0.8:1 bead to cell ratio with PBMCs in each well to activate T cells within the mixture and induce proliferation over a 18-24 hour 37°C incubation period. A volume of 110μL T cell media was then removed from each well and lentivirus encoding for the BCMA specific TAC at an appropriate MOI in 10μL PBS was added to each well without

disturbing the pellet. Cells were returned to the 37°C incubator, and were counted and fed with standard T cell media (supplemented with rhIL-2 and rhIL-7) every other day to maintain a baseline concentration of 1e6 cells/mL, and scaled up to larger flasks accordingly. Dynabeads were removed 96 hours after activation. T cells were sorted for transduced cells on day 7 using the EasySep Human CD271 positive selection kit (STEMCELL Technologies) based on manufacturer's guidelines. For HER2 TAC T cells, retrovirus was added on day 2 and removed on day 4, with standard feeding performed every other day.

5.1.4 Cryopreservation of Engineered Human T cells

On day 14 of culture, T cells were counted and re-suspended in CryoStor CS10 (BioLife Solutions) at a concentration of $20x10^6$ cells/mL in 1mL aliquots and incubated on ice for 10 minutes. Cryovials were transferred to a Mr. Frosty (ThermoFisher) cooling system and placed in -80°C overnight, before being stored in liquid nitrogen. Prior to each experiment, cryopreserved T cells are transferred on dry ice and thawed in a 37°C water bath while constantly swirled to ensure an even distribution of heat. T cells were washed in 10x volume of standard T cell media, and re-suspended with standard T cell media supplemented with rhIL-2 and rhIL-7 at a concentration of $1x10^6$ cells/mL and incubated at 37°C for 24 hours.

5.2 Functional Analysis of TAC T cells

5.2.1 Protein G Bead Coating with HER2-Fc, BCMA-Fc, LFA-3, and CD86

6-8μM Protein G Polystyrene Beads (Spherotech) are mixed and aliquoted into a microcentrifuge tube and brought up to a concentration of $5x10^6$ beads/mL with PBS + 0.1% BSA with 100ng of BCMA-Fc, 100ng of HER2-Fc, 100ng CD86, LFA-3 for RNA

experiments, and 200ng CD86, LFA-3 for screen development. Beads for RNA collection negative controls were loaded without any added protein. Beads for screen development negative controls were loaded with non-specific HER2-Fc. Beads are placed on a rotator to be coated overnight at 4°C, and spun down and re-suspended to an appropriate effector: target ratio before use.

5.2.2 In vitro 72-hour CTV Proliferation Assay

TAC T cells were counted and labelled using the CellTrace Violet Cell Proliferation kit (ThermoFisher). T cells were washed and re-suspended at a concentration of $2x10^6$ cells/mL in warm PBS and mixed with an equal volume of PBS containing 1:500 CellTrace Violet. Cells were incubated at 37°C for 20 minutes, before being quenched with 5x standard T cell media. Cells were washed and re-suspended in T cell media. $5x10^5$ T cells were plated in a U bottom 96-well plate stimulated with $5x10^5$ protein coated polystyrene protein G beads for 72 hours. Cells were washed and stained with anti-CD4-AF700 (eBioscience), anti-CD8-PerCP-Cy5.5 (eBioscience), anti-NGFR-VioBright FITC (Miltenyi Biotec), and Molecular Probes LIVE/DEAD NearIR (ThermoFisher). Cells were filtered through nylon mesh into 5mL polystyrene tubes prior to running on a BD LSR II flow cytometer. Data was analyzed by FCS Express software.

5.3 RNA sequencing and Connectivity Mapping

5.3.1 RNA Collection

Sorted populations were stimulated with Protein G polystyrene beads at a T cell: bead ratio of 1:1. Following stimulation period, T cells were collected at 4 and 72hours (Section 3.1), or 24 hours (Section 3.8) and stored as a cell pellet at -80°C for less than a week. Frozen

cell pellets were lysed and run through a QIAshredder column (QIAGEN; Cat#79654) before RNA was isolated using the RNeasy Plus Mini Kit (QIAGEN; Cat#74134) following manufacturer's guidelines.

5.3.2. RNA sequencing

Illumina sequencing was performed by the Farncombe Metagenomics Facility (McMaster University). RNA integrity was first verified using the Agilent BioAnalyzer, followed by mRNA enrichment and library prep using the NEBNext Ultra II Directional RNA Library Prep Kit along with the NEBNext Poly(A) mRNA Magnetic Isolation Module. Libraries were subject to further BioAnalyzer QC and quantified by qPCR, then pooled in equimolar amounts. Sequencing was performed with the HiSeq Rapid v2 chemistry using onboard cluster generation (2 lanes) and a 1x50 bp read length configuration.

5.3.3 Connectivity Mapping

Connectivity Mapping was performed by Anna Dvorkin (McMaster University) using the Build 02 database provided by the Broad Institute to compare transcriptional changes of known drug perturbations to the transcriptional profiles produced by costimulated TAC T cells, obtained from the RNA sequencing comparisons.

5.3.4 CMap Toxicity Assay

Toxicity of CMap compounds were evaluated on BCMA-specific TAC T cells over 24 hours. $1x10^5$ TAC T cells were plated in a 96-well plate with drug for 24 hours in cytokine supplemented media. Wells were then mixed, and cells were counted using trypan blue on the Countess Hemocytometer. Compounds were tested in 5-fold dilutions (62.5μM,

12.5µM, 2.5µM, 0.5µM, 0.1µM) with the exception of thapsigargin which also included a 0.02µM dose. DMSO treated cells (62.5µM) served as our vehicle control.

5.4.5 CMap CTV Proliferation Assay

The CTV secondary screens using BCMA-specific TAC T cells used the same method as the '*In vitro* 72-hour CTV Proliferation Assay' protocol above (Section 5.2.2), with the appropriate CMap compound dosage added to each well following bead stimulation.

5.4 Screen Development

5.4.1 72hr In vitro Live Imaging Assay

Cell images were captured at 2X on a fluorescent microscope. $1x10^4$ BCMA-specific TAC T cells were plated/well at assay set-up, unless specified otherwise. Cells were stimulated with protein-coated polystyrene G beads in U-bottomed plates for 72hours, before washing and re-suspending in PBS for staining. Cells were transferred and stained in flat-bottom optical imaging plates (Corning; Ref#353219). TAC T cells were stained with Calcein AM (Life Technologies; Cat#C3100MP) to identify nuclei and hoeschst 33342, trihydrochloride (Invitrogen; Cat#H3570) to identify dead cells. RPMI 1640 Medium, no phenol red (Gibco; Cat#11-835-030) was used to replace standard RMPI 1640 in our T cell media cocktail during the three-day bead stimulation.

5.4.2 72hr In vitro Luminescence Assay

$5x10^5$ HER2-specific TAC-LUC T cells were plated in triplicates in a white flat bottom 96-well plate stimulated with 1:1 protein coated polystyrene protein G beads for 72 hours. Plates were incubated at 37°C. 0.15mg/mL D-Luciferin (Perkin Elmer) was added per well

and incubated for 10 minutes prior to luminescence was measured using a i3 SpectraMax (Molecular Devices) across all wavelengths.

5.5 High Throughput Drug Screen

5.5.1 Screening protocol

TAC T cells were thawed and rested in cytokine supplemented media for 24 hours prior to the screen set-up. $3x10^4$ HER2-specific TAC-LUC T cells were plated in duplicate in white flat bottom 384-well plates stimulated with 1:1 protein coated polystyrene protein G beads and 10μM drug compound (from the McMaster CMCB's Biologically Active Compounds Library) or DMSO vehicle. Columns 1-2 contained DMSO and HER2-coated beads (negative control), columns 3-22 contained drug and HER2-coated beads, and column 24 contained DMSO and HER2 + CD86 + LFA-3-coated beads (positive control). Column 23 was left empty. 100nL of drug or DMSO control was plated using the Echo Acoustic Liquid Handler and Multidrop Combi nL Reagent Dispenser, respectively. 25μL of the appropriate protein-coated beads were then dispensed using the Tempest Liquid Handler, followed by 25μL of TAC-LUC T cells to all wells. Plates were incubated at 37°C under controlled CO_2 conditions for 72 hours. 0.15mg/mL D-Luciferin (Perkin Elmer) was added per well using the Combi, and incubated for 40 minutes prior to luminescence was measured using a Neo2 plate reader using the lumi fiber method.

5.6 Secondary assays

5.6.1 TCR-dependent luciferase secondary screen

The secondary screens using TAC-LUC cells used similar methods as the screening protocol above (Section 5.5.1), except with five bead conditions across one plate to test for

TCR dependent luciferase activity: Column 1 received DMSO + uncoated beads (no stimulus), column 3 received DMSO + HER2-coated beads, column 5-8 received drug + uncoated beads, column 10-13 received drug + HER2-coated beads, and column 24 received DMSO and HER2 + CD86 + LFA-3-coated beads (as a high activity control). Each uncoated or HER2-coated bead stimulated well was normalized across the plate using the % luciferase activity equation, with the low activity control matched to the respective bead stimulus control.

5.6.2 % Luciferase Activity Equation

Luciferase signal for each sample was normalized to the unstimulated and antigen stimulated controls within each plate, by calculating % luciferase activity.

Equation for % luciferase activity: [(S-L)/(H-L)] *100

S = Measured sample value

H = Mean of high activity control (positive control)

L = Mean of low activity control (negative control)

5.6.3 Dose Response Assay

The dose response assay using TAC-LUC cells used a similar method as the screening protocol above (Section 5.5.1), except columns 3-16 contained 13 compounds (isorhamnetine-3-glucoside was included twice, from two sources) over a range of 7 doses (rows A-G). Half-log doses included in this assay were: 10μM, 3.162μM, 1μM, 316nM, 100nM, 32nM, and 10nM.

5.6.4 Flow cytometry secondary screen

The CTV secondary screens using BCMA-specific TAC T cells used the same method as the '*In vitro* 72-hour CTV Proliferation Assay' protocol above (Section 5.2.2). Prior to running on the Flow Cytometer, samples were stained for dead cells, NGFR transduction marker expression, and $CD4^+$/ $CD8^+$ markers, and data was collected by flow cytometry. For analysis, samples were gated on lymphocytes, followed by live cells, $NGFR^+$ cells, and $CD4^+$/$CD8^+$ subsets. $CD4^+$ and $CD8^+$ populations were fit by FCS proliferation modelling software to determine proliferation statistics.

5.7 RNA sequencing of drug treated cells

5.7.1 RNA collection from drug treated cells

BCMA-specific TAC T cells of three different donors were thawed and rested for 24hours. At 24 hours, dead cells were removed from each culture using the Miltenyl dead cell removal kit and Miltenyl magnetic columns. Cells were then plated at $1x10^6$ cells/well in a 24-well flat bottom plate, and stimulated at a ratio 1:1 cells: antigen-coated beads in 1mL of T cell media. RNA collection and sequencing was the same as the methods above in Section 5.3.

5.7.2 RNAseq processing and results

The RNAseq data from the HiSeq run were processed by Anna Dvorkin (McMaster University) using a Linux operating system for preprocessing, and processed in R Studio. Visualizations were produced in R Studio using Bioconductor and Enhanced Volcano packages.

6. APPENDIX

6.1 Live fluorescent imaging screening method

As a screening method for T cell proliferation, we proposed to use the same three-day proliferation assay described in Section 3.1 as it reveals a pronounced difference between antigen-stimulation alone and antigen stimulation in combination with costimulation. For this assay, TAC T cells were stained with calcein (nuclei stain) to identify all cells and Hoechst dye (to identify dead cells) and cells were imaged on a fluorescent microscope at 2X. We chose this method to both qualitatively and quantitatively distinguish differences between drug conditions, and see the proportion of live to dead cells as an additional readout.

Following the three-day bead stimulation, T cells were washed with PBS to remove T cell media and transferred to optical imaging plates prior to staining. Cells were stimulated in U-bottom plates to accommodate the removal of T cell media. We performed identical experiments without a PBS wash step and found that the phenol red containing T cell media interfered with the catalytic activity of both calcein and hoechst dyes, causing the media to autofluoresce.

T cells were plated in a 5-fold dilution series and stimulated with beads for 72 hours before imaging, and the optimal plating density was determined to be 10,000 cells/well (data not shown). To test the ability to distinguish proliferation following stimulation with antigen alone and proliferation following stimulation with antigen in the presence of costimulation, bead stimulations were set-up as described in Section 3.1. We quantified the number of live cells from these images using calcein and hoescht fluorescent dyes and

Columbus spot analysis software (equation A1). To identify the optimal bead stimulation conditions, we performed a 72hr stimulation with four effector: target ratios to distinguish the biggest difference between non-specific antigen, antigen, and antigen + costimulation conditions. We chose an E:T of 1:1 for following experiments (figure A1).

As a result of washing and transferring cells between plates prior to staining and imaging, we are not confident in the accuracy of this assay. To simplify the screen and allow for a more high-throughput protocol, we repeated the assay in phenol red-free media as recommended by a ThermoFisher representative to prevent media auto fluorescence. However, after optimization of cell number and dye concentration (data not shown), the phenol-red free T cell media still exhibited a low level of auto fluorescence that interfered with spot analysis.

$$Live\ cells = Total\ nuclei\ (calcein\ spots) - Dead\ cells\ (hoescht\ spots)$$

Equation A1: Spot calculation for number of live cells in fluorescent microscopic images. Calcein and hoechst spot quantification calculated from 2X fluorescent images using Columbus imaging software spot analysis, and custom maxima script.

A.

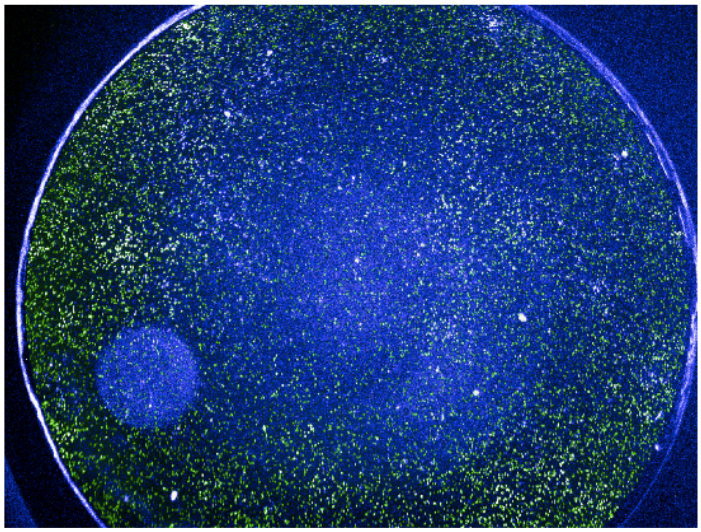

B.

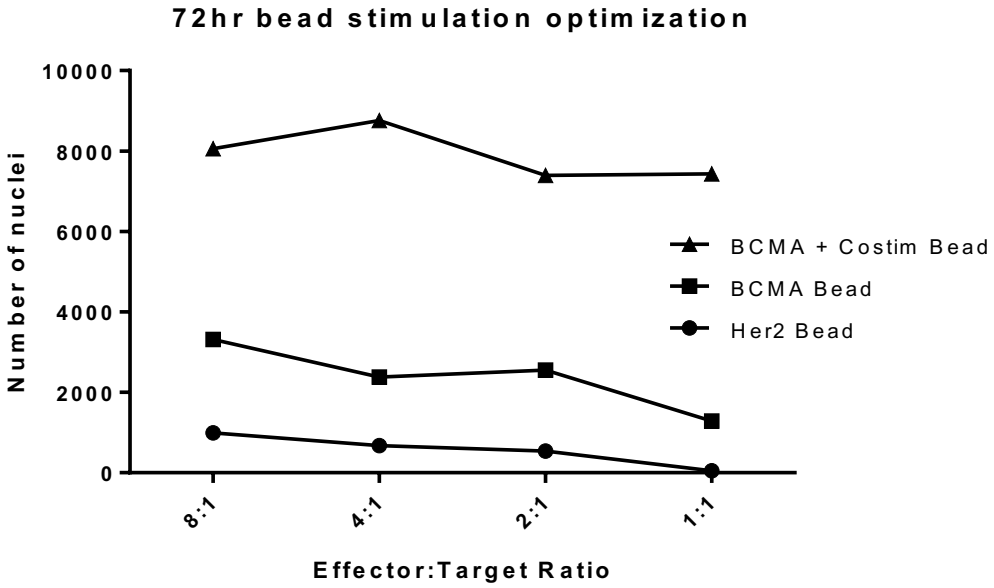

Figure A1: BCMA-specific TAC T cell effector: target bead stimulation for 72hours. **A)** Live fluorescent image of $1x10^4$ TAC T cells captured at a magnification of 2X with calcein (green) nuclei stain and hoechst (blue) cell-permeable dye. **B)** Spot analysis of the number of fluorescent nuclei counted in each image at 2X. $2x10^4$ TAC T cells stimulated with protein coated polystyrene beads at a 1:1 to 8:1 effector: target ratio with non-specific

antigen (HER2), BCMA, or BCMA+CD86+LFA3 coated beads, and washed with PBS before staining (n=1).

6.2 RNAseq ssGSEA results for Hallmark and Canonical Pathway gene sets

Gene Set	Gene Set Name	Description	# Genes in Gene Set (K)	# Genes in Overlap (k)	k/K	p-value	FDR q-value
BIOCARTA	AMI PATHWAY	Acute Myocardial Infarction	20	4	0.2	3.96E-05	3.27E-03
BIOCARTA	EXTRINSIC PATHWAY	Extrinsic Prothrombin Activation Pathway	13	3	0.2308	2.52E-04	1.25E-02
BIOCARTA	GRANULOCYTES PATHWAY	Adhesion and Diapedesis of Granulocytes	15	4	0.2667	1.16E-05	1.28E-03
BIOCARTA	INTRINSIC PATHWAY	Intrinsic Prothrombin Activation Pathway	23	4	0.1739	7.07E-05	5.13E-03
BIOCARTA	LAIR PATHWAY	Cells and Molecules involved in local acute inflammatory response	17	3	0.1765	5.82E-04	2.37E-02
BIOCARTA	LYM PATHWAY	Adhesion and Diapedesis of Lymphocytes	14	3	0.2143	3.18E-04	1.53E-02
BIOCARTA	MONOCYTE PATHWAY	Monocyte and its Surface Molecules	11	3	0.2727	1.47E-04	8.60E-03
HALLMARK	ALLOGRAFT REJECTION	Genes up-regulated during transplant rejection.	200	15	0.075	1.71E-09	1.02E-06
HALLMARK	APICAL JUNCTION	Genes encoding components of apical junction complex.	200	12	0.06	8.19E-07	1.52E-04
HALLMARK	APOPTOSIS	Genes mediating programmed cell death (apoptosis) by activation of caspases.	161	12	0.0745	7.86E-08	2.92E-05
HALLMARK	COAGULATION	Genes encoding components of blood coagulation system; also up-regulated in platelets.	138	9	0.0652	9.98E-06	1.14E-03
HALLMARK	COMPLEMENT	Genes encoding components of the complement system, which is part of the innate immune system.	200	9	0.045	1.80E-04	9.61E-03
HALLMARK	EPITHELIAL MESENCHYMAL TRANSITION	Genes defining epithelial-mesenchymal transition, as in wound healing, fibrosis and metastasis.	200	8	0.04	8.82E-04	2.82E-02
HALLMARK	ESTROGEN RESPONSE EARLY	Genes defining early response to estrogen.	200	8	0.04	8.82E-04	2.82E-02
HALLMARK	HEDGEHOG SIGNALING	Genes up-regulated by activation of hedgehog signaling.	36	5	0.1389	2.65E-05	2.39E-03
HALLMARK	IL2 STAT5 SIGNALING	Genes up-regulated by STAT5 in response to IL2 stimulation.	199	12	0.0603	7.76E-07	1.52E-04
HALLMARK	INFLAMMATORY RESPONSE	Genes defining inflammatory response.	200	10	0.05	3.28E-05	2.79E-03
HALLMARK	INTERFERON GAMMA RESPONSE	Genes up-regulated in response to IFNG [GeneID=3458].	200	19	0.095	1.71E-13	5.08E-10
HALLMARK	KRAS SIGNALING UP	Genes up-regulated by KRAS activation.	200	10	0.05	3.28E-05	2.79E-03
HALLMARK	MITOTIC SPINDLE	Genes important for mitotic spindle assembly.	199	9	0.0452	1.73E-04	9.61E-03
HALLMARK	MYOGENESIS	Genes involved in development of skeletal muscle (myogenesis).	200	9	0.045	1.80E-04	9.61E-03
HALLMARK	TNFA SIGNALING VIA NFKB	Genes regulated by NF-kB in response to TNF [GeneID=7124].	200	8	0.04	8.82E-04	2.82E-02
HALLMARK	UV RESPONSE DN	Genes down-regulated in response to ultraviolet (UV) radiation.	144	10	0.0694	1.82E-06	3.09E-04
HALLMARK	XENOBIOTIC METABOLISM	Genes encoding proteins involved in processing of drugs and other xenobiotics.	200	8	0.04	8.82E-04	2.82E-02
KEGG	ALLOGRAFT REJECTION	Allograft rejection	37	4	0.1081	4.73E-04	2.07E-02
KEGG	CELL ADHESION MOLECULES CAMS	Cell adhesion molecules (CAMs)	133	14	0.1053	6.81E-11	1.01E-07
KEGG	COMPLEMENT AND COAGULATION CASCADES	Complement and coagulation cascades	69	5	0.0725	6.05E-04	2.40E-02
KEGG	FOCAL ADHESION	Focal adhesion	199	9	0.0452	1.73E-04	9.61E-03
KEGG	GRAFT VERSUS HOST DISEASE	Graft-versus-host disease	41	4	0.0976	7.04E-04	2.58E-02
KEGG	INTESTINAL IMMUNE NETWORK FOR IGA PRODUCTION	Intestinal immune network for IgA production	48	5	0.1042	1.09E-04	6.76E-03
KEGG	LEISHMANIA INFECTION	Leishmania infection	72	8	0.1111	5.70E-07	1.30E-04
KEGG	LEUKOCYTE TRANSENDOTHELIAL MIGRATION	Leukocyte transendothelial migration	116	8	0.069	2.08E-05	2.06E-03
KEGG	SYSTEMIC LUPUS ERYTHEMATOSUS	Systemic lupus erythematosus	139	8	0.0576	7.56E-05	5.27E-03
KEGG	TOLL LIKE RECEPTOR SIGNALING PATHWAY	Toll-like receptor signaling pathway	102	6	0.0588	5.34E-04	2.30E-02
KEGG	TYPE I DIABETES MELLITUS	Type I diabetes mellitus	43	5	0.1163	6.39E-05	4.75E-03
KEGG	VIRAL MYOCARDITIS	Viral myocarditis	70	5	0.0714	6.47E-04	2.49E-02
NABA	MATRISOME	Ensemble of genes encoding extracellular matrix and extracellular matrix-associated proteins	1026	24	0.0234	9.95E-05	6.57E-03
PID	AVB3 INTEGRIN PATHWAY	Integrins in angiogenesis	74	5	0.0676	8.34E-04	2.82E-02
PID	INSULIN PATHWAY	Insulin Pathway	44	4	0.0909	9.21E-04	2.91E-02
PID	INTEGRIN2 PATHWAY	Beta2 integrin cell surface interactions	29	5	0.1724	8.83E-06	1.06E-03
PID	INTEGRIN3 PATHWAY	Beta3 integrin cell surface interactions	43	4	0.093	8.44E-04	2.82E-02
PID	VEGF VEGFR PATHWAY	VEGF and VEGFR signaling network	10	3	0.3	1.08E-04	6.76E-03
REACTOME	ADAPTIVE IMMUNE SYSTEM	Adaptive Immune System	825	24	0.0291	3.00E-06	4.70E-04
REACTOME	ANTIGEN PROCESSING CROSS PRESENTATION	Antigen processing-Cross presentation	106	6	0.0566	6.55E-04	2.49E-02
REACTOME	BILE ACID AND BILE SALT METABOLISM	Bile acid and bile salt metabolism	43	4	0.093	8.44E-04	2.82E-02
REACTOME	BIOLOGICAL OXIDATIONS	Biological oxidations	222	9	0.0405	3.88E-04	1.77E-02
REACTOME	CARGO RECOGNITION FOR CLATHRIN MEDIATED ENDOCYTOSIS	Cargo recognition for clathrin-mediated endocytosis	105	6	0.0571	6.23E-04	2.44E-02
REACTOME	CDC42 GTPASE CYCLE	CDC42 GTPase cycle	159	10	0.0629	4.45E-06	6.01E-04
REACTOME	CELL SURFACE INTERACTIONS AT THE VASCULAR WALL	Cell surface interactions at the vascular wall	194	8	0.0412	7.24E-04	2.60E-02
REACTOME	CLATHRIN MEDIATED ENDOCYTOSIS	Clathrin-mediated endocytosis	145	8	0.0552	1.02E-04	6.57E-03

REACTOME	CROSSLINKING OF COLLAGEN FIBRILS	Crosslinking of collagen fibrils	18	3	0.1667	6.93E-04	2.57E-02
REACTOME	CYTOKINE SIGNALING IN IMMUNE SYSTEM	Cytokine Signaling in Immune system	719	29	0.0403	2.17E-10	2.15E-07
REACTOME	DEVELOPMENTAL BIOLOGY	Developmental Biology	1143	25	0.0219	2.01E-04	1.03E-02
REACTOME	ECM PROTEOGLYCANS	ECM proteoglycans	76	5	0.0658	9.41E-04	2.94E-02
REACTOME	EXTRACELLULAR MATRIX ORGANIZATION	Extracellular matrix organization	301	16	0.0532	6.57E-08	2.79E-05
REACTOME	HEMOSTASIS	Hemostasis	678	19	0.028	5.31E-05	4.15E-03
REACTOME	IMMUNOREGULATORY INTERACTIONS BETWEEN A LYMPHOID AND A NON LYMPHOID CELL	Immunoregulatory interactions between a Lymphoid and a non-Lymphoid cell	191	9	0.0471	1.27E-04	7.55E-03
REACTOME	INNATE IMMUNE SYSTEM	Innate Immune System	1117	26	0.0233	5.56E-05	4.24E-03
REACTOME	INTEGRIN CELL SURFACE INTERACTIONS	Integrin cell surface interactions	85	7	0.0824	2.17E-05	2.08E-03
REACTOME	INTERCONVERSION OF NUCLEOTIDE DI AND TRIPHOSPHATES	Interconversion of nucleotide di- and triphosphates	29	4	0.1379	1.81E-04	9.61E-03
REACTOME	INTERFERON ALPHA BETA SIGNALING	Interferon alpha/beta signaling	73	5	0.0685	7.84E-04	2.74E-02
REACTOME	INTERFERON GAMMA SIGNALING	Interferon gamma signaling	93	10	0.1075	3.00E-08	1.48E-05
REACTOME	INTERFERON SIGNALING	Interferon Signaling	203	13	0.064	1.35E-07	4.00E-05
REACTOME	INTERLEUKIN 10 SIGNALING	Interleukin-10 signaling	46	4	0.087	1.09E-03	3.38E-02
REACTOME	MEMBRANE TRAFFICKING	Membrane Trafficking	629	19	0.0302	1.93E-05	1.98E-03
REACTOME	METABOLISM OF NUCLEOTIDES	Metabolism of nucleotides	98	6	0.0612	4.31E-04	1.91E-02
REACTOME	NERVOUS SYSTEM DEVELOPMENT	Nervous system development	580	15	0.0259	7.29E-04	2.60E-02
REACTOME	NEUTROPHIL DEGRANULATION	Neutrophil degranulation	479	15	0.0313	9.69E-05	6.55E-03
REACTOME	NON INTEGRIN MEMBRANE ECM INTERACTIONS	Non-integrin membrane-ECM interactions	59	5	0.0847	2.92E-04	1.42E-02
REACTOME	PEPTIDE LIGAND BINDING RECEPTORS	Peptide ligand-binding receptors	198	8	0.0404	8.27E-04	2.82E-02
REACTOME	POST TRANSLATIONAL PROTEIN MODIFICATION	Post-translational protein modification	1435	27	0.0188	1.13E-03	3.41E-02
REACTOME	RAC1 GTPASE CYCLE	RAC1 GTPase cycle	184	12	0.0652	3.36E-07	8.33E-05
REACTOME	RHO GTPASE CYCLE	RHO GTPase cycle	444	22	0.0495	8.32E-10	6.18E-07
REACTOME	RHOJ GTPASE CYCLE	RHOJ GTPase cycle	55	5	0.0909	2.10E-04	1.06E-02
REACTOME	RHOQ GTPASE CYCLE	RHOQ GTPase cycle	59	7	0.1186	1.87E-06	3.09E-04
REACTOME	SIGNAL TRANSDUCTION BY L1	Signal transduction by L1	21	3	0.1429	1.11E-03	3.39E-02
REACTOME	SIGNALING BY RECEPTOR TYROSINE KINASES	Signaling by Receptor Tyrosine Kinases	504	19	0.0377	8.18E-07	1.52E-04
REACTOME	SIGNALING BY RHO GTPASES MIRO GTPASES AND RHOBTB3	Signaling by Rho GTPases, Miro GTPases and RHOBTB3	717	22	0.0307	3.36E-06	4.99E-04
REACTOME	SIGNALING BY VEGF	Signaling by VEGF	106	10	0.0943	1.05E-07	3.48E-05
REACTOME	TRANS GOLGI NETWORK VESICLE BUDDING	trans-Golgi Network Vesicle Budding	72	5	0.0694	7.36E-04	2.60E-02
REACTOME	TRANSPORT OF SMALL MOLECULES	Transport of small molecules	728	18	0.0247	3.80E-04	1.77E-02
REACTOME	VESICLE MEDIATED TRANSPORT	Vesicle-mediated transport	724	24	0.0331	3.08E-07	8.32E-05
WP	CELLS AND MOLECULES INVOLVED IN LOCAL ACUTE INFLAMMATORY RESPONSE	Cells and Molecules involved in local acute inflammatory response	17	3	0.1765	5.82E-04	2.37E-02
WP	COMPLEMENT AND COAGULATION CASCADES	Complement and Coagulation Cascades	59	6	0.1017	2.55E-05	2.37E-03
WP	EBOLA VIRUS PATHWAY ON HOST	Ebola Virus Pathway on Host	131	7	0.0534	3.34E-04	1.58E-02
WP	EPITHELIAL TO MESENCHYMAL TRANSITION IN COLORECTAL CANCER	Epithelial to mesenchymal transition in colorectal cancer	164	7	0.0427	1.26E-03	3.73E-02
WP	FOCAL ADHESION	Focal Adhesion	202	9	0.0446	1.93E-04	1.01E-02
WP	FOCAL ADHESIONPI3KAKTMTORSIGNALING PATHWAY	Focal Adhesion-PI3K-Akt-mTOR-signaling pathway	309	13	0.0421	1.43E-05	1.52E-03
WP	GENES RELATED TO PRIMARY CILIUM DEVELOPMENT BASED ON CRISPR	Genes related to primary cilium development (based on CRISPR)	103	6	0.0583	5.62E-04	2.37E-02
WP	HIPPOMERLIN SIGNALING DYSREGULATION	Hippo-Merlin Signaling Dysregulation	123	9	0.0732	3.90E-06	5.52E-04
WP	HUMAN COMPLEMENT SYSTEM	Human Complement System	99	8	0.0808	6.47E-06	8.36E-04
WP	INSULIN SIGNALING	Insulin Signaling	161	7	0.0435	1.14E-03	3.41E-02
WP	MACROPHAGE MARKERS	Macrophage markers	9	3	0.3333	7.62E-05	5.27E-03
WP	MIRNAS INVOLVEMENT IN THE IMMUNE RESPONSE IN SEPSIS	miRNAs involvement in the immune response in sepsis	63	5	0.0794	3.97E-04	1.79E-02
WP	NONGENOMIC ACTIONS OF 125 DIHYDROXYVITAMIN D3	Non-genomic actions of 1,25 dihydroxyvitamin D3	71	5	0.0704	6.90E-04	2.57E-02
WP	PI3KAKT SIGNALING PATHWAY	PI3K-Akt Signaling Pathway	345	13	0.0377	4.48E-05	3.60E-03
WP	PLATELETMEDIATED INTERACTIONS WITH VASCULAR AND CIRCULATING CELLS	Platelet-mediated interactions with vascular and circulating cells	17	3	0.1765	5.82E-04	2.37E-02
WP	TOLLLIKE RECEPTOR SIGNALING PATHWAY	Toll-like Receptor Signaling Pathway	104	6	0.0577	5.92E-04	2.38E-02
WP	VEGFAVEGFR2 SIGNALING PATHWAY	VEGFA-VEGFR2 Signaling Pathway	438	16	0.0365	8.93E-06	1.06E-03
WP	WNTBETACATENIN SIGNALING PATHWAY IN LEUKEMIA	Wnt/beta-catenin Signaling Pathway in Leukemia	26	4	0.1538	1.17E-04	7.08E-03

Figure A3: ssGSEA revealed overlap of upregulated genes between ferutinin + BCMA– BCMA comparison and WT – SAP KO TFH CD4 T cells. Significant overlap was found between genes specific to ferutinin treatment in TAC T cells (k) and SAP

expression in CD4 T cells (K), using the Hallmark and Canonical Pathway gene sets. Q value is indicative of the false positive discovery rate. ($p<0.05$).

7. REFERENCES

Adams, J. L., Smothers, J., Srinivasan, R., & Hoos, A. (2015). Big opportunities for small molecules in immuno-oncology. *Nature Reviews Drug Discovery*, *14*(9), 603–621. https://doi.org/10.1038/nrd4596

Amor, C., Feucht, J., Leibold, J., Ho, Y. J., Zhu, C., Alonso-Curbelo, D., … Lowe, S. W. (2020). Senolytic CAR T cells reverse senescence-associated pathologies. *Nature*, *583*(7814), 127–132. https://doi.org/10.1038/s41586-020-2403-9

Annis, M.G., Ouellet, V., Rennhack, J.P. *et al.* Integrin-uPAR signaling leads to FRA-1 phosphorylation and enhanced breast cancer invasion. *Breast Cancer Res* 20**,** 9 (2018). https://doi.org/10.1186/s13058-018-0936-8

Asmal, M., Colgan, J., Naef, F., Yu, B., Lee, Y., Magnasco, M., & Luban, J. (2003). Production of ribosome components in effector CD4+ T cells is accelerated by TCR stimulation and coordinated by ERK-MAPK. *Immunity*, *19*(4), 535–548. https://doi.org/10.1016/S1074-7613(03)00268-1

Batra, S. A., Rathi, P., Guo, L., Courtney, A. N., Fleurence, J., Balzeau, J., … Heczey, A. (2020). Glypican-3-specific CAR T cells co-expressing IL15 and IL21 have superior expansion and antitumor activity against hepatocellular carcinoma. *Cancer Immunology Research*, *8*(3), 309–320. https://doi.org/10.1158/2326-6066.cir-19-0293

Berry, N., Ase, K., Kikkawa, U., Kishimoto, A., & Nishizuka, Y. (1989). Human T cell activation by phorbol esters and diacylglycerol analogues. *The Journal of Immunology*, *143*(5), 1407–1413.

Borrie, A. E., & Vareki, S. M. (2018). T Lymphocyte–Based Cancer Immunotherapeutics. *International Review of Cell and Molecular Biology Biology of T Cells - Part A*, 201–276. doi: 10.1016/bs.ircmb.2018.05.010

Calderón-Montaño, J. M., Burgos-Morón, E., Orta, M. L., Maldonado-Navas, D., García-Domínguez, I., & López-Lázaro, M. (2014). Evaluating the cancer therapeutic potential of

cardiac glycosides. *BioMed Research International*, *2014*. https://doi.org/10.1155/2014/794930

Cannons, J. L., Tangye, S. G., & Schwartzberg, P. L. (2011). SLAM family receptors and SAP adaptors in immunity. *Annual review of immunology*, *29*, 665–705. https://doi.org/10.1146/annurev-immunol-030409-101302

Cano-Gamez, E., Soskic, B., Roumeliotis, T.I. *et al.* Single-cell transcriptomics identifies an effectorness gradient shaping the response of $CD4^+$ T cells to cytokines. *Nature Communications* 11**,** 1801 (2020). https://doi.org/10.1038/s41467-020-15543-y

Chen, E. W., Brzostek, J., Gascoigne, N., & Rybakin, V. (2018). Development of a screening strategy for new modulators of T cell receptor signaling and T cell activation. *Scientific reports*, *8*(1), 10046. https://doi.org/10.1038/s41598-018-28106-5

Chen, L., & Flies, D. B. (2013). Molecular mechanisms of T cell co-stimulation and co-inhibition. *Nature Reviews Immunology*, *13*(4), 227–242. https://doi.org/doi:10.1038/nri3405

Cheng, F., Kovács, I. A., & Barabási, A. L. (2019). Network-based prediction of drug combinations. *Nature Communications*, *10*(1). https://doi.org/10.1038/s41467-019-09186-x

Demetriou, P., Abu-Shah, E., McCuaig, S., Mayya, V., Valvo, S., Korobchevskaya, K., … Dustin, M. L. (2019). CD2 expression acts as a quantitative checkpoint for immunological synapse structure and T-cell activation. *BioRxiv*, 589440. https://doi.org/10.1101/589440

Dobbs, J. F., & Katz, D. R. (1988). Human T-cell activation: Comparative studies on the role of different phorbol esters. *Immunology*, *63*(1), 133–137.

Dufva, O., Koski, J., Maliniemi, P., Ianevski, A., Klievink, J., Leitner, J., Pölönen, P., Hohtari, H., et al. (2020). Integrated drug profiling and CRISPR screening identify essential pathways for CAR T-cell cytotoxicity. *Blood*, *135*(9), 597–609. https://doi.org/10.1182/blood.2019002121

Dustin, M. L., & Long, E. O. (2010). Cytotoxic immunological synapses. *Immunological Reviews*, *235*(1), 24–34. https://doi.org/10.1111/j.0105-2896.2010.00904.x

Edwards, B. S., & Sklar, L. A. (2015). Flow Cytometry: Impact on Early Drug Discovery. *Journal of biomolecular screening*, *20*(6), 689–707. https://doi.org/10.1177/1087057115578273

Eggert, U. S., & Mitchison, T. J. (2006). Small molecule screening by imaging. *Current opinion in chemical biology*, *10*(3), 232–237. https://doi.org/10.1016/j.cbpa.2006.04.010

Esensten, J. H., Helou, Y. A., Chopra, G., Weiss, A., & Bluestone, J. A. (2016). CD28 Costimulation: From Mechanism to Therapy. *Immunity*, *44*(5), 973–988. https://doi.org/10.1016/j.immuni.2016.04.020

Fouda, A., Tahsini, M., Khodayarian, F., Al-Nafisah, F., & Rafei, M. (2017). A Fluorescence-based Lymphocyte Assay Suitable for High-throughput Screening of Small Molecules. Journal of visualized experiments : JoVE, (121), 55199. https://doi.org/10.3791/55199

Franchini, D. M., Lanvin, O., Tosolini, M., Patras de Campaigno, E., Cammas, A., Péricart, S. (2019). Microtubule-Driven Stress Granule Dynamics Regulate Inhibitory Immune Checkpoint Expression in T Cells. *Cell reports*, *26*(1), 94–107.e7. https://doi.org/10.1016/j.celrep.2018.12.014

Gabr, M. T., & Gambhir, S. S. (2020). Discovery and Optimization of Small-Molecule Ligands for V-Domain Ig Suppressor of T-Cell Activation (VISTA). *Journal of the American Chemical Society*, *142*(38), 16194–16198. https://doi.org/10.1021/jacs.0c07276

Gleisner, M. A., Navarrete, M., Hofmann, F., Salazar-Onfray, F., & Tittarelli, A. (2017). Mind the Gaps in Tumor Immunity: Impact of Connexin-Mediated Intercellular Connections. *Frontiers in immunology*, *8*, 1067. https://doi.org/10.3389/fimmu.2017.01067

Gobbi, G., Mirandola, P., Carubbi, C., Micheloni, C., Malinverno, C., Lunghi, P., … Vitale, M. (2009). Phorbol ester-induced PKCε down-modulation sensitizes AML cells to TRAIL-induced apoptosis and cell differentiation. *Blood*, *113*(13), 3080–3087. https://doi.org/10.1182/blood-2008-03-143784

Grobben, Y., Willemsen-Seegers, N., Uitdehaag, J., de Man, J., van Groningen, J., Friesen, J., van den Hurk, H., Buijsman, R. C., & Zaman, G. (2020). High-Throughput Fluorescence-Based Activity Assay for -1. *SLAS discovery : advancing life sciences R & D*, *25*(9), 1018–1025. https://doi.org/10.1177/2472555220919340

Hardman, C., Ho, S., Shimizu, A., Luu-Nguyen, Q., Sloane, J. L., Soliman, M. S. A., … Wender, P. A. (2020). Synthesis and evaluation of designed PKC modulators for enhanced cancer immunotherapy. *Nature Communications*, *11*(1), 1–11. https://doi.org/10.1038/s41467-020-15742-7

Haskard, D., Cavender, D., & Ziff, M. (1986). Phorbol ester-stimulated T lymphocytes show. *The Journal of Immunology*, *137*(5), 1429–1434.

Helsen, C. W., Hammill, J. A., Lau, V. W. C., Mwawasi, K. A., Afsahi, A., Bezverbnaya, K., … Bramson, J. L. (2018). The chimeric TAC receptor co-opts the T cell receptor yielding robust anti-tumour activity without toxicity. *Nature Communications*, *9*(1). https://doi.org/10.1038/s41467-018-05395-y

Herrant, M., Luciano, F., Loubat, A., & Auberger, P. (2002). The protective effect of phorbol esters on Fas-mediated apoptosis in T cells. Transcriptional and postranscriptional regulation. *Oncogene*, *21*(32), 4957–4968. https://doi.org/10.1038/sj.onc.1205689

Hosseinzade, A., Sadeghi, O., Biregani, A. N., Soukhtehzari, S., Brandt, G. S., & Esmaillzadeh, A. (2019). Immunomodulatory effects of flavonoids: Possible induction of T CD4+ regulatory cells through suppression of mTOR pathway signaling activity. *Frontiers in Immunology*, *10*(JAN), 1–12. https://doi.org/10.3389/fimmu.2019.00051

Huang, Y.-H. (2015). The role of SAP in antigen priming and differentiation of T lymphocytes. *University of British Columbia*. University of British Columbia. https://doi.org/10.14288/1.0220683

Ittershagen, S., Ericson, S., Eldjerou, L., Shojaee, A., Bleickardt, E., Patel, M., … Lebwohl, D. (2019). Industry's giant leap into cellular therapy: Catalyzing chimeric antigen receptor T cell (CAR-T) immunotherapy. *Current Hematologic Malignancy Reports*, *14*(1), 47–55. doi: 10.1007/s11899-019-0498-6

Janssen, E. M., Droin, N. M., Lemmens, E. E., Pinkoski, M. J., Bensinger, S. J., Ehst, B. D., Griffith, T. S., Green, D. R., & Schoenberger, S. P. (2005). CD4+ T-cell help controls CD8+ T-cell memory via TRAIL-mediated activation-induced cell death. *Nature*, *434*(7029), 88–93. https://doi.org/10.1038/nature03337

Jenkins MK, Taylor PS, Norton SD, Urdahl KB. CD28 delivers a costimulatory signal involved in antigen-specific IL-2 production by human T cells. J Immunol. 1991 Oct 15;147(8):2461-6. PMID: 1717561.

Jorgovanovic, D., Song, M., Wang, L. *et al.* Roles of IFN-γ in tumor progression and regression: a review. *Biomarker Research* 8**,** 49 (2020). https://doi.org/10.1186/s40364-020-00228-x

Kim, K. H., Kim, S. H., Jung, H. H., Moon, J. H., Jeong, S. U., Yu, K., & Lee, C. K. (2018). Thapsigargin Increases IL-2 Production in T Cells at Nanomolar Concentrations. *Immune network*, *18*(4), e26. https://doi.org/10.4110/in.2018.18.e26

Kos, F. J., Cornell, D. L., Lipke, A. B., Graham, L. J., & Bear, H. D. (2000). Protective role of IL-2 during activation of T cells with bryostatin-1. *International Journal of Immunopharmacology*, 22(8), 645–652. https://doi.org/10.1016/S0192-0561(00)00027-8

Lacey, B. M., Xu, Z., Chai, X., Laskey, J., Fradera, X., Mittal, P., Mishra, S., Piesvaux, J., et al. (2021). Development of High-Throughput Assays for Evaluation of Hematopoietic

Progenitor Kinase 1 Inhibitors. *SLAS discovery: advancing life sciences R & D*, *26*(1), 88–99. https://doi.org/10.1177/2472555220952071

Leitner, J., Herndler-Brandstetter, D., Zlabinger, G. J., Grubeck-Loebenstein, B., & Steinberger, P. (2015). CD58/CD2 Is the Primary Costimulatory Pathway in Human CD28-CD8+ T Cells. *Journal of immunology (Baltimore, Md. : 1950)*, *195*(2), 477–487. https://doi.org/10.4049/jimmunol.1401917

Lythe, G., Callard, R. E., Hoare, R. L., & Molina-París, C. (2016). How many TCR clonotypes does a body maintain? *Journal of theoretical biology*, *389*, 214–224. https://doi.org/10.1016/j.jtbi.2015.10.016

Ma, X., Shou, P., Smith, C. *et al.* Interleukin-23 engineering improves CAR T cell function in solid tumors. *Nat Biotechnol* 38, 448–459 (2020). https://doi.org/10.1038/s41587-019-0398-2

Macrì, R., Musolino, V., Gliozzi, M., Carresi, C., Maiuolo, J., Nucera, S., … Mollace, V. (2020). Ferula L. Plant Extracts and Dose-Dependent Activity of Natural Sesquiterpene Ferutinin: From Antioxidant Potential to Cytotoxic Effects. *Molecules*, *25*(23), 5768. doi:10.3390/molecules25235768

Marro, B. S., Zak, J., Zavareh, R. B., Teijaro, J. R., Lairson, L. L., & Oldstone, M. (2019). Discovery of Small Molecules for the Reversal of T Cell Exhaustion. *Cell reports*, *29*(10), 3293–3302.e3. https://doi.org/10.1016/j.celrep.2019.10.119

Martínez, G., Mijares, M. R., & De Sanctis, J. B. (2019). Effects of Flavonoids and Its Derivatives on Immune Cell Responses. *Recent Patents on Inflammation & Allergy Drug Discovery*, *13*(2), 84–104. https://doi.org/10.2174/1872213x13666190426164124

Mendu, S. K., Bhandage, A., Jin, Z., & Birnir, B. (2012). Different subtypes of GABA-A receptors are expressed in human, mouse and rat T lymphocytes. *PloS one*, *7*(8), e42959. https://doi.org/10.1371/journal.pone.0042959

Mohammad, I., Starskaia, I., Nagy, T., Guo, J., Yatkin, E., Väänänen, K., … Chen, Z. (2018). Estrogen receptor contributes to T cell–mediated autoimmune inflammation by promoting T cell activation and proliferation. *Science Signaling*, *11*(526), 1–13. https://doi.org/10.1126/scisignal.aap9415

Musa, A., Ghoraie, L. S., Zhang, S. D., Glazko, G., Yli-Harja, O., Dehmer, M., … Emmert-Streib, F. (2018). A review of connectivity map and computational approaches in pharmacogenomics. *Briefings in Bioinformatics*, *19*(3), 506–523. https://doi.org/10.1093/bib/bbw112

Ni X, Wang A, Zhang L, Shan Ly, Zhang Hc, et al. (2017) Up-regulation of gap junction in peripheral blood T lymphocytes contributes to the inflammatory response in essential hypertension. *PLOS ONE* 12(9): e0184773. https://doi.org/10.1371/journal.pone.0184773

Nichols, K. E., Koretzky, G. A., & June, C. H. (2001). SAP: natural inhibitor or grand SLAM of T cell activation? *Nature Immunology*, *2*(8), 665–666. https://doi.org/https://doi.org/10.1038/90595

Onishi, H., Fujimura, A., Oyama, Y., Yamasaki, A., Imaizumi, A., Kawamoto, M., Katano, M., Umebayashi, M., & Morisaki, T. (2016). Hedgehog signaling regulates PDL-1 expression in cancer cells to induce anti-tumor activity by activated lymphocytes. *Cellular immunology*, *310*, 199–204. https://doi.org/10.1016/j.cellimm.2016.08.003

Onishi, H., Morisaki, T., Kiyota, A., Koya, N., Tanaka, H., Umebayashi, M., & Katano, M. (2013). The Hedgehog inhibitor cyclopamine impairs the benefits of immunotherapy with activated T and NK lymphocytes derived from patients with advanced cancer. *Cancer immunology, immunotherapy : CII*, *62*(6), 1029–1039. https://doi.org/10.1007/s00262-013-1419-5

Ouyang, Y., Zhong, X., Liao, H., Zhu, P., Luo, K., & Zhu, H. (2021). A New Method for Screening Natural Products to Stimulate IFN-γ Production in Jurkat Human T Lymphocytes. *SLAS discovery : advancing life sciences R & D*, *26*(1), 130–139. https://doi.org/10.1177/2472555220922475

Oviedo-Orta, E., Perreau, M., Evans, W.H. and Potolicchio, I. (2010), Control of the proliferation of activated $CD4^+$ T cells by connexins. *Journal of Leukocyte Biology*, 88: 79-86. https://doi.org/10.1189/jlb.0909613

Parham, P., Janeway, C., & Murphy, K. (2015). *The Immune System* (4th ed.). Garland Science.

Parish, S., Kim, S., Sekhon, R., Wu, J., Kawakatsu, Y., & Effros, R. (2010). Adenosine Deaminase Modulation of Telomerase Activity and Replicative Senescence in Human CD8 T Lymphocytes. *The Journal of Immunology*, *184*(6), 2847–2854. https://doi.org/10.1038/jid.2014.371

Ramakrishna, S., Barsan, V., & Mackall, C. (2020). Prospects and challenges for use of CAR T cell therapies in solid tumors. *Expert Opinion on Biological Therapy*, *20*(5), 503–516. https://doi.org/10.1080/14712598.2020.1738378

Ramakrishna, S., Highfill, S. L., Walsh, Z., Nguyen, S. M., Lei, H., Shern, J. F., … Fry, T. J. (2019). Modulation of target antigen density improves CAR T-cell functionality and persistence. *Clinical Cancer Research*, *25*(17), 5329–5341. https://doi.org/10.1158/1078-0432.CCR-18-3784

Roy, M., Liang, L., Xiao, X., Feng, P., Ye, M., & Liu, J. (2018). Lycorine: A prospective natural lead for anticancer drug discovery. *Biomedicine & pharmacotherapy = Biomedecine & pharmacotherapie*, *107*, 615–624. https://doi.org/10.1016/j.biopha.2018.07.147

Santos, J., Ogando, J., Lacalle, R. A., & Mañes, S. (2020). A flow cytometry-based method to screen for modulators of tumor-specific T cell cytotoxicity. *Methods in enzymology*, *631*, 467–482. https://doi.org/10.1016/bs.mie.2019.02.040

Siegel, R. L., Miller, K. D., & Jemal, A. (2019). Cancer statistics, 2019. *CA: A Cancer Journal for Clinicians*, *69*(1), 7–34. doi: 10.3322/caac.21551

Skånland, S. S., Moltu, K., Berge, T., Aandahl, E. M., & Taskén, K. (2014). T-cell co-stimulation through the CD2 and CD28 co-receptors induces distinct signalling responses. *Biochemical Journal*, *460*(3), 399–410. https://doi.org/10.1042/BJ20140040

Song, D. G., Ye, Q., Poussin, M., Harms, G. M., Figini, M., & Powell, D. J. (2012). CD27 costimulation augments the survival and antitumour activity of redirected human T cells in vivo. *Blood*, *119*(3), 696–706. https://doi.org/10.1182/blood-2011-03-344275

Sterner, R.C., Sterner, R.M. CAR-T cell therapy: current limitations and potential strategies. (2021) *Blood Cancer J.* 11**,** 69. https://doi.org/10.1038/s41408-021-00459-7

Stewart, G. A., Lowrey, J. A., Wakelin, S. J., Fitch, P. M., Lindey, S., Dallman, M. J., … Howie, S. E. M. (2002). Sonic Hedgehog Signaling Modulates Activation of and Cytokine Production by Human Peripheral CD4 + T Cells. *The Journal of Immunology*, *169*(10), 5451–5457. https://doi.org/10.4049/jimmunol.169.10.5451

Subramanian, A., Narayan, R., Corsello, S. M., Peck, D. D., Natoli, T. E., Lu, X., … Golub, T. R. (2017). A Next Generation Connectivity Map: L1000 Platform and the First 1,000,000 Profiles. *Cell*, *171*(6), 1437-1452.e17. https://doi.org/10.1016/j.cell.2017.10.049

Tian, Y., Li, Y., Shao, Y. *et al.* (2020). Gene modification strategies for next-generation CAR T cells against solid cancers. *J Hematol Oncol* 13**,** 54. https://doi.org/10.1186/s13045-020-00890-6

To, J., Quackenbush, D., Rowell, E., Li, L., Reed, C., Lo, F., & Horman, S. R. (2021). A biomimetic assay platform for the interrogation of antigen-dependent anti-tumor T-cell function. *Communications biology*, *4*(1), 56. https://doi.org/10.1038/s42003-020-01565-1

Veillette, A., Dong, Z., & Latour, S. (2007). Consequence of the SLAM-SAP Signaling Pathway in Innate-like and Conventional Lymphocytes. *Immunity*, *27*(5), 698–710. https://doi.org/10.1016/j.immuni.2007.11.005

Vilar, M. L. L. V., Frutuoso, M. S., Arruda, S. M., Lima, D. M., Bezerra, C. S., & Pompeu, M. M. L. (2011). The role of the SLAM-SAP signaling pathway in the modulation of CD4

+ T cell responses. *Brazilian Journal of Medical and Biological Research*, *44*(4), 276–282. https://doi.org/10.1590/S0100-879X2011007500038

Waller, A. (2019). Metabolic reprogramming of T cells to optimize adoptive T cell therapy. *Boston University*. Retrieved from https://hdl.handle.net/2144/36720

Wang, X., Chuang, H. C., Li, J. P., & Tan, T. H. (2012). Regulation of PKC-Θ function by phosphorylation in T cell receptor signaling. *Frontiers in Immunology*, *3*(JUL), 1–8. https://doi.org/10.3389/fimmu.2012.00197

Yuan, B., Clark, C. A., Wu, B., Yang, J., Drerup, J. M., Li, T., … Li, R. (2021). Estrogen receptor beta signaling in CD8 + T cells boosts T cell receptor activation and antitumor immunity through a phosphotyrosine switch. *Journal for ImmunoTherapy of Cancer*, *9*(1). https://doi.org/10.1136/jitc-2020-001932

Yusuf, I., Kageyama, R., Monticelli, L., Johnston, R. J., DiToro, D., Hansen, K., … Crotty, S. (2010). Germinal Center T Follicular Helper Cell IL-4 Production Is Dependent on Signaling Lymphocytic Activation Molecule Receptor (CD150). *Journal of Immunology Research*, *185*(1), 190–202. https://doi.org/10.4049/jimmunol.0903505.Germinal

Zhang, X., Lu, X. A., Yang, J., Zhang, G., Li, J., Song, L., Su, Y., Shi, Y., et al. (2020). Efficacy and safety of anti-CD19 CAR T-cell therapy in 110 patients with B-cell acute lymphoblastic leukemia with high-risk features. *Blood advances*, *4*(10), 2325–2338. https://doi.org/10.1182/bloodadvances.2020001466